

**ECONOMIC GEOLOGY  
RESEARCH UNIT**

University of the Witwatersrand  
Johannesburg

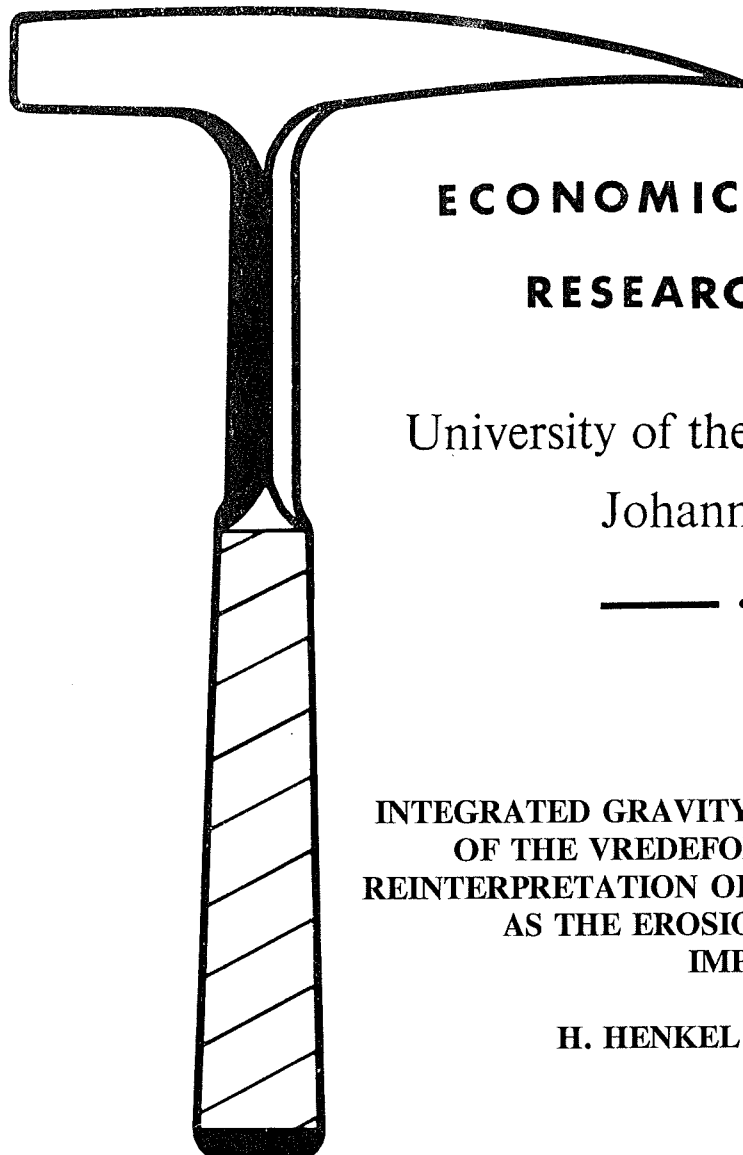
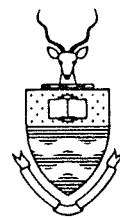
---

**INTEGRATED GRAVITY AND MAGNETIC MODELLING  
OF THE VREDEFORT IMPACT STRUCTURE -  
REINTERPRETATION OF THE WITWATERSRAND BASIN  
AS THE EROSIONAL REMNANT OF AN  
IMPACT BASIN**

**H. HENKEL and W.U. REIMOLD**

---

**INFORMATION CIRCULAR No. 299**



**ECONOMIC GEOLOGY  
RESEARCH UNIT**

University of the Witwatersrand  
Johannesburg

— • —  
**INTEGRATED GRAVITY AND MAGNETIC MODELLING  
OF THE VREDEFORT IMPACT STRUCTURE -  
REINTERPRETATION OF THE WITWATERSRAND BASIN  
AS THE EROSIONAL REMNANT OF AN  
IMPACT BASIN**

**H. HENKEL and W.U. REIMOLD**

— • **INFORMATION CIRCULAR No. 299**

UNIVERSITY OF THE WITWATERSRAND  
JOHANNESBURG

**INTEGRATED GRAVITY AND MAGNETIC MODELLING  
OF THE VREDEFORT IMPACT STRUCTURE -  
REINTERPRETATION OF THE WITWATERSRAND BASIN  
AS THE EROSIONAL REMNANT OF AN  
IMPACT BASIN**

by

**H. HENKEL<sup>1</sup> and W.U. REIMOLD<sup>2</sup>**

(<sup>1</sup> Department of Geodesy and Photogrammetry,  
Royal Institute of Technology,  
S-100 44 Stockholm, Sweden

<sup>2</sup> Geology Department, University of the Witwatersrand,  
P/Bag 3, WITS 2050, South Africa)

**ECONOMIC GEOLOGY RESEARCH UNIT  
INFORMATION CIRCULAR No. 299**

May, 1996

**INTEGRATED GRAVITY AND MAGNETIC MODELLING OF THE  
VREDEFORT IMPACT STRUCTURE - REINTERPRETATION OF THE  
WITWATERSRAND BASIN AS THE EROSIONAL REMNANT OF AN IMPACT  
BASIN**

**CONTENTS**

	<b>Page</b>
<b>INTRODUCTION</b>	1
Meteorite impact cratering	1
The case of the Vredefort Structure	3
<b>GEOLOGY OF THE VREDEFORT DOME AND ITS ENVIRONS</b>	8
<b>GEOPHYSICAL DATA</b>	14
Gravity and magnetic data	14
Petrophysical data	17
Magnetic susceptibility	17
Density	21
Remanent magnetization	26
Seismic data	28
The 'Background' crustal structure	29
<b>GEOPHYSICAL MODELLING</b>	30
The starting model	31
Modelling of gravity sources	32
Topographic elevation	33
Modelling of magnetic sources	33
<b>RESULTS</b>	34
The gravity model	34
<i>The central uplift</i>	36
<i>The northwest-southeast profile</i>	38
<i>The south-southwest-north-northeast profile</i>	39
The magnetic model	42
<b>DISCUSSION</b>	43
The three stages of impact cratering	43
Reconstructing the Vredefort Crater	46
<i>Restoring the extension of the modified crater (MC)</i>	46
<i>The pre-impact cover thickness</i>	48
<i>Estimation of the extension of shock effects</i>	48
<i>Extent of the plastic deformation regime</i>	49
<i>Estimate of the extent of melt formation</i>	52
<i>Effects of the excavation flow</i>	52
<i>The collapse flow</i>	53
<i>Position of melt bodies after collapse</i>	54

## CONTENTS (continued)

### DISCUSSION (continued)

Comparison with modelling results	54
Characteristic geological features created by the crater-forming sequence of events	57
<i>Shock effects and mass flow</i>	57
<i>Transient crater wall and rim</i>	58
<i>Rim collapse</i>	59
<i>Central rise collapse</i>	60
Remaining effects of the impact event on the crust	62
<i>Post-impact thermal effects</i>	64
<i>Possible occurrences of impact breccias</i>	65
What is missing in the Vredefort Structure?	66
<i>Ejecta</i>	66
<i>Impact melt</i>	66
<i>Injecta</i>	67
<i>The Projectile</i>	67
"Impact tectonics" and metamorphism	68
<i>The crater region</i>	68
<i>The ring basin</i>	68
<i>The central rise</i>	69
SUMMARY AND CONCLUSIONS	70
ACKNOWLEDGEMENTS	73
REFERENCES	74
APPENDIX	83
I. Comparison of measured magnetic properties of central core rocks	83
II. Calculation of flow lines	83
III. Calculation of how to delimit the viscosity factor for modelling of the central rise formation	87
IV. Calculation of impact energy	87
V. Calculation of seismic magnitude	87
VI. Calculation of melt extension from the extension of HEL	87
VII. Calculation of displaced masses	88

\_\_\_\_ oOo \_\_\_\_

Published by the Economic Geology Research Unit  
Department of Geology  
University of the Witwatersrand  
1 Jan Smuts Avenue  
Johannesburg 2001  
South Africa  
ISBN 1 86838 203 6

**INTEGRATED GRAVITY AND MAGNETIC MODELLING OF THE  
VREDEFORT IMPACT STRUCTURE - REINTERPRETATION OF THE  
WITWATERSRAND BASIN AS THE EROSIONAL REMNANT OF AN IMPACT  
BASIN**

**ABSTRACT**

Integrated modelling of gravity and aeromagnetic data, supported by constraints from reflection and refraction seismics, as well as drilling results and petrophysical data, along northwest-southeast and northnortheast-southsouthwest traverses across the Vredefort Dome and the surrounding region resolved that the area of the structurally preserved Witwatersrand Basin represents the eroded remnant of an originally at least 250 kilometer diameter, complex impact structure. The Vredefort Dome constitutes the central uplift terrane of this impact structure, and the surrounding basins attain depths between 6 and 14 kilometres. The remaining structural uplift in the central rise region was modelled to be of the order of 8 kilometres, with a maximum uplift at the base of the crust of about 4 kilometres. It is estimated that some 8 kilometres of upper crust have been eroded since impact times at 2025 Ma ago. The crust-on-edge model for the Vredefort Dome is not supported by the results of this integrated modelling; nor is it likely that upper mantle lithologies could have been transferred into currently surface-near positions.

Based on the results of this modelling exercise, impact scaling and cratering mechanical considerations provide some first-order understanding of the extents of zones dominated by brittle and plastic deformation, as well as that characterised by impact melt formation in the environs of the point of impact. These results allow predictions about the subsurface composition and structure in the ring basin regions surrounding the Vredefort Dome.

\_\_\_\_ oOo \_\_\_\_

# INTEGRATED GRAVITY AND MAGNETIC MODELLING OF THE VREDEFORT IMPACT STRUCTURE - REINTERPRETATION OF THE WITWATERSRAND BASIN AS THE EROSIONAL REMNANT OF AN IMPACT BASIN

## INTRODUCTION

### Meteorite impact cratering

In the course of the last 40 years it has been comprehensively documented that impact cratering has represented the most important surface-forming and -modifying process on all planetary bodies in the Solar System. Detailed remote sensing and chronological studies on lunar and meteorite samples have demonstrated that major impact activity occurred prior to about 3.8 Ga ago throughout the Solar System. Since then, the influx of projectiles onto the terrestrial planets has decreased exponentially. However, the July 1995 impact of large fragments of comet Shoemaker-Levy 9 into the atmosphere of Jupiter has dispelled the myth that impact cratering catastrophes are a threat of the past.

Since the early 1960's, a relatively small number of geologists and planetologists have carried out remarkably comprehensive studies of impact cratering processes and of the terrestrial impact cratering record (e.g., Melosh, 1989). This has led to a rather good conception of the physical and chemical processes involved in large-scale impact cratering and associated rock and mineral deformation, established the criteria for recognition of impact structures, and has shown that terrestrial impact structures can be of significant economic potential (e.g., Grieve and Masaitis, 1994; Reimold, 1995c; Grieve et al., 1996).

At present, the terrestrial impact cratering rate is estimated to have been of the order of  $1.5 \cdot 10^{-14} \text{ km}^2 \text{a}^{-1}$ , for impact craters  $\geq 20$  kilometres in diameter. The cratonic shield areas of the Earth, consisting of crustal rocks older than 2 Ga, have been affected by a substantial number of such large events: on an area of  $10^6 \text{ km}^2$  about 30 such craters would have formed during the last 2 Ga of Earth's evolution. Erosion has levelled most of the smaller craters, but remnants of impact structures in excess of 100 kilometres in diameter would be expected to remain on shield environments for very long times. Contrary to this argument, to date only three very large impact structures have been identified on Earth: the 65 Ma old and about 180 kilometres wide Chicxulub crater structure at the coast of the Yucatán peninsula in Mexico (e.g., Hildebrand et al., 1991), the Sudbury Structure in Ontario of estimated 200-250 kilometres diameter (Deutsch et al., 1995) and 1.85 Ga age, and the Vredefort Structure in South Africa, for which an age of 2.02 Ga (Kamo et al., 1995) has been obtained and which has been estimated to have been 250- $>300$  kilometres in diameter (Theriault et al., 1993, 1995; this work). Two other very large impact structures are suspected to exist in Scandinavia, the about 320 km wide Uppland Structure (Henkel and Lilljequist, 1992), and in South Africa, the Morokweng Structure in the Northern Cape Province (Andreoli et al., 1995; Corner, 1994; Corner et al., 1996). Whereas extensive data on large impact structures have been obtained from remote sensing studies of such features on other planetary bodies, only this small sample of large terrestrial impact structures can provide first-hand and hands-on data crucial for satisfactory knowledge of the impact cratering processes involved in such catastrophic events.

The origin of the Vredefort Structure within the region of the economically important Witwatersrand Basin in South Africa has been controversial for much of this century. While the presence of abundant pseudotachylitic breccias and shatter cones, of coesite and stishovite in association with a few pseudotachylitic veinlets, and of microdeformation features in quartz from Vredefort rocks has been cited as evidence in favour of an impact origin for this structure, a large school of mainly South African geologists favoured, until quite recently, an endogenic origin for the Vredefort Dome (see, for example, review by Reimold, 1993). However, in the past few years new evidence confirmed that the microdeformations in Vredefort quartz indeed represent bona fide impact-diagnostic shock metamorphic effects (Leroux et al., 1994), and Kamo et al. (1995) reported on planar deformation features and granular shock texture in zircon from Vredefort rocks. Furthermore, a detailed Re-Os isotopic study (Koeberl et al., 1996) of the enigmatic Vredefort Granophyre (e.g., Reimold et al., 1990a) proved the presence of a small meteoritic component in this rock type - thereby confirming that the Granophyre represents impact melt rock. This leaves no further doubt as to the origin of the Vredefort Structure by the impact of a large asteroid or comet. Kamo et al. (1995) also reported a  $2025 \pm 4$  Ma U-Pb age determined for zircons grown from a pseudotachylitic melt breccia sampled near the center of the Vredefort Dome. These authors interpret this age as a close approximation of the time of the formation of the Vredefort impact structure. (In the following we will refer to the 'Vredefort Structure' as the whole impact structure, whereas the term 'Vredefort Dome' only refers to the about 45 kilometres wide erosional remnant of the crystalline *core* of the central uplift feature of the Structure and the surrounding *collar* of up- or overturned supracrustals).

Somewhat uncertain is, however, still the original size of the Vredefort impact structure, because of the severe degradation caused by 2 Ga of erosion. Based on the spatial distribution of shock deformation (planar microdeformation, shatter cones), Therriault et al. (1993, 1995) estimated that the structure could have been as large as >300 kilometres, thus encompassing the whole of the Witwatersrand Basin. Several workers have discussed that the Vredefort impact event had a significant effect on the Archaean ore deposits of the basin (e.g., Reimold, 1994; Grieve and Masaitis, 1994; Trieloff et al. 1994; Reimold, 1995c).

The purpose of this geophysical modelling study was to investigate the present distribution of lithologies within the Vredefort Structure, aiming at better defining the most likely original diameter of the structure and to determine the extent to which the Vredefort event may have perturbed the crust of this part of the Kaapvaal Craton. This modelling is, thus, not part of the discussion whether or not there is a Vredefort *impact* structure. As discussed, there is sufficient evidence that a very large impact event occurred at this site at about 2 Ga ago.

Two models for the geological structure in and around the Vredefort Dome have been proposed in the past: *The crust-on-edge model* (Slawson, 1976; Hart et al., 1981) for the cross-section of crustal rocks in the area of the Dome was originally used to present endogenic mechanisms for the formation of the Vredefort Dome. This idea left the surrounding Witwatersrand terrane as ordinary sedimentary basin formations. *The impact model* explains the Vredefort Dome as the central uplift of a large impact structure, but the effects that this event would have had on the whole geological region of central South Africa have not been challenged to date. An impact event causing the formation of a 40-kilometres-wide (at the present level of erosion) crystalline central uplift must have had a profound

effect on a wider region of, at least, 150 kilometres radial extent. The enormous energies imparted on the target region in such an impact catastrophe would have caused seismic and tectonic deformation in addition to the direct impact destruction and, thus, affected all strata in, and probably beyond, this region. Anything left today in this region will have been impact-affected in one way or another. To quantify the extent of such impact deformation will only be possible after thorough multidisciplinary examination of the known, large terrestrial impact structures. A first attempt at such integrated modelling of a large impact structure is reported here.

### The case of the Vredefort Structure

At present, the Vredefort Structure does not resemble the typical complex impact structures encountered in the Solar System (Figure 1): the original impact scar has been levelled by post-impact tectonic modification and 2 Ga tectonic and erosional activity. It may, however, be possible to assess these post-impact processes and their effects, once the approximate original margin of the crater structure, and its extension at depth, has been restored. The prospect to see beyond the time of impact and to unravel pre-impact geological structures within the crater is more difficult and could prove futile. An impact event is so catastrophic that nothing but seriously disturbed lithologies remain. The chaos left by an impact event, although in a new impact-generated order, is almost inconceivable by traditional geological thinking regarding structural, thermal, or geochemical patterns - a phenomenon evidenced by the many and extremely complicated non-impact explanations given for almost all known impact craters before their impact status could be confirmed. The impact-induced geological processes are characterized by extremely high pressures, exceeding by far those experienced in crustal processes. They operate on unusually short time scales of seconds to a few minutes. Table 1 provides an overview of some of the parameters relevant to impact cratering, and Figure 2 indicates the pressure-temperature regime of impact processes as compared to terrestrial metamorphic processes.

Parts of the pre-impact cover sequences may become preserved in the ring depressions of a large impact structure and deeper crustal horizons are brought to surface in the region of the central rise. This implies that large impact structures are the very places where substantial vertical sections of crustal lithologies can be studied, potentially surpassing the sections accessible by deep continental drilling.

To present an impression of such re-organized crust, a photograph of the sedimentary ring around the approximately 60-km-diameter Siljan impact structure, which has an about 20 kilometres wide central core composed of granitoids, is shown in Figure 3. In the limestone quarry (Figure 3A) an approximately 250 metres wide and 30 metres high section displays an array of more or less intensely brecciated blocks. Brecciation (Figure 3B) occurs at all scales from sub-millimetre to over 10 metres. What is more - if the field of view would permit, it could be observed at a kilometre scale as well. On maps, the chaotic mega-block patterns are obscured because of lack of outcrop and because of the cartographer's habit to draw continuous borders between lithologies. At a more detailed mapping scale, the mega-brecciated character of these ring deposits is more evident (Figure 4, after Hische, 1991).

"Ordered chaos" is not the only unique aspect to impact geology. The other one is the enormous speed at which impact deformation occurs. Strain rates at impact deformation have been estimated to be  $10^6$  to  $10^8$  times higher than in normal tectonic events (e.g., Spray,

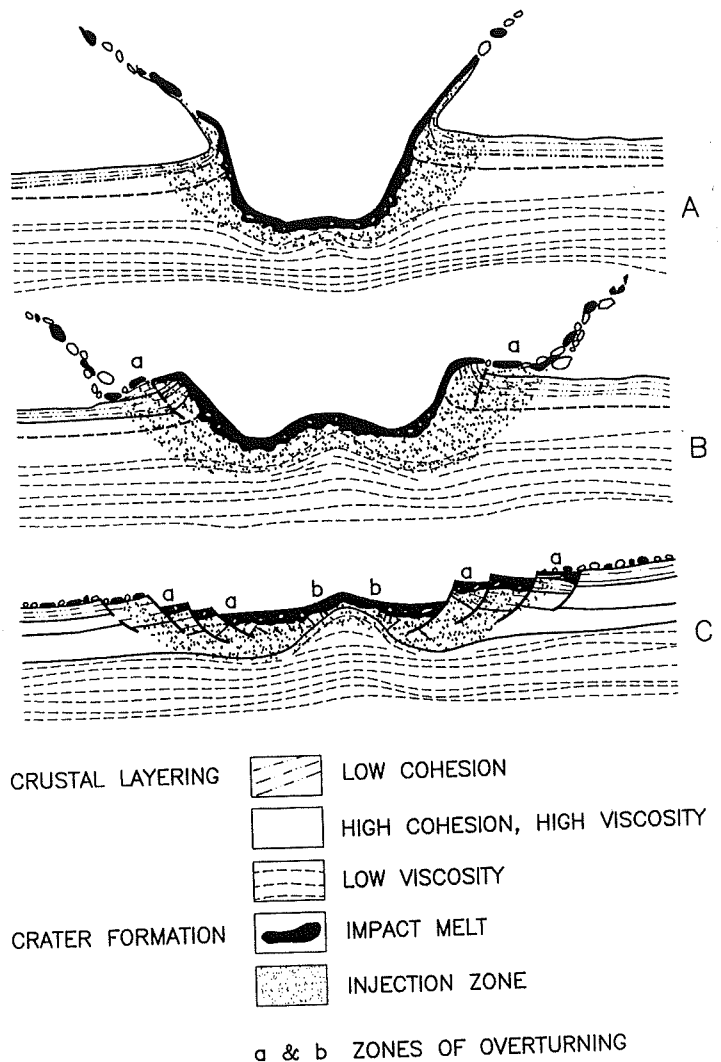


*Figure 1: Evolution of a complex impact structure. The entire structure, even if several 100km in diameter, is formed within a few minutes. Modified after Melosh (1989). Note upturning of the cover sequence along the evolving crater wall and the soon evolving central rise. The final crater consists of 3 major structural units: a collapsed rim, the ring basin, and a central rise. Depending on the amount of erosion, these will be exposed at different levels.*

**Table 1. Aspects of Impact Cratering**

<i>impact stages:</i>	<i>main factors determining:</i>		
	SPATIAL DIMENSIONS	TIME SCALE	PRODUCTS
<b>SHOCK ZONATION</b>	ENERGY OF PROJECTILE	SHOCK WAVE	THERMODYNAMICS OF PROJECTILE AND TARGET
<b>CRATER FORMATION (EXCAVATION, EJECTION + INJECTION)</b>	ENERGY TRANSFERED + RHEOLOGY OF TARGET	RAREFRACTION WAVE	THERMODYNAMICS AND RHEOLOGY OF TARGET
<b>CRATER SHAPE</b>	GRAVITY + RHEOLOGY	GRAVITY	TERRESTRIAL OR MARINE ENVIRONMENT
<b>LATE ADJUSTMENTS</b>	RHEOLOGY	THERMAL DIFFUSION	HYDROTHERMAL ACTIVITY

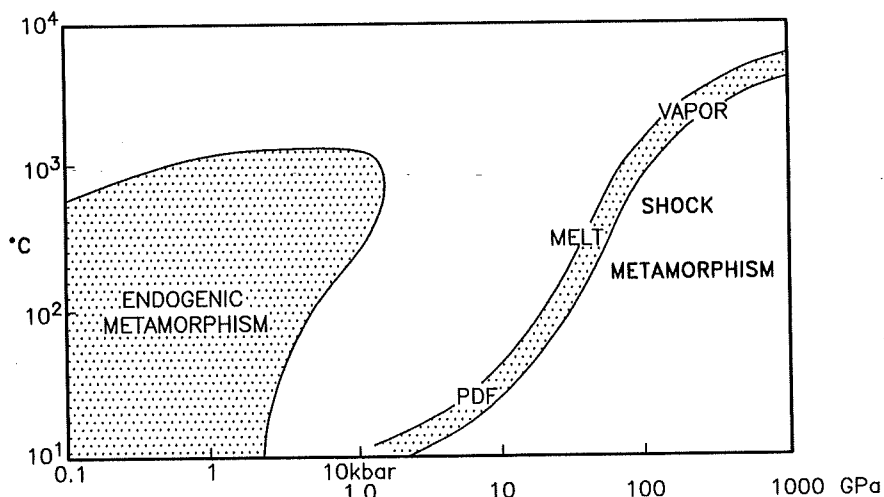


*Figure 2: Pressure-Temperature diagram showing the difference between normal endogenic and impact (shock)-induced metamorphic regimes. For the latter, the extremely high pressures are the most important characteristic.*

1992). An impact crater is formed and collapses within a few minutes. The huge volumes of crustal material comprising a central uplift move over distances of many kilometres within seconds, as does the material of the collapsing transient crater wall (cf. Discussion). Huge amounts of vaporized, melted, and fragmented target material are formed instantaneously and are deposited within a short interval in and around the crater. The details of impact cratering as a geological process were comprehensively reviewed by Melosh (1989). The erosional remnant of the impact melt body and the overlying ejecta deposits formed within the Sudbury Structure, of similar size magnitude as the Vredefort Structure, measures about 60 x 40 km at the surface and is about 4 kilometres thick (Grieve et al., 1990; Deutsch et al., 1995). Similar, possibly larger, volumes of impact melt and ejecta can be expected to have been produced in the Vredefort impact event.

The Sudbury Structure is, like the Vredefort Structure, deeply eroded, but, as the existence of still thick impact lithologies (melt and ejecta) and crater fill sediments demonstrates, not as deeply as the Vredefort Structure. In contrast, the similar-sized Chicxulub Structure, like Vredefort formed in a terrane that consisted of granitoid basement overlain by sedimentary supracrustals, is fully preserved under a thick pile of post-impact sedimentary deposits (e.g., Hildebrand et al., 1991; Sharpton et al., 1993). Thus, comparison of three different erosional sections through large, complex terrestrial impact structures, which may well be of the 'multi-ring basin' type (Spudis, 1994), should provide a multitude of important data for the understanding of impact structures in general.

Exposures within the Vredefort Dome are of such an extent that detailed lithological and structural studies are possible within this central part of the Vredefort impact structure. However, much of the surrounding Witwatersrand basin is covered by post-Vredefort deposits, mainly of the Permo-Jurassic Karoo Supergroup and by alluvium. Obviously geophysical methods are required to obtain detailed information about the non-exposed parts of the wider Vredefort impact structure. It is for this reason that we embarked on an integrated gravity-aeromagnetic modelling exercise, supported, where possible, by drilling and vibroseis information. Previous modelling of geophysical data over the Vredefort-

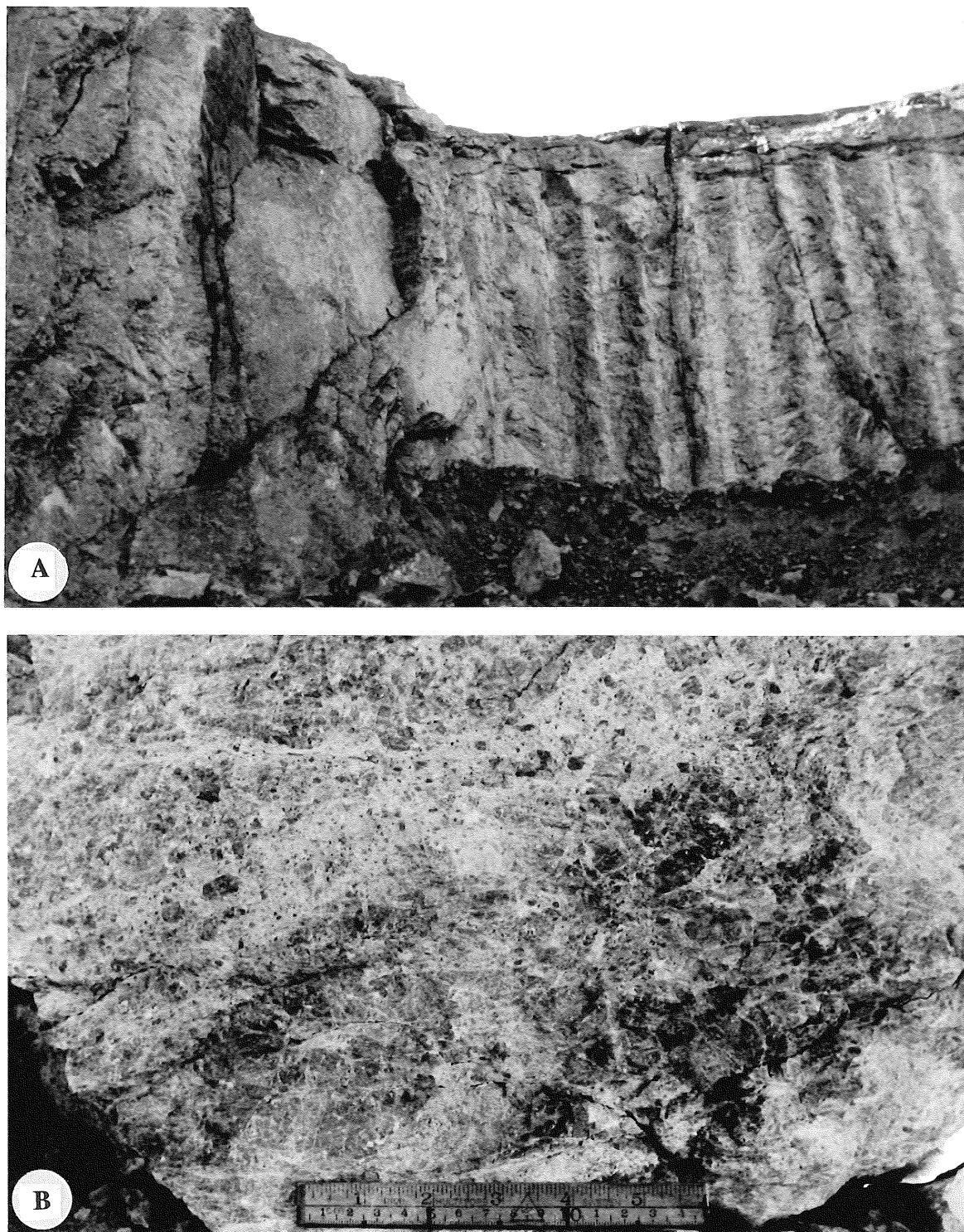


*Figure 3: Part of a limestone quarry in the mega-breccia ring of the 60km Siljan crater. The scarp is about 30m high. A: Large rotated blocks of limestone, 10-50m in size, are surrounded by curved gliding surfaces (black) of different orientations. B: Large rock volumes are finely brecciated, down to sub-mm size, while others appear less distorted with clearly visible layering. Photographs by H. Henkel. Upper scale in inches, lower one in centimetres.*

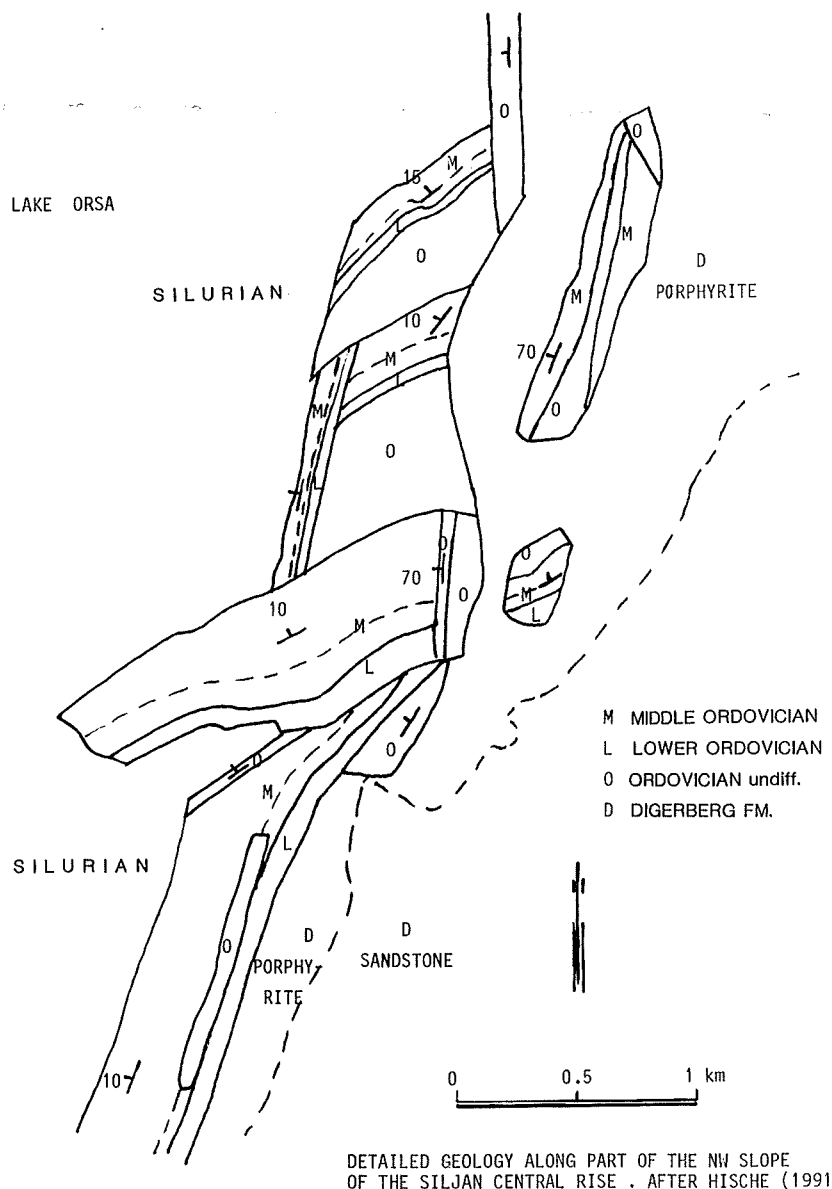


*Figure 4: Map of part of the NW sector of the Siljan crater showing the typical block pattern of the megabreccia ring where it abuts against the crystalline central rise (to the right). Simplified after Hische (1991).*

Witwatersrand region has been reported by Corner and Wilsher (1989), Corner et al. (1990), and Antoine et al. (1990).

The success of any modelling of the Vredefort impact structure not only depends on the quality and accessibility of data, but also on how open-minded the geological community will address the question of re-interpretation of the vast amount of geological and geophysical data existing for the realm of the Witwatersrand Basin. A thorough reinterpretation of the geology of the Basin must have significant effects on the understanding of its ore deposits and their future exploration.

## GEOLOGY OF THE VREDEFORT DOME AND ITS ENVIRONS

The Vredefort Dome is located about 120 kilometres to the southwest of Johannesburg, near the geographical center of what is known as the erosional remnant of the Witwatersrand Basin (Figure 5). This illustration shows the shape of the Witwatersrand Basin as delineated by outcrop or suboutcrop of strata belonging to the about 2.72 to 2.9 Ga old Witwatersrand Supergroup. Locally around the margin of the Basin older rocks belonging to the about 3.074 Ga Dominion Group, comprising felsic metasediments and mafic metavolcanics, or basement granitoids are encountered. Some of these granitoids have been dated at 3.2 to 2.9 Ga, with two distinctive maxima in the age database around 3.2 and 3.075 Ga, respectively. The interior of the Basin is filled with the Witwatersrand, the about 2.7 Ga old Ventersdorp, and the about 2.5 to 2.25 Ga Transvaal Supergroups (Figure 6). The Ventersdorp Supergroup consists to a large extent of mafic, in portions ultramafic, metavolcanics, besides some sedimentary formations. The Transvaal Supergroup is mainly composed of carbonates and siliciclastic rocks, with some intercalated volcanic formations. For a detailed summary of the stratigraphy of the Witwatersrand Triad (Dominion to Ventersdorp) and Transvaal Supergroups, refer to SACS (1980). A comprehensive summary of chronological information for this region can be found in Robb and Meyer (1995) and in Walraven et al. (1990).

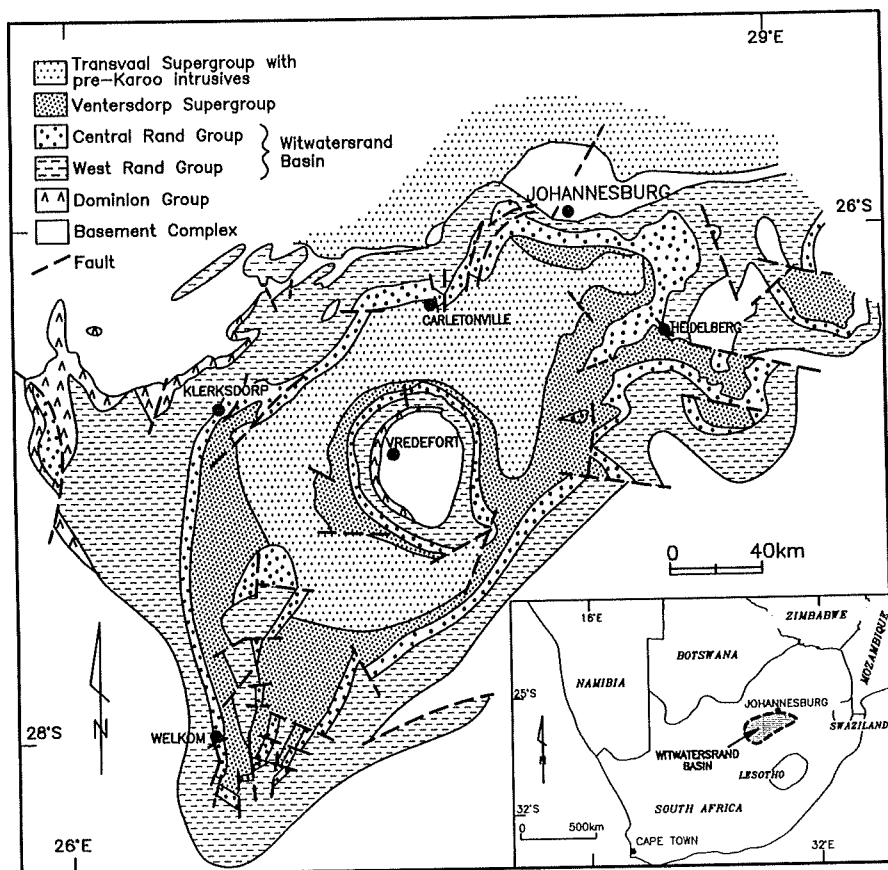


*Figure 5: Schematic geology of the Witwatersrand Basin as defined by the distribution of Witwatersrand Supergroup rocks. Inset: Location in southern Africa.*

Surface geology over the region of the Witwatersrand Basin and surrounding areas is schematically shown in Figure 7 (based on the 1: 1 Million geological map by the Geological Survey of South Africa, 1984). Most obvious is the near-complete cover of the southern part of the study area by Permo-Jurassic Karoo volcanics and sedimentary rocks. Exposures of Archaean crystalline basement are limited to the region of the Vredefort Dome, the Johannesburg Dome in the northeast, several outliers along the northern and western margins of the Witwatersrand Basin, and the Devon Dome to the southeast of the Johannesburg Dome.

The central part of the Witwatersrand Basin contains Archaean to early Proterozoic Witwatersrand, Ventersdorp, and Transvaal strata, all of which are exposed in the form of up- or overturned strata around the Vredefort Dome. The region around the northern part of the Dome, comprising a thick pile of these strata, is known as the Potchefstroom Synclinorium. A schematic stratigraphic column for this region is given as Figure 6. The surface geology over major parts of the Basin is limited to Transvaal and Cenozoic cover rocks. In this context it is significant that the Vredefort Dome represents an overturned (i.e., synformal) basement structure, unlike the other basement domes around the Witwatersrand Basin, which are antiformal structures.

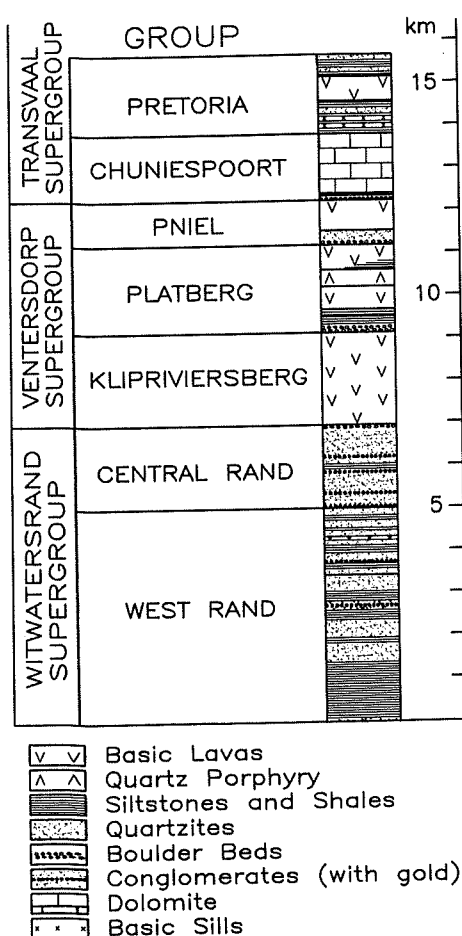


*Figure 6: Schematic stratigraphic column for the Witwatersrand, Ventersdorp, and Transvaal Supergroups in the region of the Witwatersrand Basin (after Fletcher and Reimold, 1989).*

Figure 7 also demonstrates the extension of the two study profiles, along near-perpendicular southwest-northeast and northwest-southeast trends. These traverses were chosen in order to cross the Witwatersrand Basin along its main axes. They intersect at the center of the Vredefort Dome. Figure 5 also indicates where the main gold mining areas are located in the areas around the towns of Welkom, Klerksdorp, Carletonville, and to the south and east of Johannesburg - in relation to the extension of the Witwatersrand Basin and in an annular geometry with respect to the position of the Vredefort Dome.

A schematic geological map of the Vredefort Dome is provided by Figure 8. Generally, the Dome is subdivided into the 40 km diameter *core* consisting of Archaean basement and the surrounding *collar* of up- or even overturned, severely faulted and folded, supracrustals belonging to the Dominion Group and the Witwatersrand, Ventersdorp, and Transvaal Supergroups. The *Dominion Group* in the western part of the Witwatersrand Basin consists of bimodal felsic and mafic metavolcanics, besides some meta-sediments. In the Vredefort area only the metavolcanics (amphibolites) occur with a substantial thickness. The maximum thickness of this unit described from the collar of the Vredefort Dome is about 400 metres (Jackson, 1994). The *Witwatersrand Supergroup* strata, subdivided into the lower West Rand and the upper Central Rand Groups (SACS, 1980), consist to a large extent of quartzitic and shale formations. The *Ventersdorp Supergroup* comprises mainly andesitic meta-lavas, but also some intercalated meta-sediments. The bulk of the *Transvaal Supergroup* consists of carbonates and quartzites, but this interval also encompasses a number of mafic intrusions, for example the Hekpoort Andesite Formation, which is also well-exposed to the north and northwest of the Dome.

The core of the Vredefort Dome is well-exposed in the northern part, but largely covered by Karoo rocks in the south. Besides a few granite gneiss windows, such as the one on the farm Broodkop in the southeastern sector (Colliston and Reimold, 1990), several small exposures of Lower Witwatersrand strata in the east and southeast and a large terrane of Archaean greenstones, the so-called *Greenlands Greenstone Complex* (Minnitt et al., 1994), provide insight into the composition and structure of the crust in this part of the Dome. Preliminary dating results (Reimold et al., 1988a) suggest that this Complex could be as old, or older than, 3.3 Ga. The central part of the core granitoid terrane (Figure 8) consists of rather homogeneous, variably foliated, K-feldspar-quartz rich gneiss termed the *Inlandsee Leucogranofels* (ILG - Stepto, 1990). This terrane is of low-pressure granulite metamorphic grade (e.g., Stevens et al., 1996). Stepto also described a series of felsic to mafic granulites, amphibolites, and charnockitic rocks, as well as high-grade meta-pelites, all of which apparently occur in the form of mega-xenoliths within Inlandsee Leucogranofels. Hart et al. (1981), based on whole rock isotopic studies, suggested that some of these rocks could be older than 3.5 Ga.

In addition to the frequently observed millimeter-sized pockets of granophytic quartz-feldspar intergrowths in ILG, which are thought to be the product of local melting - either due to anatexis or to impact melting, a small body of biotite-granite has been described from the eastern shore of the central Inlandsee pan (Figure 8). Hart et al. (1981) obtained a whole rock Rb-Sr age of  $1.95 \pm 0.06$  Ga for this lithology and considered it a Proterozoic intrusive body. Consequently they termed it the 'Central Intrusive Granite'. A drillcore since obtained from this locality revealed, at depth, gradational contacts between this biotite-granite and ILG, and Hart et al. (1991) suggested that this small body could rather represent the result

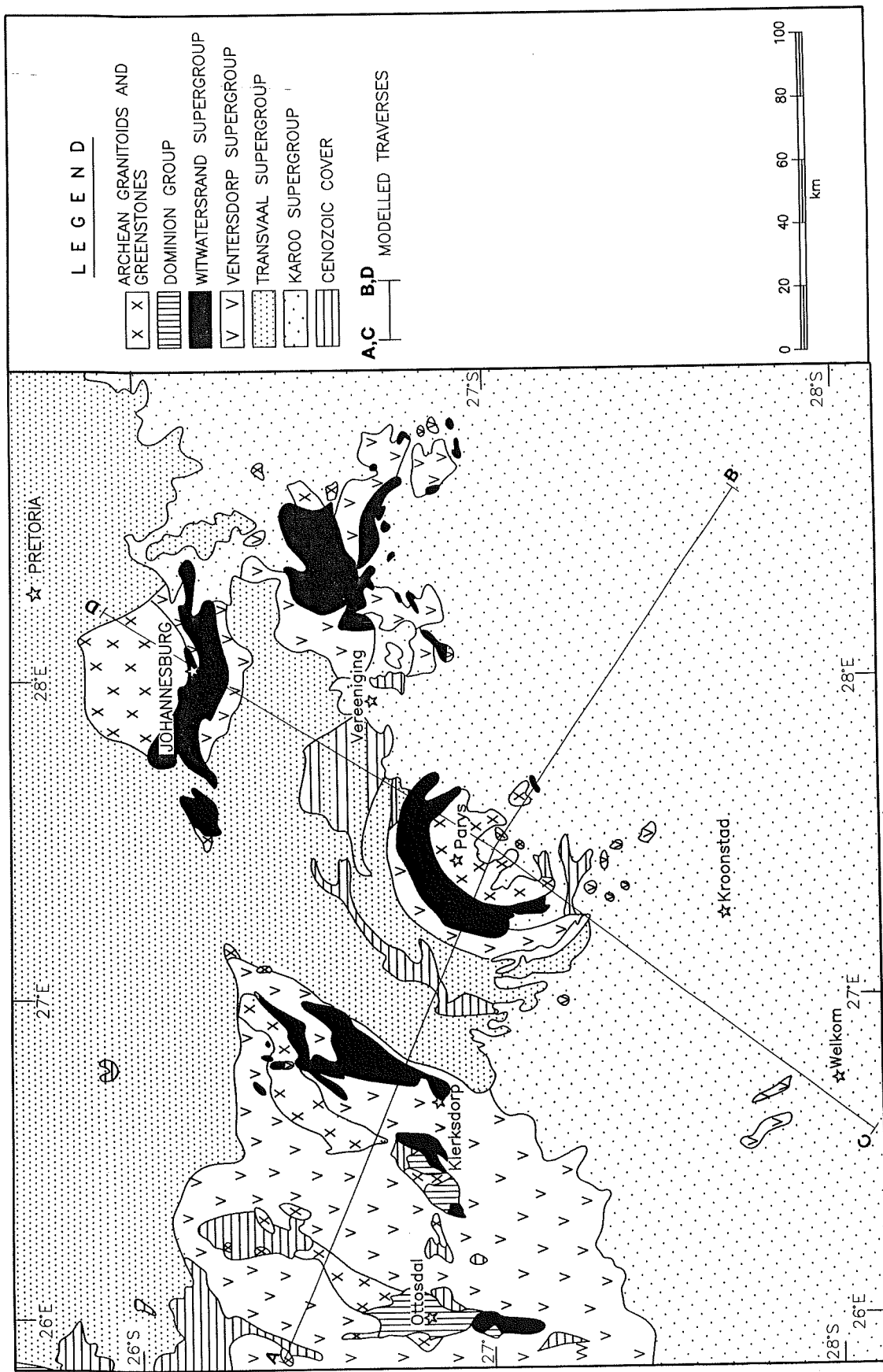


Figure 7: Surface geology in the study region. After the 1:1000 000 geological map of South Africa (Geological Survey of South Africa, Geological Survey of South Africa, 1984). Also shown are the locations of the two profiles along which integrated geophysical modelling was carried out.

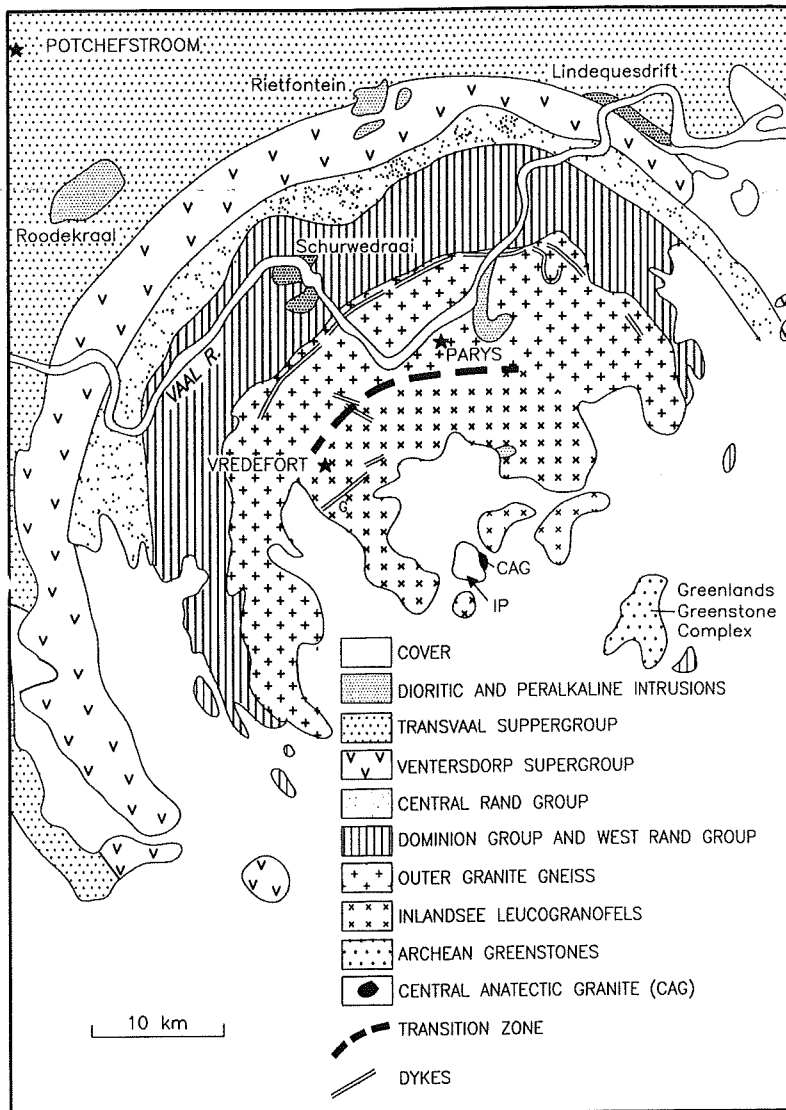


Figure 8: Simplified geological map of the Vredefort Dome. See text for detail.

of partial melting of ILG material and, accordingly, renamed it the '*Central Anatetic Granite*' (Fig. 8). It has been suggested that this lithology could represent impact melt rock or is the result of local anatexis during pre- to syn-impact (regional) high-grade metamorphism.

A small mafic body, the *Winddam wehrlite*, occurs several kilometres to the north of the Inlandsee. Numerous mafic intrusions have been described from the core and the collar of the Dome (e.g., Nel, 1927; Bisschoff, 1969, 1972a,b; Pybus et al., 1995; Pybus, 1996). Pybus, in his comprehensive mineralogical, chemical, and isotopic investigation of these intrusions, determined that the metamorphosed bodies can be confidently related to Ventersdorp magmatism at about 2.7 Ga ago. These Ventersdorp-related so-called *epidiorites* are most abundant in the collar rocks, where they form up to 30% of the stratigraphic thickness of the collar. It also became obvious in Pybus' study that not many Bushveld (2.06 Ga) related intrusions are found within the area of the Vredefort Dome, with the notable exception of the Losberg Complex (Coetze and Kruger, 1989) near Fochville to the north. A number of *gabbroic intrusions*, including the Anna's Rust Sheet, just northeast of the town

of Parys, of distinct chemical and isotopic characteristics were identified and dated at about 1.08 Ga (Pybus et al., 1995).

Hart et al. (1990a) reported on mafic to ultramafic, pyroxenitic and harzburgitic lithologies intersected in a borehole near the center of the Dome. These authors reported chemical and isotopic results that allegedly indicated that these rocks might be of Archaean age and possibly represented upper mantle exposed in the center of the Dome. They cited this evidence as further support of the crust-on-edge model, first invoked by Slawson (1976), which postulates that on a radial traverse, from the outer edge of the Dome towards its center, successively deeper crustal, and possibly upper mantle, rocks, are encountered. However, the composition of these borehole rocks was shown by Moonsamy (1995) to be very similar to chemical compositions of lithologies related to the Bushveld Complex of 2.06 Ga age.

In an annular region of the core, surrounding the ILG terrane, occur heterogeneous, strongly migmatized gneisses, which are collectively known as the *Outer Granite Gneiss* (OGG) (Stepto, 1990). These granitic-granodioritic gneisses are of lower metamorphic grade than the ILG and attained only amphibolite facies grade. As only the inner collar rocks have amphibolite metamorphic grade, whereas further outwards a sharp transition into greenschist facies is reached, this metamorphic succession has also been considered as support for the crust-on-edge model. However, this model has not been supported yet by detailed structural data from the gneissic terrane (e.g., Reimold and Colliston, 1994; Minnitt et al., 1994).

According to Hart et al. (1990b), the OGG and ILG terranes are separated by the so-called *Transition Zone* (Figure 8), which is characterized by an abundance of pseudotachylitic breccia, mafic intrusions, and charnockitic rocks. These authors proposed that within this zone a major intracrustal discontinuity, the so-called *Vredefort Discontinuity*, occurred, along which the upper crustal OGG and supposed lower crustal ILG had been juxtaposed. The approximate position of this inferred Transition Zone is shown in Figure 8. Again it must be emphasized that this Zone has, to date, not been mapped in detail. Some workers favour a gradational transition from OGG to ILG.

For a long time it was thought that the OGG gneisses were formed at 3.08 Ga ago (Hart et al., 1981). However, recent Argon chronological studies (e.g., Reimold et al., 1995a,b) and U-Pb zircon dating (Kamo et al., 1995) indicated that both the ILG and OGG gneisses were formed between 3.1 and 3.3 Ga ago and experienced a first metamorphic overprint at about 3.08 Ga.

Other intrusions into the collar include *alkali granitic complexes* (Schurwedraai, Rietfontein, Lindequesdrift) with associated mafic to ultramafic rocks (Bisschoff, 1973). A chronological study of the Schurwedraai alkali granite and nepheline syenite complex (Figure 8) suggested an age of 2.15 to 2.2 Ga for this suite (Walraven and Elsenbroek, 1991).

With the exception of the Anna's Rust Sheet-related gabbros, the Winddam wehrellite, and the Central Anatetic Granite, all other lithologies in the area of the Dome were subjected to strong macro- and microdeformation, for example in the form of brecciation (the Vredefort Dome is the type locality for pseudotachylite - Shand, 1916; however, different types of breccias, clastic and melt breccias, have been collectively termed Vredefort

'pseudotachylite', so that here the term 'pseudotachylitic' breccia is preferred; cf. Reimold, 1995a), shatter coning, or planar microdeformation in quartz.

*Pseudotachylitic breccias* are particularly abundant in two annular zones within the core (Fletcher and Reimold, 1989). One occurs along the inside of the core-collar boundary and is less than 2 kilometres wide. A much wider zone follows the so-called Transition Zone between OGG and ILG in the northern and northwestern parts of the core. However, whereas Hart et al. (1990b) postulated a semi-annular shape of the Transition Zone, the breccia-rich zone appears to be extended in northeast-southwesterly direction and was interpreted as a linear, northeast-southwest trending décollement by Fletcher and Reimold (1989).

In the core and along the core-collar boundary occur exposures of a suite of dykes of a breccia type, which superficially closely resemble the pseudotachylitic breccias. This material is characterized by a unique and regionally extraordinarily homogeneous composition (e.g., French et al., 1989; Reimold et al., 1990a; Therriault, 1992). Because of the large proportion of micropegmatitic (granophytic) matrix, this rock type is known as the *Vredefort Granophyre*. It has long been suspected that these dykes represented remnants of the Vredefort impact melt, but because of the complete absence of shock metamorphic effects in clasts within the Granophyre, no unequivocal evidence supporting this suggestion could be forwarded. Recently, however, a Re-Os isotopic study of Granophyre and major Vredefort country rock types by Koeberl et al. (1996) provided the proof that a small meteoritic component, relic of the meteoritic projectile, is mixed into the crustal melt that constitutes the Granophyre. The Granophyre was finally confirmed as impact melt rock. It is thought that these dykes formed by gravitational settling of impact melt into fractures in the crater floor below a now eroded impact melt body (Therriault, 1992; Therriault et al., 1993, 1996).

Overall, the Vredefort Dome does not show complete symmetry. Whereas the collar rocks are up- or overturned in the western and northern sectors, drilling information has revealed that the southeastern equivalent is characterised by shallow dips not exceeding about 45° and, where it was possible to establish dip orientations, dipping south-eastwards. It has been speculated in the past (Reimold and Wallmach, 1991) that this asymmetry could be the result of an oblique impact, of northwards tilting of the Dome and subsequent differential erosion, or of post-impact tectonic modification, such as the northwest-directed Kibaran thrust tectonics proposed by Friese et al. (1995).

## GEOPHYSICAL DATA

A large number of good geophysical data sets are available for the Vredefort area. These include refraction and reflection seismic (Durrheim et al., 1991, Durrheim and Green, 1992), gravity, and magnetic data, as well as compilations of petrophysical data (Smit and Maree, 1966).

### Gravity and magnetic data

Gravity and magnetic data from two approximately 300 kilometres long profiles shown in Figure 7 were analyzed. The data source was the data base of the Department of Geophysics, University of the Witwatersrand, which mainly comprised open-file data generated by the Geological Survey of South Africa. The average station spacing for gravity

measurements is about 1 to 5 kilometres. These data were converted into a grid with 1 kilometre spacings, from which data points were interpolated along the profiles at 1 kilometre intervals.

The magnetic data were originally measured as total intensities of the geomagnetic field along 1 kilometre spaced flightlines at 120 metres altitude. A grid with 0.75 kilometre spacings was generated, from which data points were interpolated along the two profiles at 1 kilometre intervals. Extremely low values of the magnetic field were truncated. The gridding and interpolation of the potential field profiles were carried out by Dr. Luc Antoine of the Department of Geophysics at Wits.

The locations of gravity and magnetic data points along the profiles are identical. Maps of the magnetic field and of the gravity of the whole region of the Witwatersrand Basin were used for assessment of regional source structures, their orientations, and extensions. These maps (Figures 9 and 10) were made available by the Geology Division of Gold Fields of South Africa (Pty.) Limited.

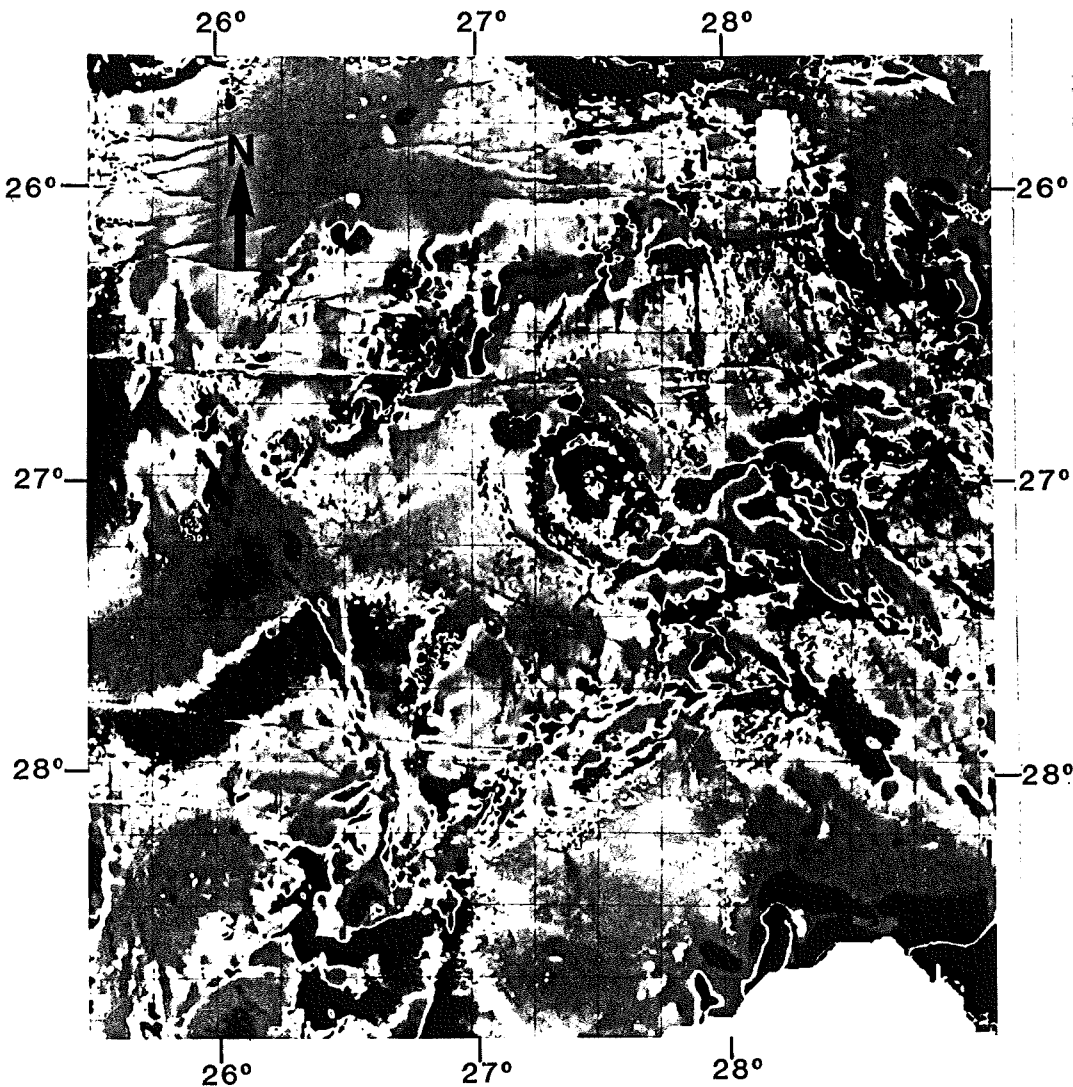


Figure 9: Aeromagnetic map of the region of the Witwatersrand Basin and surrounding areas. After Corner et al. (1990).

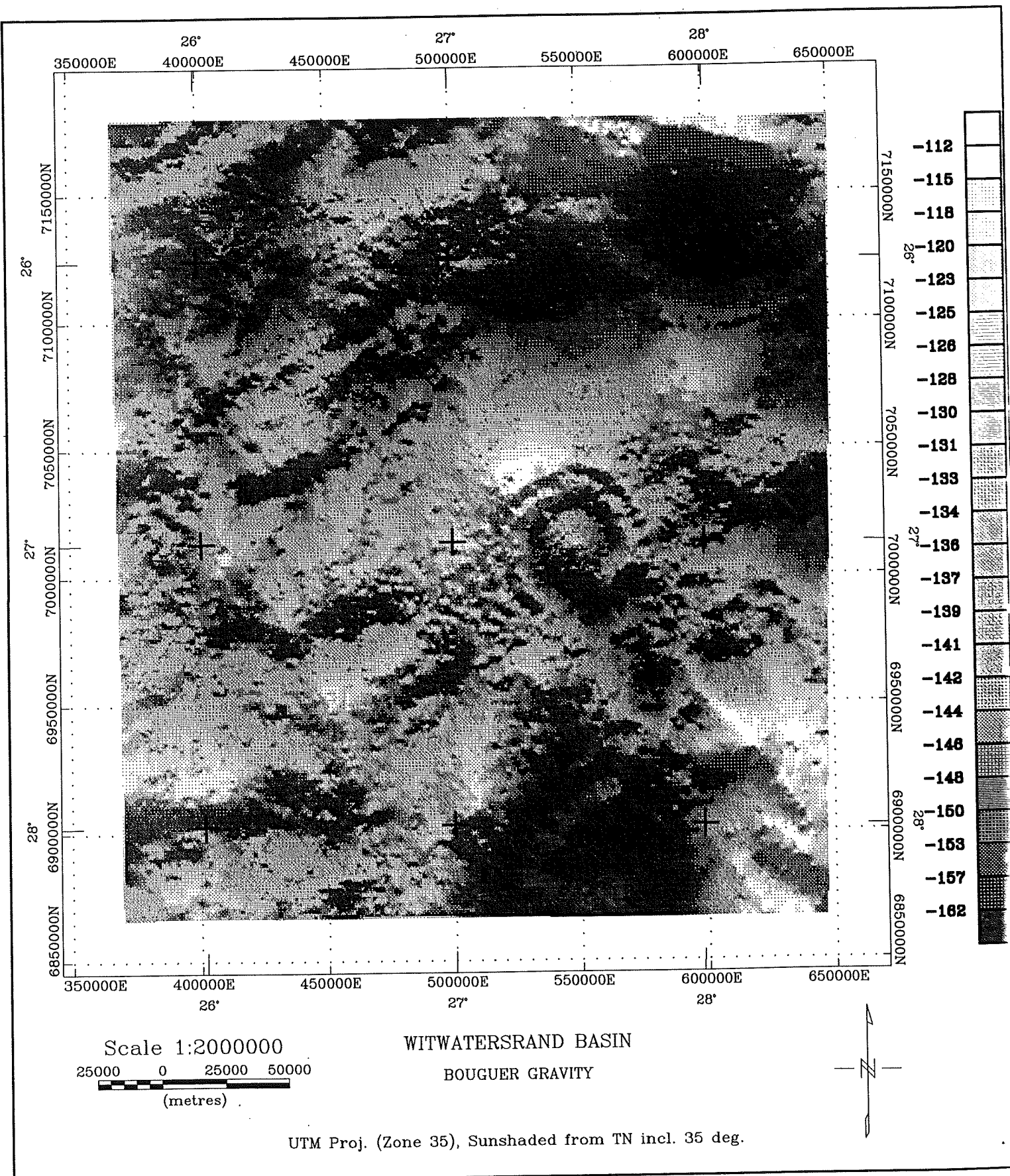


Figure 10: Gravity (Bouguer anomalies) map of the Witwatersrand region. Courtesy of Geology Division, Gold Fields of South Africa (Pty) Limited.

## Petrophysical data

A general review of crystalline rock densities and magnetizations for a large variety of shield rocks was given by Henkel (1991) and is shown in Figures 11A and B. These rocks typically display higher densities where compositions change from felsic to mafic. There are lower limits of density and magnetic susceptibility values, respectively. With regard to their magnetic properties, the rocks are generally bimodal, with a population of low paramagnetic characteristics and another of higher ferrimagnetic properties. The rocks of this latter group also define the upper limit of susceptibility of terrestrial rocks. The complex magnetic behaviour is related to the mineralogical compositions of the rocks. Iron-containing silicates are generally paramagnetic, whereas some oxides and sulphides of iron may have ferrimagnetic properties (Figure 11B; cf. also Henkel, 1994). It should be noted that the highest remanent magnetizations are related to ferrimagnetic pyrrhotite, leading to q-ratios (the ratio between remanent and induced magnetizations) as high as 200. Pronounced remanence is, however, an unusual property for cratonic rocks, as demonstrated in Figure 11C, where the average q-value is about 0.2 and, accordingly, induced magnetization is the normal situation.

Data on physical properties of rocks from the Vredefort Structure and its surroundings were compiled mainly from existing sources (Smit and Maree, 1966; Stepto, 1979; Jackson, 1982). A few additional measurements were made of densities and magnetic susceptibilities of lithologies that were not yet represented in the existing data bases and for calibration purposes. However, the regional coverage with petrophysical data is still incomplete for parts of the sedimentary supracrustal sequences and almost completely lacking for crystalline rocks occurring along the margins of the Witwatersrand Basin. The available data for major lithologies have been compiled as histograms (Figures 12 and 13) and are summarized in Tables 2 - 6. From these data average properties for specific rock formations were calculated. Measurements of natural remanent magnetizations are largely confined to lithologies from the crystalline core of the Vredefort Dome.

## Magnetic susceptibility

For a number of lithologies from the central core region, magnetic susceptibility data were reported by Jackson (1982). These values have also been applied by Hart et al. (1995). In the collar, magnetic rocks are either mafic intrusives (which were shown by Pybus (1996) to be in their majority related to the Ventersdorp Supergroup) or magnetic shale layers, whereas quartzitic and dolomitic horizons generally have low magnetic characteristics. We were able to measure magnetic susceptibilities for some critical lithologies, for which average values are listed in Table 5.

Granitoid rocks from the core terrane have type values, according to Jackson (1982), of  $5 \cdot 10^{-3}$  and  $2 \cdot 10^{-2}$  SI, for OGG and ILG rocks, respectively. These values match our own in situ results (Figure 12A) very well. For OGG rocks typical values around  $3 \cdot 10^{-3}$  SI and for ILG rocks values around  $8 \cdot 10^{-3}$  SI were obtained. Charnockitic rocks, for which a number of measurements were obtained within the so-called Transition Zone, typically have much higher values around  $2.5 \cdot 10^{-2}$  SI. Values for intrusive rocks from the central core region are also listed in Table 6.

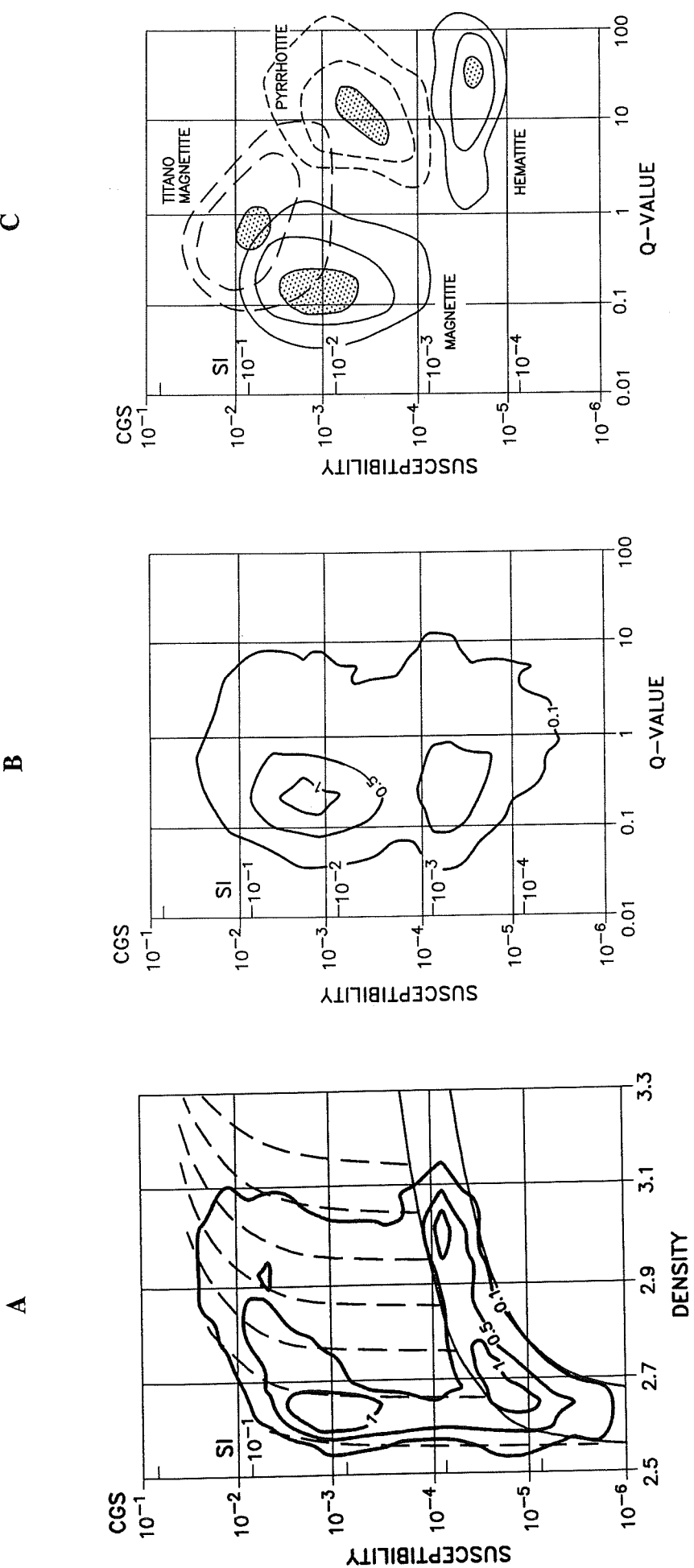


Figure 11: Typical rock physical properties for crystalline shield rocks of the Baltic Shield (from Henkel, 1991). A: Density and magnetic susceptibility; B: Magnetic susceptibility and  $q$ -value (ratio of remanent to induced magnetization) for rocks with different magnetic carrier minerals (data from Henkel, 1994); C: Magnetic susceptibility and  $q$ -value; note low (on average 0.2)  $q$ -values implying that induced magnetization is dominant.

**Table 2. Petrophysical Data for the Background Model and Characteristics of Important Stratigraphic Packages.**

Unit		Density, Mgm <sup>-3</sup>	P-wave velocity, kms <sup>-1</sup>
Upper crust	granitic	2.65	
	granodioritic	2.70	6.0
	dioritic	2.77	6.3
Lower crust		2.98	6.7
Eclogitic layer		3.30	7.5
Upper mantle		3.32	8.2
Karoo Supergroup		2.608	
Transvaal, all basins		2.830	
Ventersdorp, NW and NE basin		2.800	
“	SW basin	2.780	
“	SE “	2.980	
Witwatersrand, NW, SW, and NE basin		2.700	
“	SE basin	2.720	

**Table 3. Petrophysical Properties of Core Formations (measurement sites shown in Figures 40B and C).**

Rock Type	Density, Mgm <sup>-3</sup>		Magnetic Susceptibility, SI 10-5		
	No.	Data	Type	Value	Site
Granitoids	71	2.621			
OGG			48	H14,H21,H22	300
ILG			93	H15-20	800
Granophyre	7	2.787	25	E6	1000
Alkali granite			5	E1	40
Amphibolite facies gneiss			10	E2	250
Granulite facies gneiss			18	E3	1000
Mafic granulite			7	E3	350
Charnockite			36	E4, H23	2500
Anna's Rust Sheet			11	H6	2900

**Table 4. Petrophysical Properties of Basin Formations (measurement sites shown in Figures 40B and C).**

Rock Type	Density, Mgm <sup>-3</sup>		Magnetic Susceptibility, SI 10 <sup>-5</sup>		Type Value
	No.	Data	No.	Data	
Intermed. volcanics	6	2.82	46	H1,H5-7,H12	100
Mafic volcanics	3	3.068			
Low-magn. quartzites and shales			42	E7,H2-4,H10	30
Magnetic shales	20	3.0	89	E5	10000
Quartzites (Rt)	58	2.712			
Cherts	16	2.644			
Dolomites	36	2.866			
Quartzites (Rj,Rg,Rh)	25	2.59			

**Table 5. Results of Control Measurements  
of Densities.**

Rock Type	No.	Data	Density, Mgm <sup>-3</sup>
ILG	2		2.599
OGG	4		2.659
Quartzites	5		2.60

**Table 6. Control Measurements of Magnetic Susceptibilities of Core Granitoids.**

<i>Data by</i>	<i>No. Data</i>	<i>Magn. Susceptib. SI 10<sup>-5</sup></i>
Henkel	75	500 to 3000
Hart	45	600
Jackson	16	1000

A detailed susceptibility profile was measured across the so-called type section for the Vredefort Discontinuity along the Schulpspruit stream bed (Hart et al., 1990b; 1991), the alleged boundary between amphibolite and granulite terranes of the central core. Figure 12E displays the measured data together with the resulting distribution. The amphibolite facies rocks have a type value of  $5 \cdot 10^{-3}$  SI, whereas the granulite facies rocks have a type value of  $3 \cdot 10^{-2}$  SI, which is very similar to the value reported by Jackson (1982). Clearly, amphibolite and granulite facies rocks vary continuously over a short interval (ca. 3 kilometers), which is more consistent with a gradational than a sharp contact between OGG- and ILG-type lithologies.

### Density

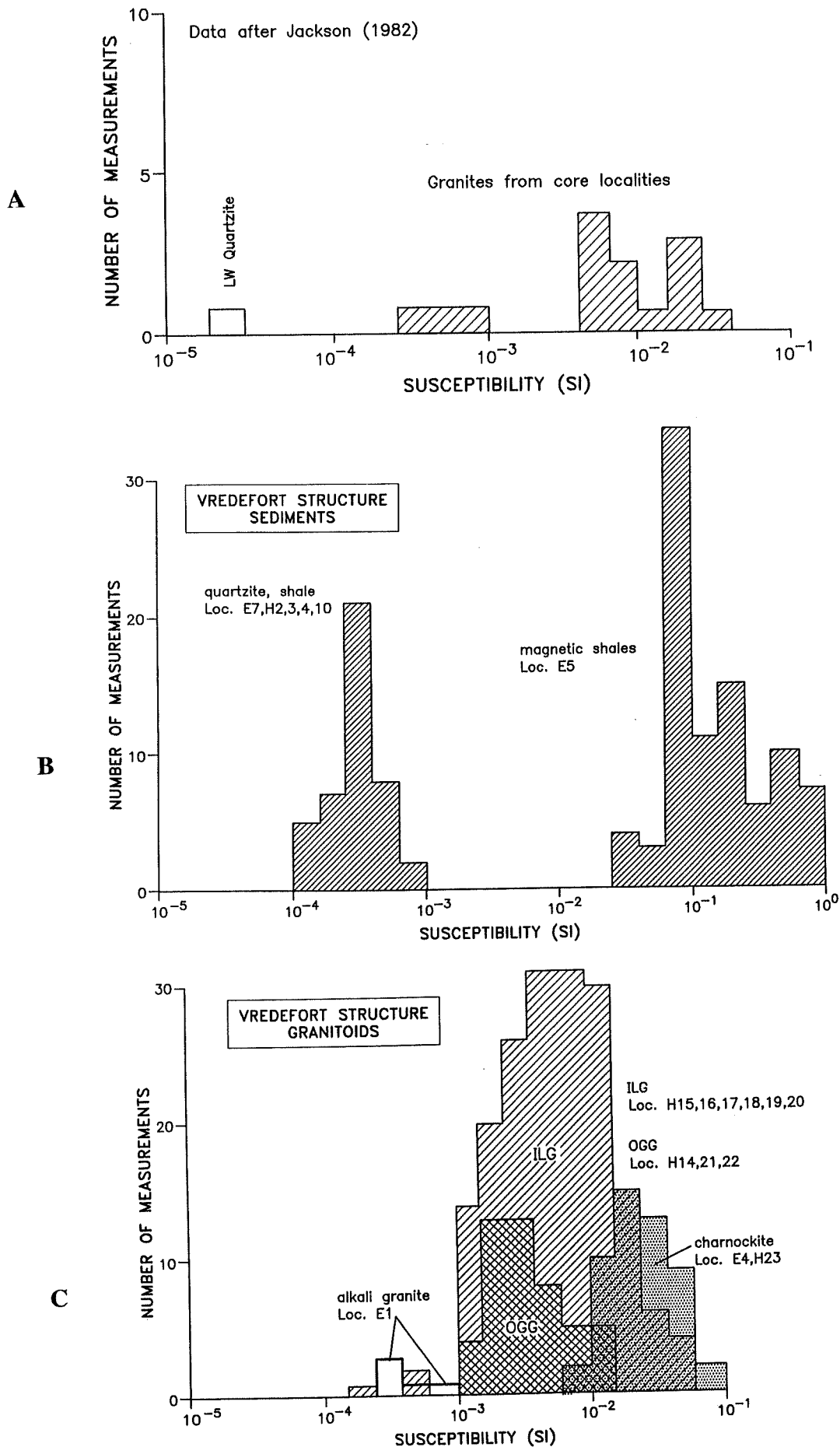
Stepto (1979) presented density values for the granitoid rocks of the central core terrane of the Vredefort Dome. The dominantly granitic lithologies have a rather uniform density distribution (Figure 13F), with a rather low characteristic value of  $2.61 \text{ Mgm}^{-3}$  (average value:  $2.621 \text{ Mgm}^{-3}$ ). Testing whether there is a typical difference between densities of OGG and ILG specimens revealed that ILG data fall into the lower part of this distribution (approximately around  $2.599 \text{ Mgm}^{-3}$ ) and that densities of OGG samples plot into the higher part (approximately around  $2.659 \text{ Mgm}^{-3}$ ). Densities for less abundant lithologies in the core region are listed in Table 3.

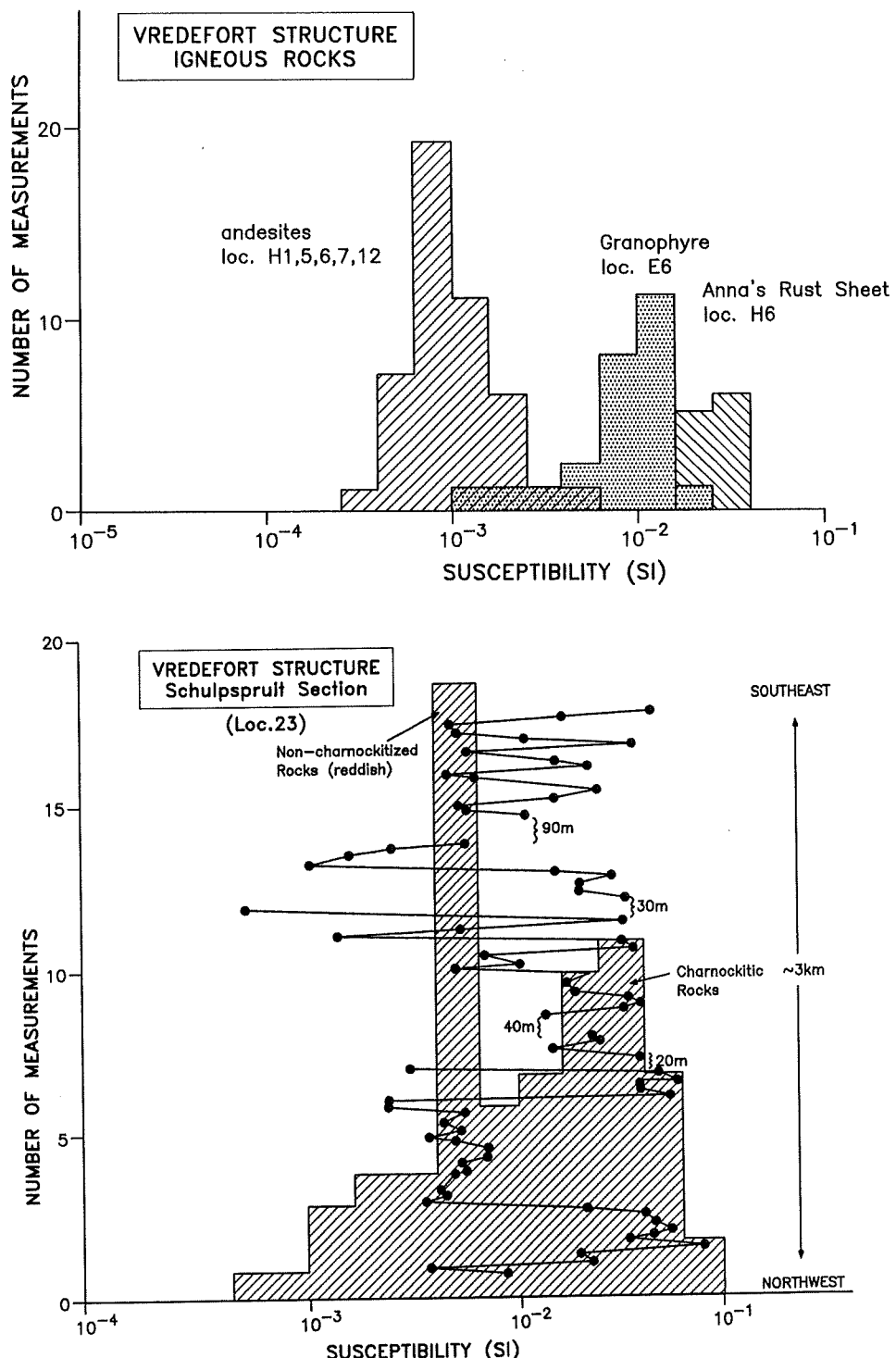
Densities of lithologies from the collar surrounding the crystalline core region are part of a national petrophysical data base (Smit and Maree, 1966). These data are listed as average values, also giving the numbers of measurements and the range of individual values per stratigraphic unit analysed. Data compilations (Figure 13A-E) were made from this source for the major lithologies - quartzite, dolomite, shale, chert, and Ventersdorp extrusives. Weighted averages for these lithologies are compiled in Table 4. Control measurements carried out by us on collar rocks provided the results of Table 5.

The Karoo cover rocks in the Vredefort region mainly consist of sediments (shale, sandstone) and mafic (dolerite) sills. Average densities for these rock types are  $2.52$  (Smit and Maree, 1966) and  $2.962$  (Stepto, 1979)  $\text{Mgm}^{-3}$ , respectively.

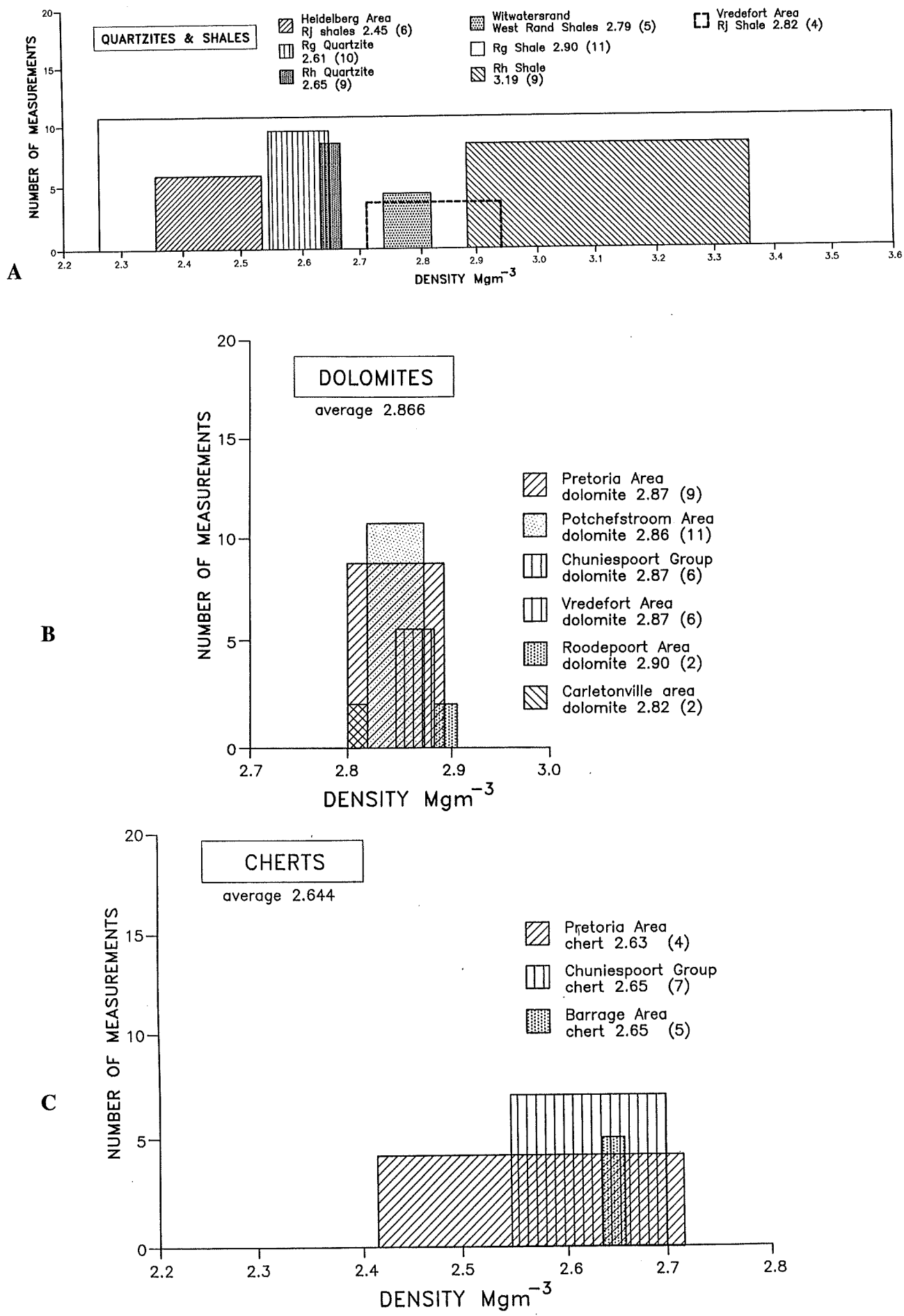
Average densities were then calculated for stratigraphic packages (namely the Witwatersrand, Ventersdorp, and Transvaal Supergroups) occurring in each quadrant of the Witwatersrand Basin traversed by the two profiles. These calculations were performed on the basis of available data regarding stratigraphic rock type variations and thicknesses, as constrained by drilling information obtained from various industry sources or estimated from stratigraphic sources, such as SACS (1980) or P. Fletcher (pers. commun., 1995).

For the Karoo cover in this region an average amount of 20% dolerite was adopted, which resulted in a combined average of  $2.608 \text{ Mgm}^{-3}$ . An average density of  $2.735 \text{ Mgm}^{-3}$  was assigned to the Witwatersrand Supergroup. For the Ventersdorp Supergroup average values of  $2.78 - 2.80 \text{ Mgm}^{-3}$  (specific for different basins) were calculated, and for the Transvaal Supergroup a value of  $2.83 \text{ Mgm}^{-3}$  was adopted.





*Figure 12: Magnetic susceptibilities of rocks from the Vredefort Structure. A: Rocks of the crystalline core (after Jackson, 1982); B: Sedimentary rocks; C: Granitoids of the core region; D: Other igneous rocks; E: Measurements carried out every 5m along a profile across the so-called Vredefort Discontinuity; the resulting histogram indicates two distributions of data which can be related to the different metamorphic grades of the studied rocks (cf. text); there is, however, no indication for a spatial trend between these distributions.*



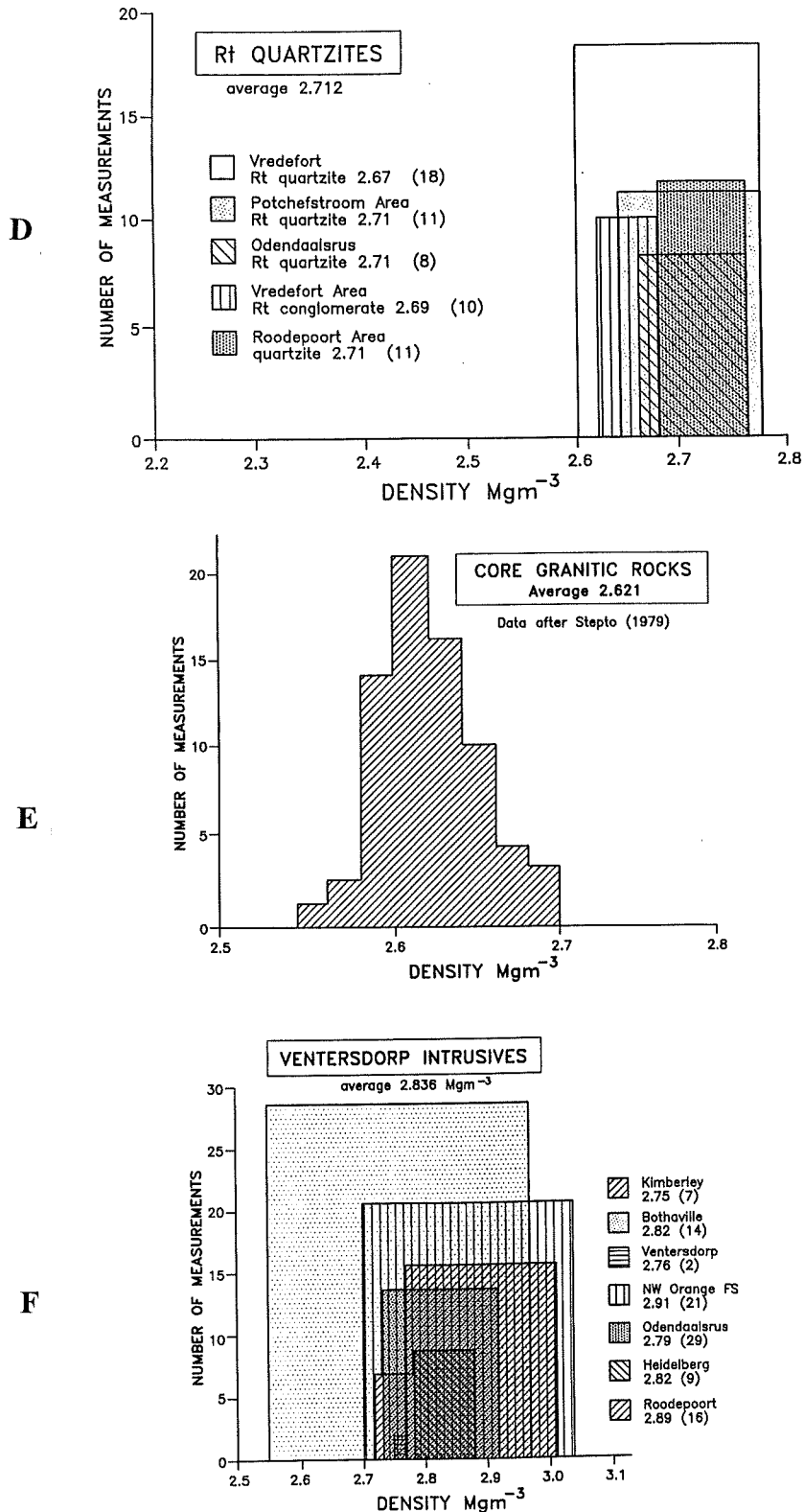


*Figure 13: Density data for some typical lithologies from the Vredefort Structure (data after Smit and Maree, 1966). Note that the diagrams show range and number of measurements for each rock type - they are, thus, not pure histograms. A: Data for quartzites and shales; B: for dolomites; C: for cherts; D: for Rt quartzites; E: data for granitoids from the core and granophyre (data after Stepto, 1979); F: data for Ventersdorp intrusives.*

### Remanent magnetization

The report by Jackson (1982) contains detailed information of remanent magnetizations at 18 sampling sites in the central core region. The cleaned (in a standard demagnetizing field) vectors appear to fall along a great circle (Figure 14) between the type remanence (declination 25°, inclination 56°) and the viscous remanence parallel to the present field (declination -20°, inclination -60°). Jackson assumed that this remanence also occurs in the magnetic shales and presented a set of model calculations that verified this assumption.

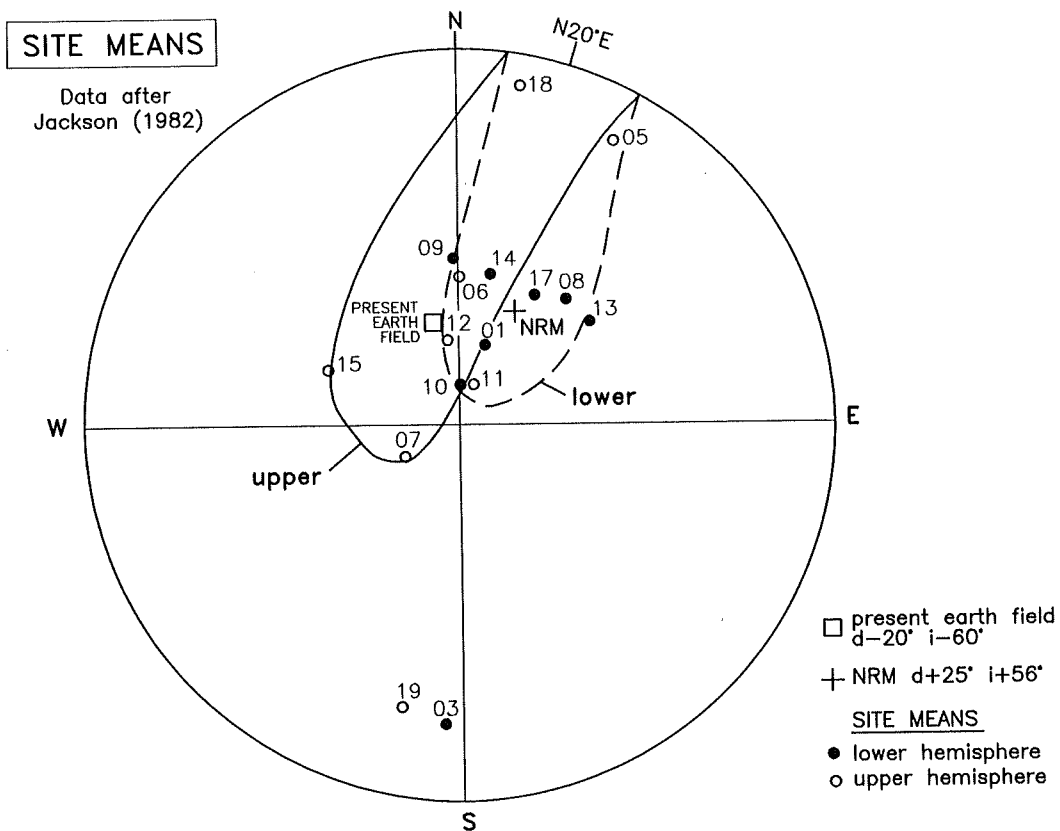
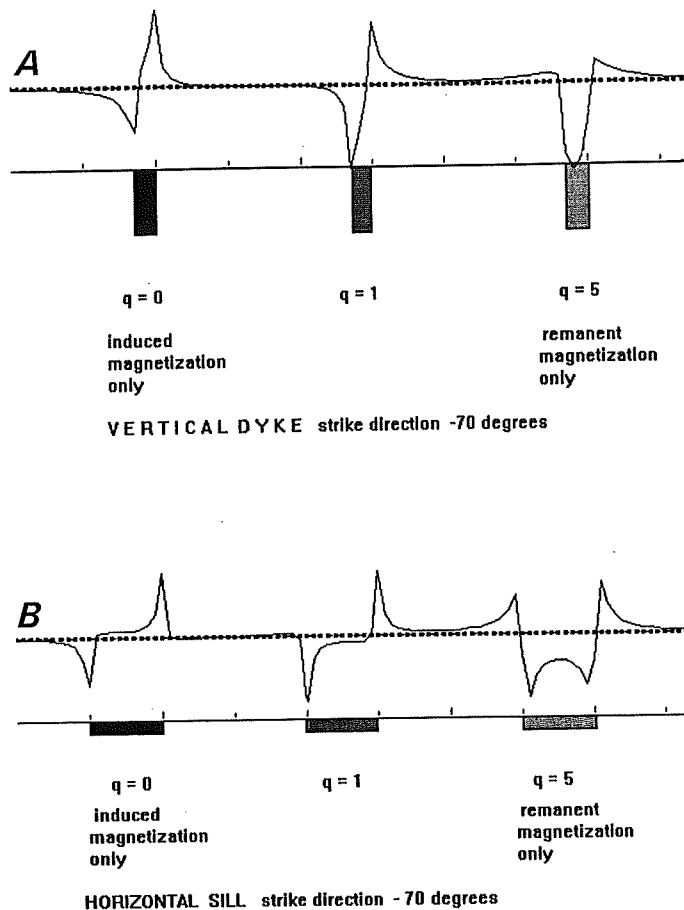


Figure 14: Natural remanent magnetization of rocks from the core region. Measurements from Jackson (1982). The diagram shows both remanences close to the present geomagnetic field and remanences with positive inclination obtained in a reversed geomagnetic field.

The total field magnetic anomalies generally reflect the effect of the volume, orientation, and total magnetization of the source structures. The total magnetization may contain variable amounts of remanence, as reflected in the q-ratios of the rocks. In Figure 15A a set of models are shown that illustrate the effect of two types of sources (sills and dykes, respectively). As the two magnetizations involved occur in different quadrants in the plane of magnetization, very different anomaly shapes will result, when the amount of remanence is varied (Figure 15B). The ability to keep a high amount of remanence is an effect of the amount of highly coercive minerals, usually of the ferrimagnetic type, of small grain sizes that occur in the rock. Minerals that typically show this effect are titanomagnetite,



*Figure 15: A: Two geometrically different structures (a dyke and a sill) were given induced and remanent magnetizations to illustrate the resulting complexity of the magnetic anomaly. B: Total magnetization vectors as seen in the NW-SE plane of modelling, showing a strong effect from variable  $q$ -values. This complexity is different in the SSE-NNW modelling plane.*

in mafic lithologies where exsolution lamellae of ilmenite subdivide magnetite grains, or very fine-grained magnetite precipitates formed by metamorphic processes such as the prograde transition to granulite facies. In the mineralogical study across the alleged Vredefort Discontinuity reported by Hart et al. (1991), fine-grained magnetite (often decorating planar microdeformations in quartz) was reported to occur along the entire traverse studied. The modelling by Jackson (1982) indicated, however, that the obtained remanence intensities were a factor 10 too high to provide an acceptable fit to measured magnetic anomalies. The extremely high  $q$ -ratios cited by Hart et al. (1995) are very unlikely and seem to be the result of calibration problems of the remanence measurements, as already suspected by Jackson (1982) [cf. further discussion in Appendix I]. See also the diagram of typical  $q$ -values of rocks with various magnetic carrier minerals (Figure 11B). The locations of new petrophysical measurement sites are shown in Figure 16.

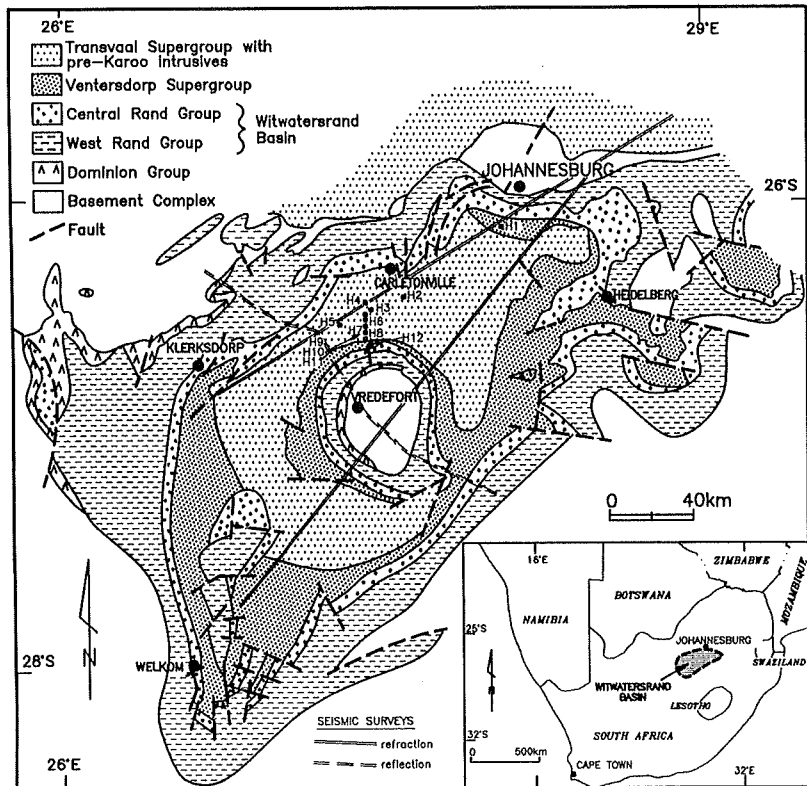


*Figure 16: Geology of the Witwatersrand Basin with localities where samples for density measurements were collected and susceptibility measurements were performed. Also shown are the two refraction seismic profiles discussed by Durrheim and Green (1992) and the reflection seismic profile interpreted by Durrheim et al. (1991).*

### Seismic data

Two sets of seismic data relevant to this study were available. First, the work by Green and Chetty (1990), who reported results of refraction seismic experiments from the area of the Vredefort Dome. Second, refraction seismic data were collected along two 250 kilometres long traverses (Figure 16) extending southwest-northeast across the Vredefort Structure (Durrheim and Green, 1992). From these data a general seismic velocity-depth profile for the Kaapvaal Craton was constructed. This profile is generally similar to profiles for other shield regions and, therefore, the general sequence of shield crustal layering established for the Baltic shield by the combined modelling of the FENNOLORA refraction seismic transect by Henkel et al. (1990) was used together with the velocity characteristics of the Kaapvaal craton. The seismic p-wave velocities obtained from a refraction seismic model can be transformed into densities via the empirical relation after Henkel et al. (1990), which is shown in Figure 17.

A single reflection seismic survey along a 200 kilometres profile across the northwestern part of the Witwatersrand Basin and the Vredefort Dome was carried out by the Geological Survey of South Africa. Some of these results were published by Durrheim et al. (1991). A second profile across the southeastern sector of the Dome and adjacent terrane further to the southeast was made available for this study by A. Friese (Department of Geology, Wits; cf. Friese et al., 1995). These reflection seismic data provide structural

detail, which has been used as constraints on the subsurface structure and stratigraphy of the Basin throughout the modelling procedure for this study.

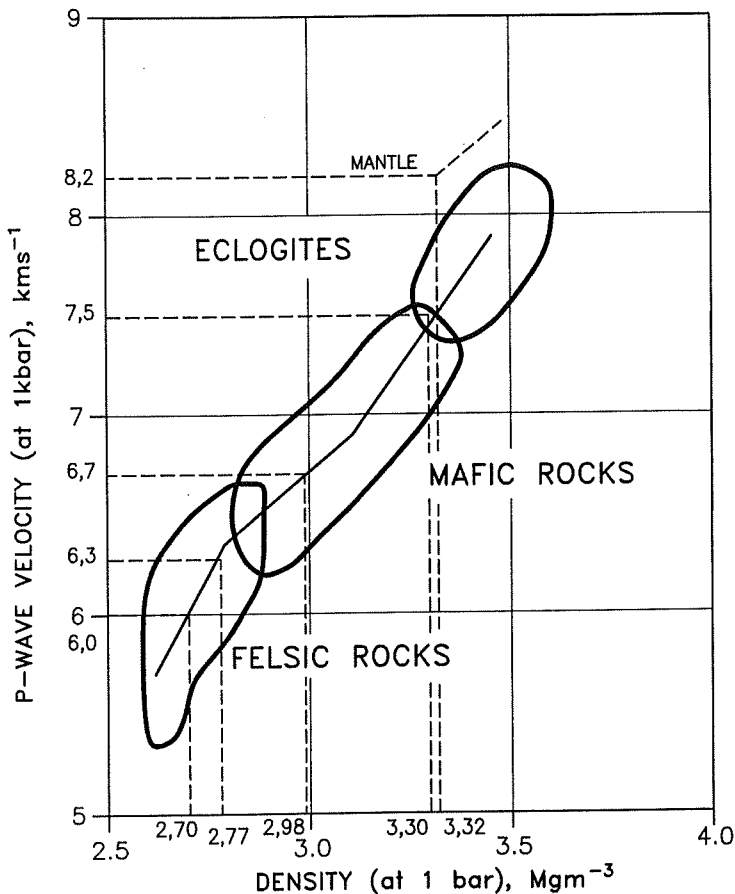


*Figure 17: Relation between seismic p-wave velocity and density. The velocities are given for pressures at 1 k/bar, whereas the densities are given for atmospheric pressure. Global data for plutonic rocks collected by Carmichael (1989) and compiled by Henkel et al. (1990).*

### The 'Background' crustal structure

From the refraction seismic model of the Kaapvaal Craton by Durrheim and Green (1992) the background crustal structure, that is the craton structure prior to the Vredefort impact event, can be derived (Figure 18). The different velocity regimes were identified according to the refraction seismic model and a density was assigned to each velocity regime by making use of the relation shown in Figure 17. The background crustal model consists of an upper crustal layer, extending from the surface to a depth of 14 kilometres, of  $2.70 \text{ Mg m}^{-3}$  density, an upper crustal layer from 14 to 20 kilometres depth with a density of  $2.77 \text{ Mg m}^{-3}$ , a lower crustal layer from 20 to 33 kilometres depth with a density of  $2.98 \text{ Mg m}^{-3}$ , a lower crustal layer from 33 to 36 kilometres depth of  $3.30 \text{ Mg m}^{-3}$  density, and an upper mantle below 36 kilometres depth, with a density of  $3.32 \text{ Mg m}^{-3}$ . Boundaries between layers were located where the velocity-depth variation changes its gradient. The mid-velocity was used to represent a density for a specific layer. The density interfaces do not necessarily represent major lithological changes; they are merely the representation of discrete

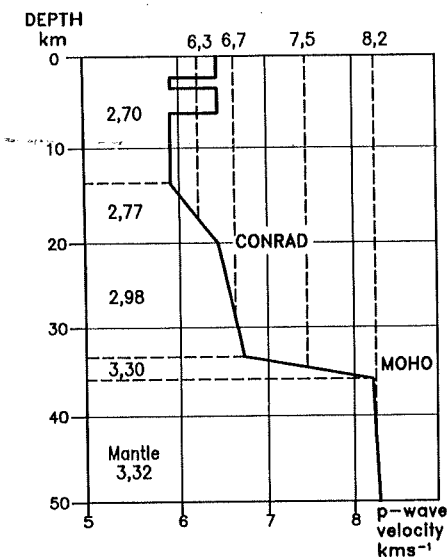


Figure 18: Background crustal density model, based on the seismic p-wave velocity model by Durrheim and Green (1992).

boundaries as interpreted in the refraction seismic velocity (density)-depth variation. The background density of  $2.99 \text{ Mgm}^{-3}$  for a 50 kilometres thick upper lithosphere is the weighted average of the densities of the individual layers within this section. It should be noted that the deepest crustal layer with rather high p-wave velocity (and, thus, density) is the equivalent, in this modelling, to the eclogite layer introduced for the Baltic shield, which explains how variable crustal thickness is uncorrelated to gravity variation (Henkel et al., 1990). The upper boundary of the eclogite layer is a pressure dependent interface, adjusting to prevailing lithostatic conditions and, thereby, levelling the effects of a variable Mohorovičić discontinuity (Moho) at greater depth.

## GEOPHYSICAL MODELLING

The selected profiles across the study region (Figure 7), however optimized they were with respect to the position of the structure to be modelled, will arbitrarily cut across local gravity or magnetic anomalies (compare Figures 9 and 10). The modelling software must, therefore, contain an algorithm, which allows gravity or magnetic sources, which may have arbitrary strike lengths and orientations with respect to the selected profile, to be located off-profile (Figure 19). The software GAMMA (Geovista, 1994) can cope with these complexities. The software is, however, limited to the treatment of a maximum of 20 individual source bodies, which constitutes a serious restriction of the modelling of long profiles. This problem can be circumvented by slicing the model profile into sections, which are then modelled one at a time. The GAMMA software requires an IBM PC/AT or compatible computer with a minimum of 540 kb free RAM, an IBM VGA, EGA, and a math co-processor operating with MS DOS 2.10 or later versions. A selection of printing facilities is supported with specific driving routines.

The modelling concept applied to the data for the Vredefort region generally followed the ideas about integrated crustal modelling discussed in Henkel et al. (1990). Seismic refraction profiles can provide a good indication of vertical segmentations and velocity structures of the crust, but they are not an effective means for resolving lateral heterogeneity

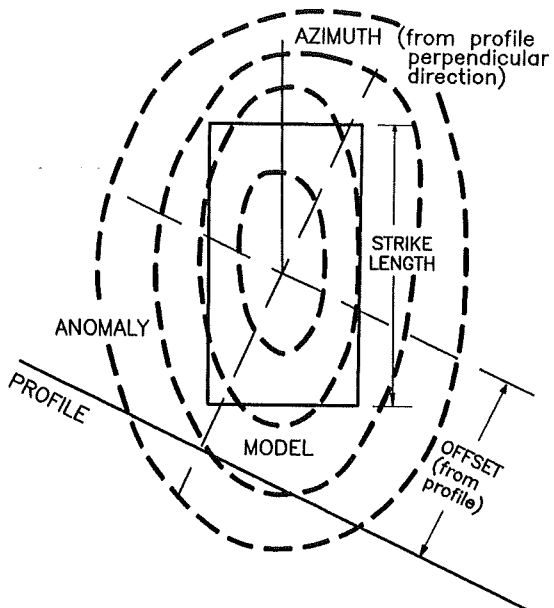


*Figure 19: Off-profile magnetic or gravity sources (anomaly indicated by broken line) will influence the anomaly along the modelling profile. The modelling software used can cope with strike length variation, offset, and rotated source bodies.*

within the upper and middle crust. Gravity and magnetic field data, on the other hand, mainly reflect lateral heterogeneity of the upper crust. These data do not have strong capacity to resolve layering within the crust or broad-scale lateral changes in crustal type and thickness, which give rise to anomalies of long spatial wavelength. In contrast, an integrated interpretation of gravity, magnetic, and seismic data uses each of these data sets to constrain the possible range of interpretations of the others. The seismic data provide the broad-scale crustal framework, which assists in explaining long wavelength gravity and magnetic anomalies. The potential field data define upper crustal structures and constrain lithological contrasts occurring at depth. Thus, combined interpretation eliminates the danger of illusive separation of potential fields of different spatial wavelengths.

For this modelling project, densities were assigned to the crustal layers in accordance with the relationship between p-wave velocity and density (Figure 17). Individual bodies were then inserted into the upper crust to explain the short wavelength gravity and magnetic anomalies. These bodies and their extensions were constrained, wherever possible, by geological information from regional geological maps, and their physical properties (e.g., densities) by data from actually analysed rock types. Each source structure is assigned its own observed or estimated physical properties. Shapes and properties of the various layers and near-surface bodies were then changed within prescribed limits, until an acceptable fit between observed and calculated gravity and magnetic anomaly profiles was achieved.

### The starting model

The concept of a large, complex impact structure requires the consideration of a central uplift region, where deeper crustal layers would occur at relatively shallow depths, as well as of a ring-shaped basin structure of down-warped strata surrounding the central

uplift. The central rise anomaly has, therefore, been modelled as a rise of crustal layers, whereas the anomalies of the ring basin were modelled with down-warped sedimentary layers. In this concept the need for isolated source bodies is limited. A simple perturbation of the background crustal model was used as the starting model. This initial model was characterized by a central rise consisting of deep crustal layers and by a surrounding down-warped basin filled with metasedimentary and metavolcanic supracrustals. The portion of the regional stratigraphic column, which was involved in the cratering event, was subdivided into the Witwatersrand, Ventersdorp, and Transvaal Supergroups. In addition, a discordant cover sequence of Karoo lithologies was introduced. Respective depth extents of these layers were varied according to drilling information (for example, after Fletcher and Reimold, 1989) and information provided by the Geology Division of Gold Fields of South Africa (Pty.) Limited. The background crustal model and the starting model indicated that a shift of the gravity field by -460  $\mu\text{g}$  was required to be able to match the average regional gravity level. In order to avoid edge effects, the starting model for each profile was extended by an additional 100 kilometres, on each side, beyond the 300 kilometres wide cross-sections across the Witwatersrand Basin that were to be modelled in detail.

### Modelling of gravity sources

Sources of gravity anomalies are, on the one hand, crustal layers of variable densities and, on the other, single sources of limited extent within these layers. The gravity anomaly of such an individual source depends on the distance ( $d$ ) from measurement to source, the density contrast ( $c$ ) to the surrounding lithologies, and a function  $F$  of the volume ( $V$ ) and the shape ( $S$ ) of the source structure:

$$\text{anomaly} = (1/d)^2 \cdot c \cdot F(V, S)$$

As long as crustal layers are undisturbed and have a horizontal attitude, no gravity anomaly would be produced. In contrast, any vertical perturbation will result in gravity anomalies. Variable interfaces with large density contrasts between adjacent rocks will produce distinct anomalies, if they are located close to the surface. The technique used here of approximating crustal layers with specific densities may result in an exaggerated density contrast along the interfaces between adjacent bodies. In such cases the modelling will result in subdued topography of these interfaces.

An additional complexity arises in the case of the Vredefort Structure from the inverted density stratification of the pre-impact regional stratigraphic column, with dense supracrustal rocks (such as the Transvaal carbonate strata) overlying crystalline basement of relatively lower density. This complexity can not be resolved with gravity modelling alone. It is, therefore, extremely important to make optimum use of constraints on the thicknesses of the various sedimentary packages, as provided by seismic data (Durrheim and Green, 1992; Durrheim et al., 1991) or drilling information. The central core of the Vredefort Dome has previously been modelled as a rise consisting of dense lower crustal material (Stepto, 1990). This rise constitutes a source of restricted strike length within the crustal layers, a complexity which has been considered in this study.

In addition to the crustal layers, the Karoo cover was also modelled as a layer on top of other crustal sources and to depths restricted by drilling information. Neither Dominion Group rocks, nor Cenozoic cover material (cf. Figure 6) were considered as individual formations in the modelling procedure. Where significant thicknesses of Dominion Group rocks had to be taken into account - especially in the western region of the Witwatersrand Basin (Figure 7), these stratigraphic thicknesses were combined with Witwatersrand strata. The gravity effect from the Cenozoic cover was assumed to be negligible within the limits of the modelling accuracy.

### Topographic elevation

As the Vredefort region is characterized by relatively high ground elevations (on average 1500 metres), the applied Bouguer correction with the standard density of  $2.67 \text{ Mg m}^{-3}$  will result in residual anomalies whenever the actual rock densities are different from the standard value. For Transvaal Supergroup rocks this results in an anomaly of +102 gu, and for the granitoids of the central core in an anomaly of -38 gu - a combined amplitude of 140 gu. Also the vertical gradient of mass acceleration may not coincide with the standard value of  $-3.086 \text{ gu} \cdot \text{m}^{-1}$  used for the Free Air correction. A variation between -2.946 and -3.266 (representing the estimated range of variation (Militzer and Weber, 1984)) would result in a difference of 420 gu at 1500 m elevation. None of these effects has been taken into account in this modelling, as the number of source bodies is restricted to 20 (each of the surface-reaching bodies would have to be divided into one part above the correction datum and one part below). The vertical gradient of mass acceleration is usually not sufficiently well known to be taken into account - if it is a different constant valid for the whole region, the result would be a constant shift in gravity. On the other hand, the previously mentioned compensation with -460 gu for both profiles may actually contain much of these elevation-related effects. Other sources for this difference may arise from the conversion of seismic velocities to densities or the indicated boundaries of crustal layers, both from the refraction seismic interpretation. Until better constraints can be obtained, these effects will contribute to the uncertainty on any interpretation. It must be pointed out that the shapes of the modelled structures will only be marginally affected by these problems.

### Modelling of magnetic sources

Single magnetic sources produce anomalies which are dependent on distance ( $d$ ) from measurement to source structure, volume ( $V$ ), shape ( $S$ ), and orientation ( $O$ ), in addition to the magnetization contrast ( $m$ ) to their surroundings:

$$\text{Anomaly} = (1 / d)^3 \cdot m \cdot F(V, S, O)$$

The magnetization contrast is the vector sum of the induced ( $I$ ) and remanent magnetizations ( $R$ ), where the induced magnetization depends on the magnetic susceptibility of the rock volume and the local total intensity of the geomagnetic field ( $H$ ):

$$m = s \cdot H + R$$

It must be emphasized that the magnitude of a magnetic anomaly decreases rather

rapidly with distance, a characteristic which is different from the characteristics of gravity anomalies and which results in, comparatively, significantly reduced depth sensitivity of magnetic measurements. The combination of the total magnetization vector and the orientation of the source structure creates magnetic anomalies of complex shapes. The anomaly of a single source structure usually has both positive and negative parts. This is well illustrated in Figure 15A, which demonstrates the remanence effect on the magnetic anomalies of two different source structures of simple geometries.

Generally, magnetic sources constitute crystalline basement rocks, intrusions into these and into sedimentary rocks, and sediments with anomalously high contents of magnetite or pyrrhotite. According to the survey of rock magnetic properties, magnetic intrusions are common constituents throughout the column of sedimentary supracrustals, and several horizons of strongly magnetic shales are known in outcrop and from drilling. Where magnetic crystalline basement occurs within a few kilometres depth, the magnetic anomalies reflect the location of the upper surface of these rocks.

For magnetic modelling of the Vredefort Structure, the potential effects on magnetic fields from high temperature overprinting due to granulite facies metamorphism and impact-induced heating need to be considered. Both these effects may result in increased magnetite contents and a specific remanence. The change of magnetic properties associated with the prograde transition to granulite metamorphism is described, for example, by Olesen et al. (1991).

The final gravity model was used as the starting model for the magnetic modelling. Magnetic sources were preferentially located within the corresponding Supergroup determined by gravity modelling. This procedure reduced the need to crosscut important stratigraphic boundaries.

## RESULTS

The result of this modelling effort is the distribution of densities within the crust of the region of the Witwatersrand Basin along two profiles, as obtained from the gravity modelling. Furthermore, the distribution of magnetic material in the uppermost part of the crust was computed, through magnetic modelling along parts of the NW-SE profile. This is the first time that a large, complex impact structure has been modelled with this technique and on the basis of integration of so many data sets.

### **The gravity model**

The results of the gravity modelling are shown in Figures 20 and 21. The crystalline basement rocks are characterized by densities that systematically increase with depth, as defined by the observed p-wave velocities. The most important interface is the so-called Conrad Discontinuity between upper and lower crust, which is characterized by a density contrast of  $0.21 \text{ Mgm}^{-3}$  in these models. The Moho at the base of the crust is slightly below the expected reversible eclogite transition depth. The dominant density interface is, therefore, the lower crustal eclogite transition zone, which has a minimum topography (due to its nature as a zone of dominantly pressure-dependent phase transition). Here the expected density

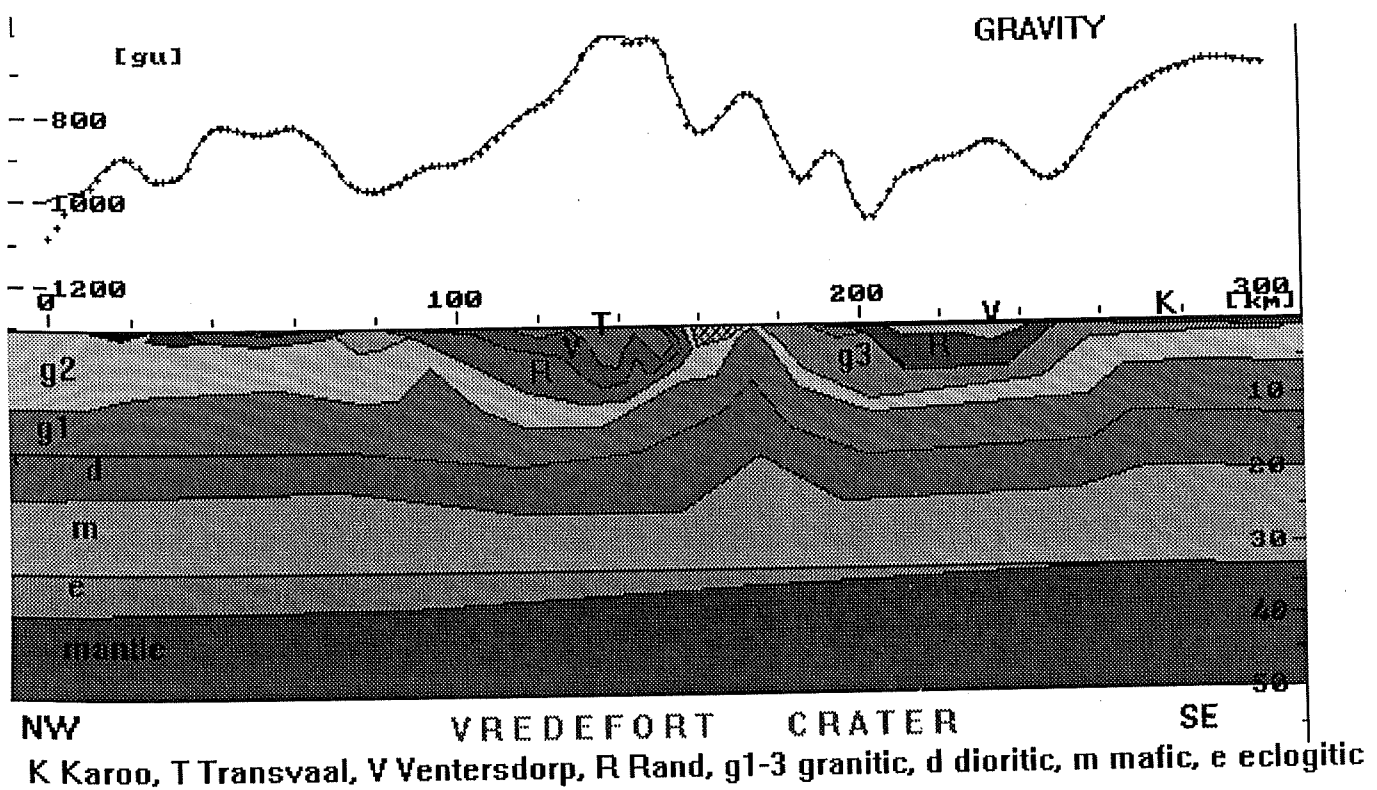


Figure 20: Gravity model along the NW-SE profile across the Witwatersrand Basin. For profile location see Figure 7.

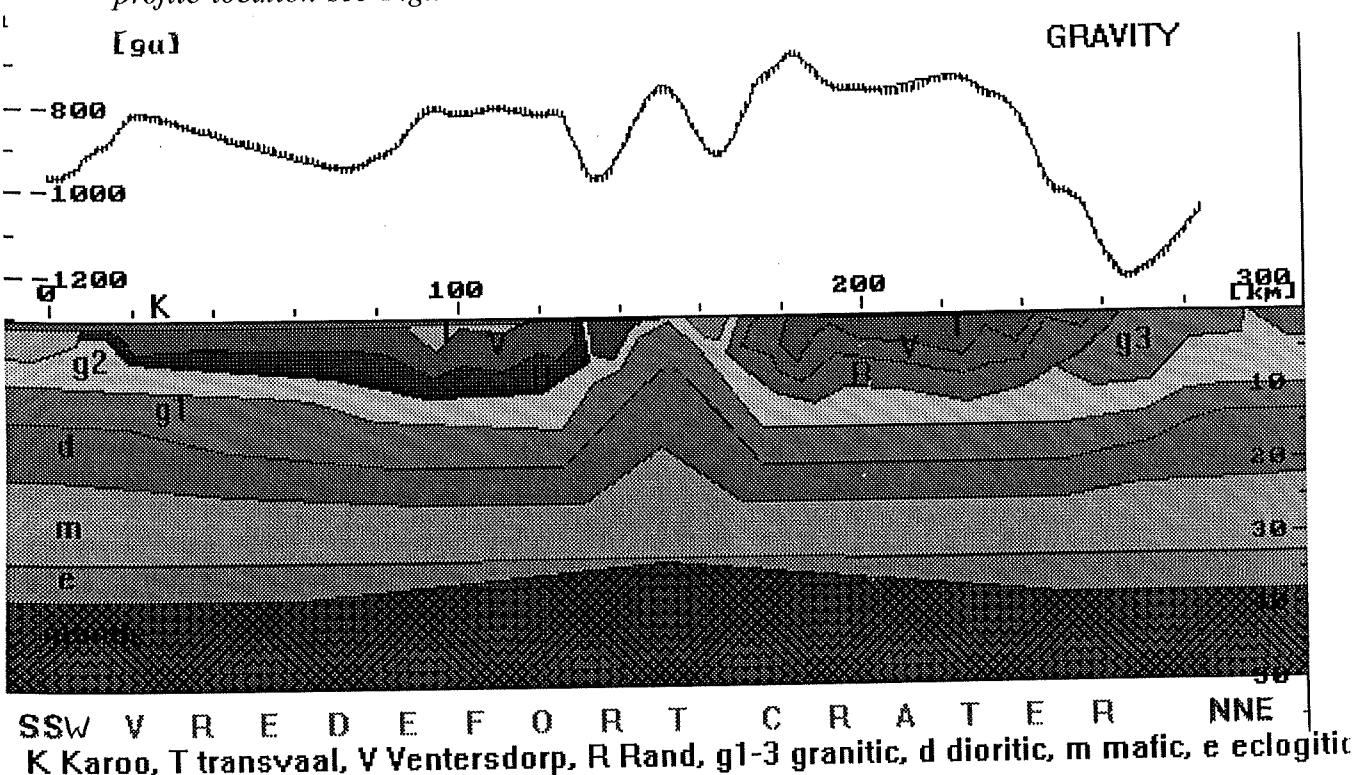


Figure 21: Gravity model along the SSW-NNE profile across the Witwatersrand Basin (compare Figure 7). The two profiles of Figures 20 and 21 intersect at the gravity maximum in the centre of the core.

contrast is  $0.32 \text{ Mgm}^{-3}$ . The uppermost crystalline basement layer is granitic to granodioritic in composition, in accordance with the observed p-wave velocity, and has a density of  $2.65 \text{ Mgm}^{-3}$ . These basic constraints allow the insertion of low density granitic bodies in the uppermost crystalline crust, wherever this is required by an observed low gravity anomaly.

The metasedimentary and metavolcanic supracrustal column has generally high densities, in comparison with the underlying crystalline basement. Within this column, the stratigraphically lowest unit (Witwatersrand Supergroup) has the relatively lowest density, and the upper Transvaal Supergroup package the highest. This inversion of the density-depth relationship introduces a major ambiguity and calls for additional constraints at least for parts of the stratigraphy. These constraints were provided by reflection seismic data from the NW-SE Geological Survey profile, various drillcore logs, and from expert stratigraphic knowledge (e.g., P.Fletcher, pers. commun.).

In the eastern and southern portions of the Vredefort Structure, more or less extensive Karoo cover is evident (Figures 7 and 8). The density applied to this sequence of sedimentary and extrusive magmatic rocks was calculated from measured data and taken as regionally constant. This simplification is justified, as this cover sequence is regionally rather thin with regard to the overall depth of this model.

In judging the results of this modelling it is important to remain conscious of the fact that this modelling was performed on a regional scale. It is, therefore, inherent to the technique that the effects of small-scale features less than a few kilometres across can not be represented with any precision.

### *The central uplift*

The structure of the central uplift region, the Vredefort Dome, has been the focus of attention by many workers (e.g., papers in Nicolaysen and Reimold, 1990; review by Reimold, 1993). The gravity signature of this region consists of a rather smooth central gravity high of 300 gu amplitude, which is surrounded by a complete, ring-shaped gravity low (Antoine et al., 1990; Corner et al., 1990). Stepto (1990) attempted to model this feature by isolating the gravity high of the central uplift from a smoothed regional field. This author suggested that an approximately 10 kilometres deep body of  $2.84 \text{ Mgm}^{-3}$  density could fit the central gravity residual of 300 gu. The surface densities used for this model were, however, generally higher than the observed values. The diameter of the high density body was calculated at about 15 kilometres. This model does, however, not fit the seismic velocity structure for the central core region published by Green and Chetty (1990). The seismically determined high velocity structure comes to surface over a distance of about 8 kilometres in the central core and then slopes gently outwards to about 1 kilometre depth at a distance of 16 kilometres from the centre.

In our model, all density anomalies have been accounted for in the lateral and vertical surroundings of the Dome, making a separation from residual gravity fields unnecessary. There are, however, limitations in the complexity that can be modelled even with a 2.5-d software. The central rise has, therefore, been modelled in two ways. First, the deeper layers of the crust were treated as layers extending to far distances perpendicular to, as well as

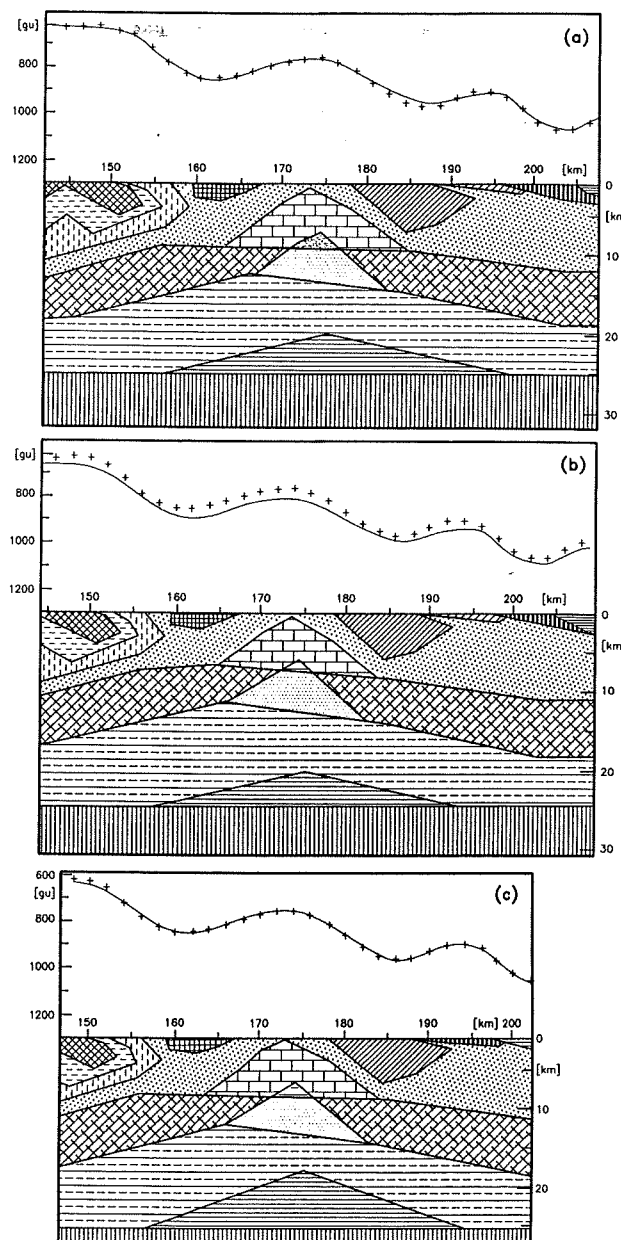


*Figure 22: Calculation of the effect of limited strike extension of the core structures.*

*A: Model with infinite strike extension of core structures and subdivision into structures with limited strike extension. B: Model with strike-restricted extension inserted, which reduces the calculated gravity. C: Model with lower crust interface adjusted upward by approximately 4km, which reproduces the observed gravity anomaly with regard to amplitude and wavelength. Measured gravity values are indicated by (+), calculated values by a thin line.*

along, the profile. Second, the central rise was modelled as a combination of strike-restricted sub-models within each layer, with the same perpendicular extension as that along the profile. The difference is a long wavelength gravity anomaly of -95  $\mu\text{g}$  extending far beyond the central uplift. This anomaly is completely accounted for by rising the mid-crustal density interface by about 4 kilometres. The whole procedure is illustrated in Figure 22.

Along the surface, observed densities of the granitoids can be used as constraints. The modelling shows that these low density rocks occur in a ring-like fashion around the centre, where the crustal layer with  $2.70 \text{ Mgm}^{-3}$  density almost approaches the surface. At the southeastern flank of the central rise, a high density mafic source structure has been inserted to account for the occurrence of Archaean greenstones in this area (Minnitt et al., 1994). These mafic rocks have a restricted volume and no connection with deeper high density layers.

The ring-shaped gravity low is related to the volume of near-surface low-density granitoids of the central core region. The gravity high, on the other hand, is related to the uprise of deeper crustal layers with an amplitude of up to 13 kilometres as compared to the base of the surrounding sediment-filled ring basin. Compared to the surrounding, undisturbed layering of the crust, the amplitude of the uplift is about 8 kilometres, a figure that is in excellent agreement with recently published figures derived from detailed metamorphic analysis of the core granitoids (Gibson and Wallmach, 1995; Stevens et al., 1995, 1996).

#### *The northwest-southeast profile*

The location of this profile is shown in Figure 7 and the corresponding gravity model in Figure 20. This profile is located parallel to the shortest lateral dimension of the Vredefort Structure. The reflection seismic profile discussed by Durrheim et al. (1991) was used as constraint for this model. The seismic interpretation shows clearly the change of reflective patterns when the crater structure is approached. Some deep crustal reflectors are terminated, others change orientation. These terminations have been used as constraints for the lateral onset of the impact-reworked crustal patterns - resulting in a lack of systematic reflectors. It can also be seen that the Moho-related reflectors begin to bend upwards, when the structure is approached. This rise has been taken into account in the modelling. The width of this crustal perturbation is approximately 100 kilometres. We interpret this zone as the region within which yielding by plastic deformation dominated in the shock zoning of the Vredefort impact structure (cf. below, Discussion).

The stratigraphy of the sedimentary basin along the northwest-southeast profile is constrained by surface intersections of the various lithologies and by some drillcore profiles. The anticlinal structure seen in surface data and in the seismic reflection pattern at depth has been maintained in the model. The greatest depth of this basin, reaching 5.3 s TWT in the interpretation of Durrheim et al. (1991), could, however, not be verified by this gravity modelling. This interface could only be placed at a maximum depth of 10 kilometres.

All sedimentary basins along this profile are characterized by positive gravity anomalies. The internal basin structures have been modelled from gravity anomalies only. The northwest sector shows strong perturbations. The causes for these disturbances are not

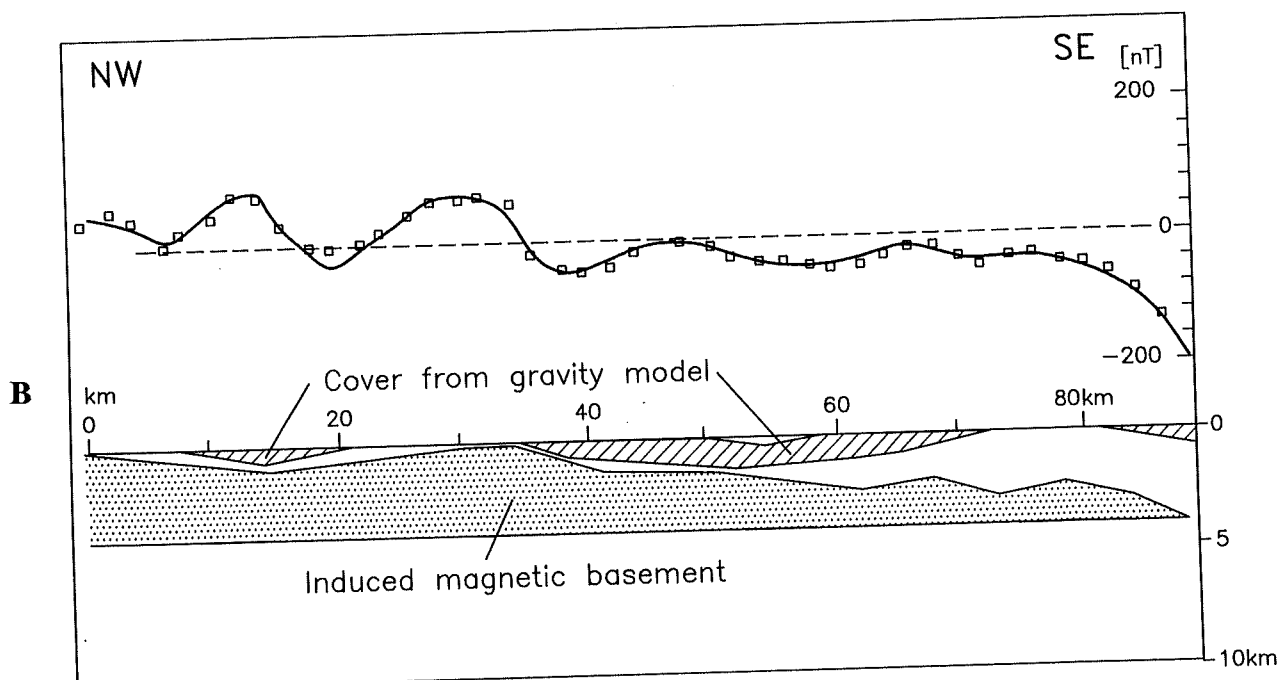
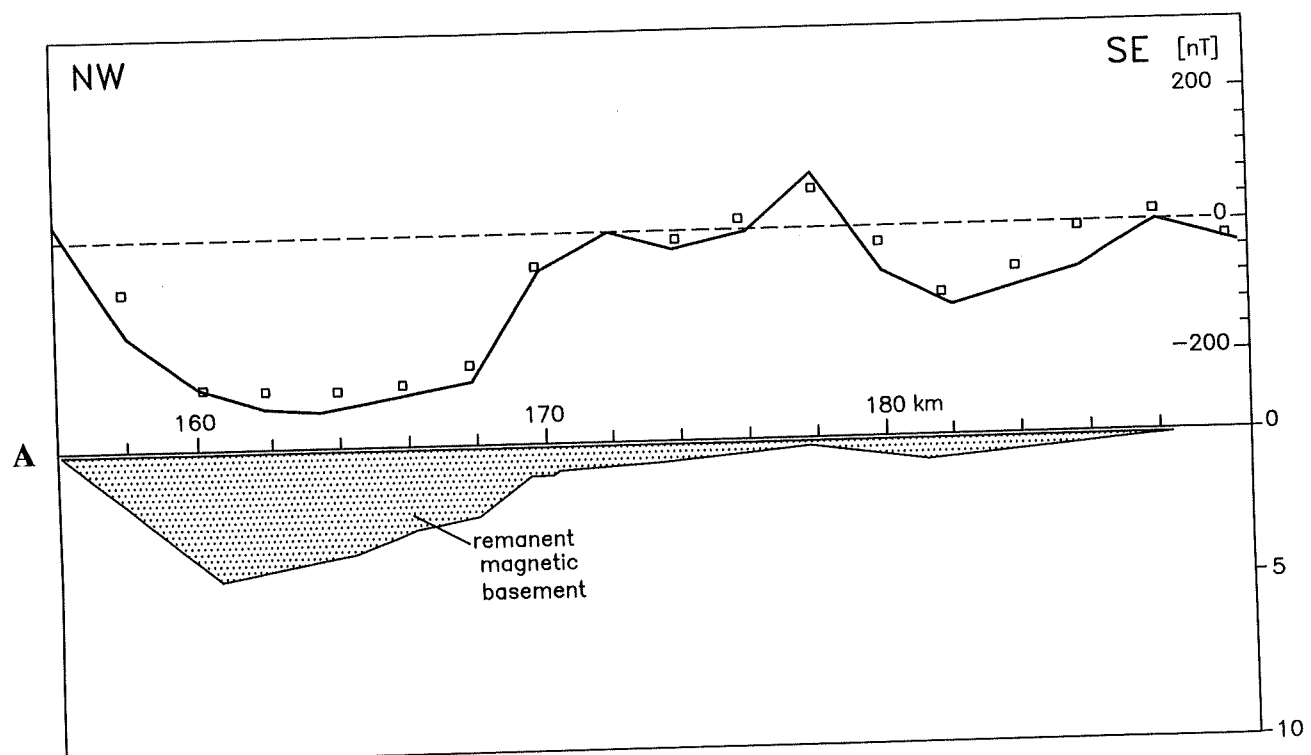
clear and not well constrained. Perhaps detailed evaluation of the unmigrated reflection seismic data may yield further insight. The maximum depth of the northwest basin is about 13 kilometres below the Karoo cover. The southeast section of this profile shows a relatively small gravity high, which could be interpreted as the result of lesser volumes of high density sediments (in comparison with the northwest section) and/or a lower depth of this basin. In the modelling a rather schematic basin depth of about 6 kilometres was assumed, which turned out to be reasonable, when the reflection seismic data for this southeast sector (Friese, pers. commun.) became available. The detailed structure of this basin can be improved by taking into account the details visible in these reflection seismic data. No high density Transvaal rocks have been included in the model of the southeast basin in accordance with geological constraints that were mainly derived from drilling information.

The overall crustal structure along the outer parts of the northwest-southeast profile, as seen in the gravity model, shows two rather shallow sedimentary basins in the northwest sector and minor perturbations of the deeper crustal structure. Within the actual crater structure, as defined by reflection seismic data, a thinning of the uppermost granitic crust is seen under very deep sedimentary basins. Closer to the central uplift region, the whole crust is strongly disturbed. This is the likely reason why the northwest reflection seismic profile yielded unsatisfactory detail of the crustal structure in the region of the Vredefort Dome. The northwesterly sedimentary basin abuts against the crystalline core with an overturned edge. This overturning is not seen at the southeastern flank of the central rise. The southeastern sedimentary basin is less deep than its northwesterly counterpart and is terminated in the southeast by a crustal flexure. This flexure elevates deeper crustal layers and the upper mantle by about 4 kilometres.

#### *The south-southwest-north-northeast profile*

The location of this traverse is also shown in Figure 7 and the corresponding model in Figure 21. This profile extends parallel to the longest dimension of the Vredefort Structure. The central uplift region is modelled in accordance with the description of the previous model. It is noteworthy that the sedimentary basins abut against the uplifted central crystalline core with overturned structure on both flanks of the rise. The sedimentary basins are much more extensive than those in the other profile, and the accumulation of dense sedimentary rocks is also seen in the rather high gravity anomaly, especially in the northeast sector. The sedimentary basins reach modelled depths of 13 kilometres. The anomalies are accounted for by the observed surface lithologies. At depth, a thicker pile of Transvaal rocks has been modelled in the northeastern sector to account for a part of the higher gravity anomaly. An alternative solution could be obtained by modelling an increased amount of Ventersdorp extrusives, resulting in a still higher formation density (the NW and NE basins have already been modelled with a somewhat higher Ventersdorp formation density of 2.80  $Mgm^{-3}$ , whereas  $2.78 Mgm^{-3}$  was used for the SW basin).

The perturbations of the deeper crustal structures are similar to those observed in the northwest-southeast profile. A slight rise of the Moho of about 2 kilometres has been introduced under the central rise, which, however, does not produce a noticeable gravity effect, as the rise is located below the eclogite transition depth. The gravity low to the northeast is related to the granitoid rocks of the Johannesburg Dome. Further to the



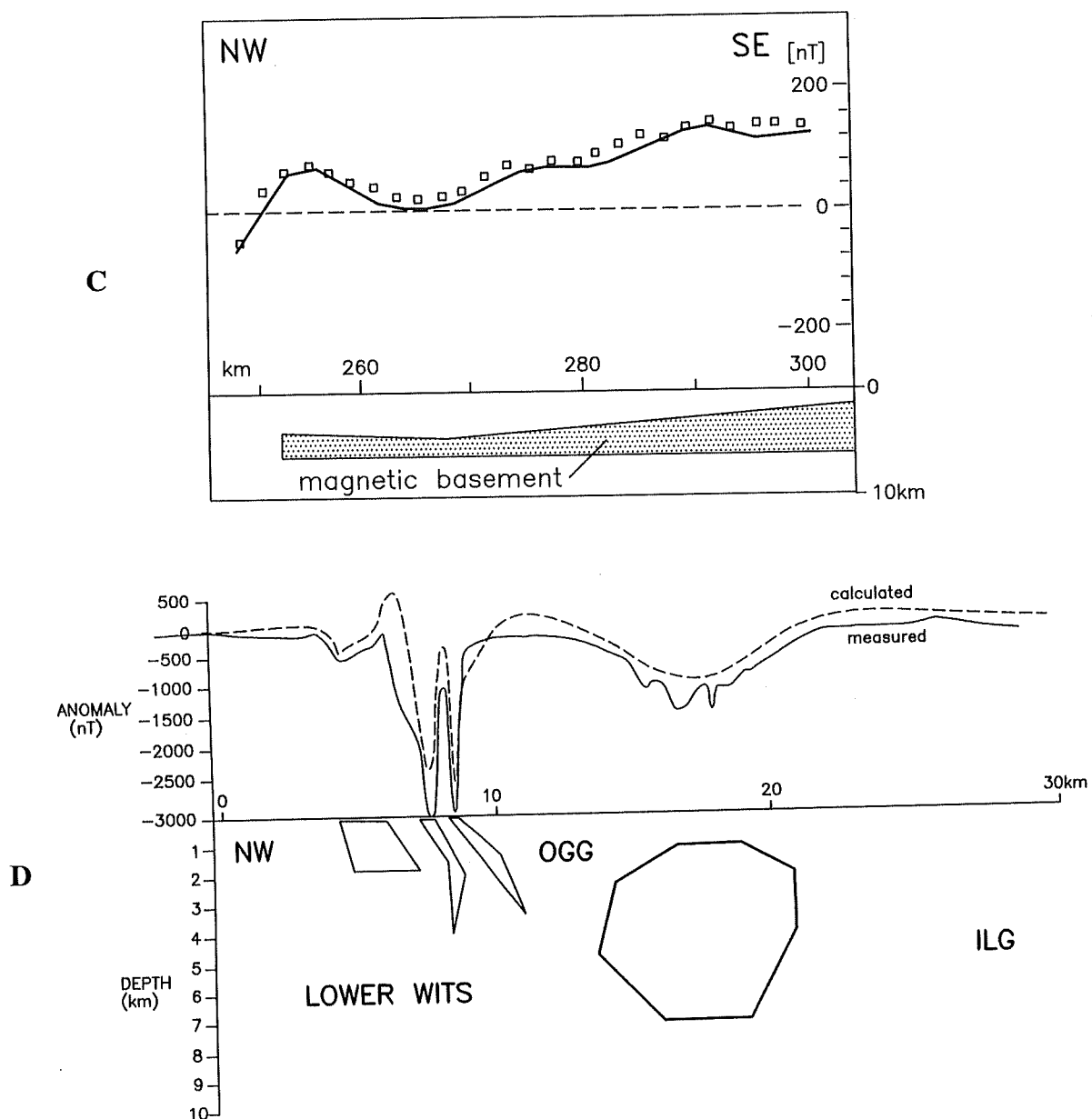


*Figure 23: Magnetic models obtained from this study (measured anomalies are indicated by squares and calculated ones by a thin line): A: The model of the central rise along the NW-SE profile. The magnetic low anomaly is caused by the thickness variation of a remanent magnetic structure at the top of the central core. B: Model of the NW collar region of the Vredefort Dome, from Jackson (1982), showing in some detail the negative magnetic effect from remanent magnetized shales. Note: The rounded body at 10km is, however, better modelled according to the model shown in A. C: Magnetic model of the NW edge of the Witwatersrand Basin. The magnetic anomalies are caused by the depth to induced magnetized crystalline basement rocks. D: Magnetic model of the SE edge of the Witwatersrand Basin. The magnetic anomalies are caused by the depth to induced magnetized crystalline basement.*

northeast, a schematic model has been introduced accounting for the positive edge effect of the nearby Bushveld Complex.

### The Magnetic Model

As mentioned previously, the detectable magnetic sources are confined to the uppermost few kilometres of the crust. Deeper sources will only generate magnetic anomalies, if they are very voluminous. For the magnetic modelling, the final gravity model was used as starting model. The number of gravity sources was reduced where no magnetic anomalies were found.

The strong negative magnetic anomalies over part of the central core region and the sedimentary collar have been discussed in earlier literature (Antoine et al., 1990; Corner et al., 1990; Hart et al., 1995, and references in these publications). The thesis by Jackson (1982) represents the first detailed study of this aspect. Observed rock magnetic properties were used to model the observed anomalies. The modelling results are presented for the central uplift region and the surrounding sedimentary basins in Figure 23A-D.

Two types of magnetic structures were found, both of which have remanent magnetizations of the same direction. The first type corresponds to overturned magnetic shale layers within the Witwatersrand Supergroup sequence of the collar. The second type is related to magnetic sources within the crystalline basement core (Figure 23A). Jackson's (1982) modelling, shown in Figure 23B, was found to be correct with regard to all essential aspects. However, this author observed that the remanence intensities of the models must be lower by an order of magnitude than the values calculated from actual measurements on rock samples. (For an account of all the different approaches of how to measure rock magnetic properties, refer to Appendix I). Jackson's model concerning the overturned sedimentary units of the collar is more detailed than the one that could be achieved by us, because of the lesser spatial resolution that could be applied here. In our model, the remanence direction determined by Jackson was used together with measured susceptibilities and with more moderate q-values.

The central core magnetic anomalies can be explained with a model discordant to the density structure determined by the gravity modelling. It reflects the basal topography of a remanent magnetic structure in the top of the central rise. The thickness of such a remanent magnetic layer is largest - nearly 4 kilometres thick - in the northwestern sector of the core and lowest in the central and southwestern sectors, where it is at most 1 kilometre thick. The overturned magnetic sedimentary rocks have the same remanence as the core sources and they occur only in an arcuate arrangement symmetrical to the northwest-southeast profile. They are lacking in the southeastern sector.

The magnetic anomalies within the region of the sedimentary basins in the environs of the Dome have not yet been modelled completely. This is due to the rather strong complexity of the involved structures, which in part are located off-profile. In addition, the constraints on the magnetic properties of the rocks involved are largely unknown. The first attempts at modelling these structures, however, indicate that induced magnetizations seem to be sufficient to explain most of the occurring anomalies. In a few cases strong negative

magnetic anomalies must be modelled with high remanent magnetization.

The exterior regions of the Vredefort Structure contain low gradient magnetic highs, which can all be modelled as the depth variation of the upper surface of an induced magnetized upper crustal layer, as seen in Figures 23C and D. Susceptibilities similar to those observed in the granitic central core region were used for modelling purposes. This topography does, however, not match in all detail that of the gravity modelling of the sedimentary basins. Observed discrepancies are related to the higher sensitivity of the magnetic method for structures at shallow depths and the occurrence of crystalline rocks of low magnetic properties.

## DISCUSSION

### The three stages of impact cratering

Meteorite impact structures (craters) are scars in the Earth's crust, the size and shape of which are dependent on the kinetic energy of the projectile and its transfer to the crust. Naturally, this process depends on the thermodynamic and rheological characteristics of both the projectile and the target rocks. Melosh (1989) presented a detailed account of the processes involved and their physical/mathematical treatments; the subsequent discussion generally follows Melosh's outline. Several of the processes overlap in time and space, and it is important to note that, in comparison to endogenic geological processes, all impact processes occur within very short time intervals (minutes) and affect extensive rock volumes (thousands of km<sup>3</sup>). Figure 24 summarizes the impact-related processes in a time-space diagram. The main sequence of events affecting a target area begins with the formation of a *shock wave* and associated compression of the target material. This is followed by *excavation* and subsequent *modification* of the crater and terminates with *late adjustments* of the crustal environment. Each of these stages is characterized by a typical geometric pattern interacting with the pre-existing structure of the crust, as illustrated in Figure 25 for a complex crater. The simplified Earth's crust is shown as a rheologically layered medium with a cover sequence, a felsic crystalline upper crust, and a mafic lower crust. The prevailing thermal gradient will influence the actual rheological status, and, accordingly, two cases are illustrated for a low geothermal gradient (typical of present shields) and an enhanced geothermal gradient (due to higher radioactive heat production) which might be more representative of cratons at 2 Ga ago.

The first impact-induced processes are the effects of a shock wave, creating a series of *spherical shells*, eccentrically arranged around the point of contact between projectile and target, with shock pressures and associated shock metamorphic effects decreasing in intensity outwards from the point of impact. Along a radial profile, the innermost shell is represented by plasma formation, followed outwards by shells characterized by vapor and melt formation, plastic deformation, and brittle deformation features, respectively. The volume of each shell depends on the energy of the projectile (its velocity and mass) and the thermodynamic properties of the target rocks.

The crater evolves out of these shells by an explosion that redistributes the near-surface material within its surroundings. The geometry of the evolving structure now changes

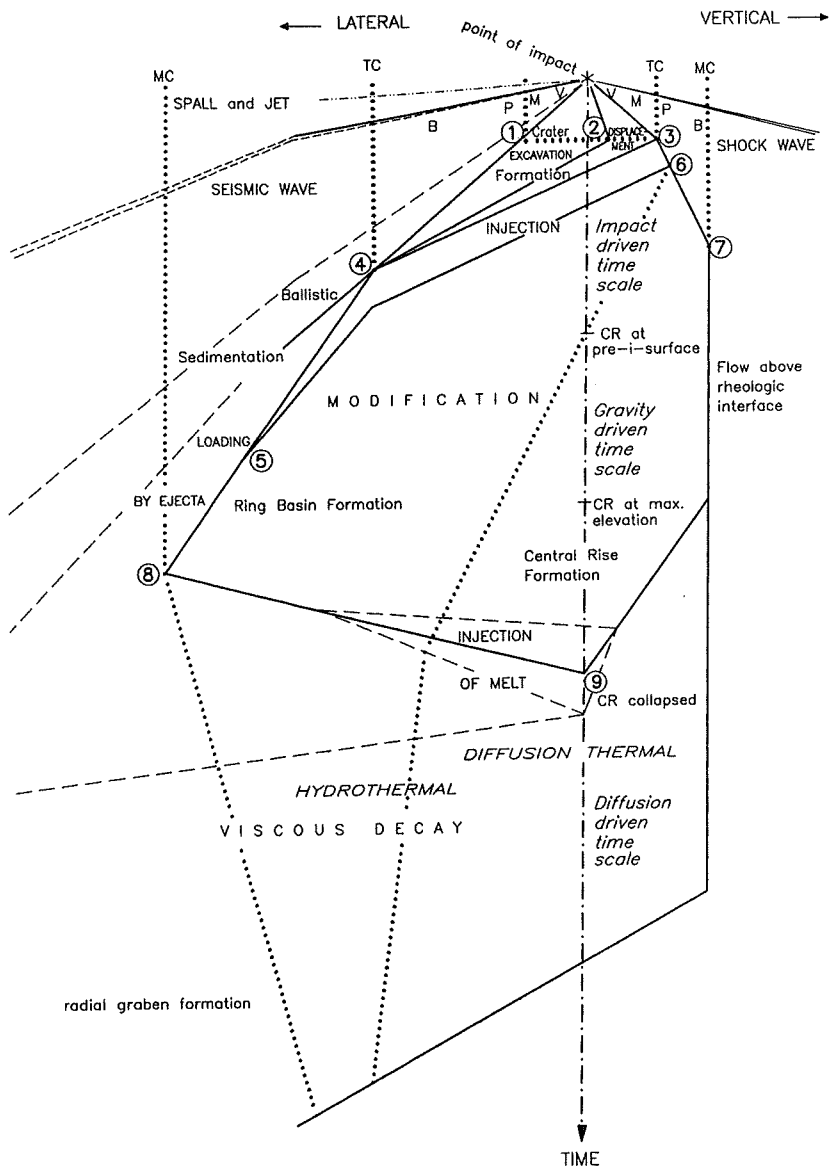


*Figure 24: Space (vertical and lateral dimension) and time (vertical axis) diagram showing the sequence of events that form an impact crater. The expansion of a shock wave through the crust converts rocks into (plasma), vapour (V), melt (M), plastically (P), and brittly (B) deformed states, creating a typical shock zonation. The excavation flow leads first to the formation of a symmetrical crater (1-2-3), which then widens laterally until its final shape is attained (3-4). The deformation flow injects material into the crater floor and wall (5-6). The central rise forms early in complex craters and moves vertically above the pre-impact surface, before it collapses in the modification flow. The crater wall, on the other hand, collapses into the crater - thereby enlarging its lateral dimensions significantly. After the modification stage, thermal disequilibrium (with the geothermal gradient) changes the crater shape further due to viscous decay.*

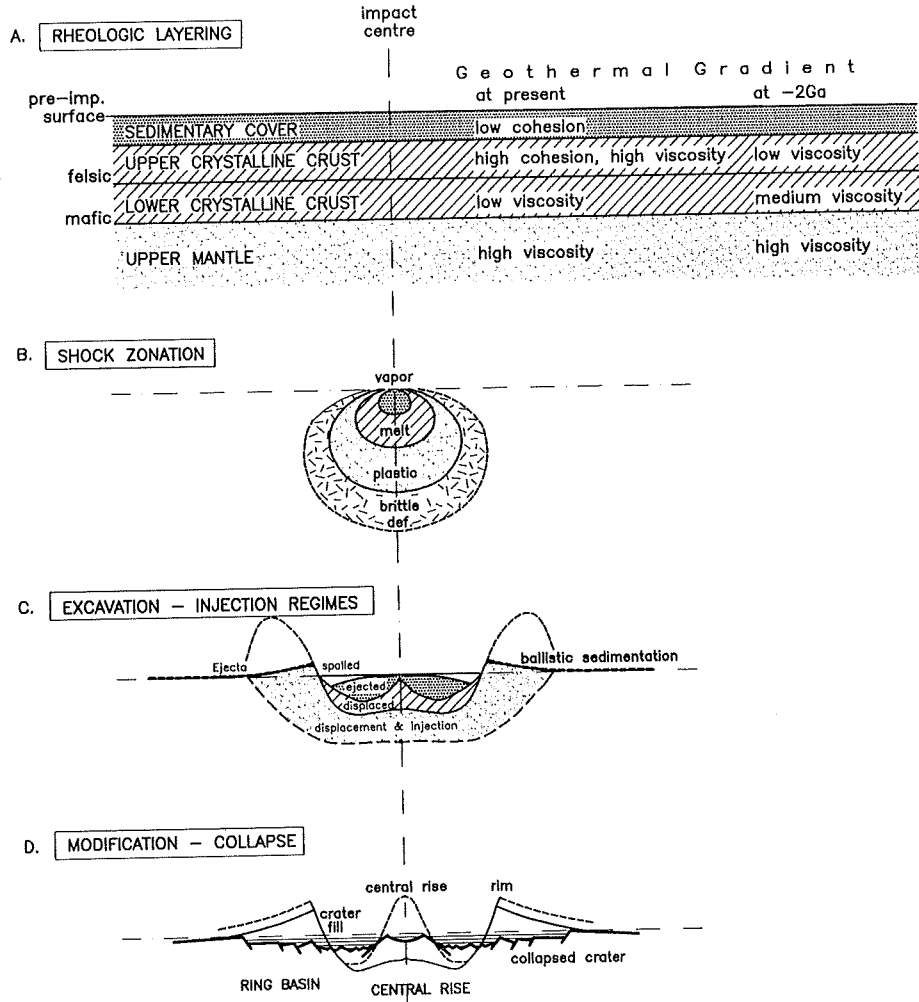


*Figure 25: The different geometric patterns resulting from impact cratering. A: Approximate rheological structure of the target area (a craton with sedimentary cover); B: Shock-induced zonation of irreversible phase changes is essentially spherical, with the spherical shells emanating from the explosion centre; C: Excavation and injection flow cause a ring-shaped symmetry with different mass displacement regimes around the impact epicentre; D: The final crater form results from modification flow, which enhances the ring-shaped geometry by bringing up a substantial central rise feature; collapse starts with an overheightened relief and results in less relief than the transient cavity; the collapsed crater may either become filled with sediments or become eroded to variable depths.*

to a flow pattern, as a result of which material is moved radially downwards and away from the point of impact. Some of this material is ejected out of the evolving crater, while most of it is pushed or injected into the crust. The ejecta deposited outside the evolving crater and the removal of material from within the crater change the load of the crust. The geometry of the structure has now changed to a *ring shape*. The material left in the crater represents the excavated crater (EC) and the displacement of material terminates with the creation of a new free surface, the outline of the *transient crater* (TC). This surface, lined with breccia and impact melt, is, to variable extents, preserved in the new structures formed. The formation time for a transient crater of the size applicable to the original Vredefort Structure

(cf. below) is about 2 minutes. As the diameter of various shock-induced structures grows faster than the crater diameter, craters may, with increasing size, form entirely in brittle or plastically (beyond the HEL - the Hugoniot Elastic Limit) deformed rock, or in liquid (melt) rock.

The formation of the TC marks the shift to the collapse of the crater, where material flow is now essentially reversed to downward and inward flow directions. The collapse flattens the TC to a fraction of its transient depth and creates a completely anomalous (in comparison to endogenic crustal processes) juxtaposition of former crustal entities, the *modified crater* (MC). The typical structural features of a MC are *a ring shaped basin (RB) around a central rise (CR)* (compare Figure 1). Eventually, the remaining topographic low may be filled with post-impact sediments, which, in the case of an impact crater formed in a marine environment, will contain thick piles of basal breccia moved in from the crater surroundings (Lindström et al., 1994). The collapse of the initial transient crater occurs on a time scale similar to that of its formation, i.e. another 2 minutes. The entire impact structure is, thus, created within 4 minutes. The volume involved in the formation of a Vredefort-sized impact structure is at least  $7 \cdot 10^5 \text{ km}^3$ .

## Reconstructing the Vredefort Crater

### *Restoring the extension of the modified crater (MC)*

Following the recent confirmation of the presence of unambiguous shock metamorphic deformation features of impact-diagnostic value (cf. chapter Geology) in several minerals from rocks of the Vredefort Dome, the structure, geology, and mineralogy of this terrane force the conclusion that the Dome represents the central rise (CR) of a large, complex impact structure. Its impressive dimensions, in the order of 40-50 kilometers across the basement core alone, at the present surface, indicate the original existence of a very large impact structure. The sedimentary basin, the 'Witwatersrand Basin', surrounding the Vredefort Dome to date has not been interpreted as an impact ring basin (RB). The impact association is disguised by the fact that it does not appear as an impact-characteristic ring basin. The fortuitous circumstance that the Archaean basin-fill is sediment-dominated has, in the past, prompted all discussion of the evolution of the 'Witwatersrand Basin' to be governed by conventional geological thinking. It is now recognized that, whereas the realm of the 'Witwatersrand Basin' originally was part of a sedimentary basin environment, the remaining, structurally preserved, basin, which now is known as the 'Witwatersrand Basin', represents the eroded remnant of an impact ring basin. This was formed at ca. 2025 Ma ago within the older sedimentary cover and extended into the crystalline basement.

Approaching the problem of the nature of this basin from a pure impact point of view leads to a first-order assumption that the non-circular shape must essentially be a post-impact deformation feature (most impact structures - and other explosion craters - are essentially circular, but may assume a more irregular shape on marginal gravity collapse; the typical impact basin is, thus, roughly circular and centered around the well-defined central rise). Restoring the approximately circular shape of the original ring basin, in the Vredefort case results in a diameter of about 250 kilometers, provided that the long axis of the present basin was not extended due to post-impact tectonic deformation. (It also should not contain parts

of potentially formed radial basins that could have evolved due to viscous decay of parts of the crater - cf. below). The gravity modelling generally confirms this figure: at a radius of about 125 km, the basin deepens and extends in a similar fashion up to the central rise.

Restoring a near-circular shape of the ring basin requires up to 65 km outward displacement of parts of the northwestern edge of the present 'Witwatersrand Basin'. The inward-facing lobe in this sector (Figure 26) is most likely the result of post-impact thrusting directed from the northwest (as a potential consequence of the post-2000 Ma Kheis orogeny - Duane and Kruger, 1991). The southeastern boundary of the Basin is rather straight and extends southsouthwest-northnortheast. Restoration of this sector outwards by an amount of one third of the crater basin radius can be achieved by reversing the uplift of the southeastern segment along a fairly straight lineament, along which the southeastern block was lifted by about 4 km.

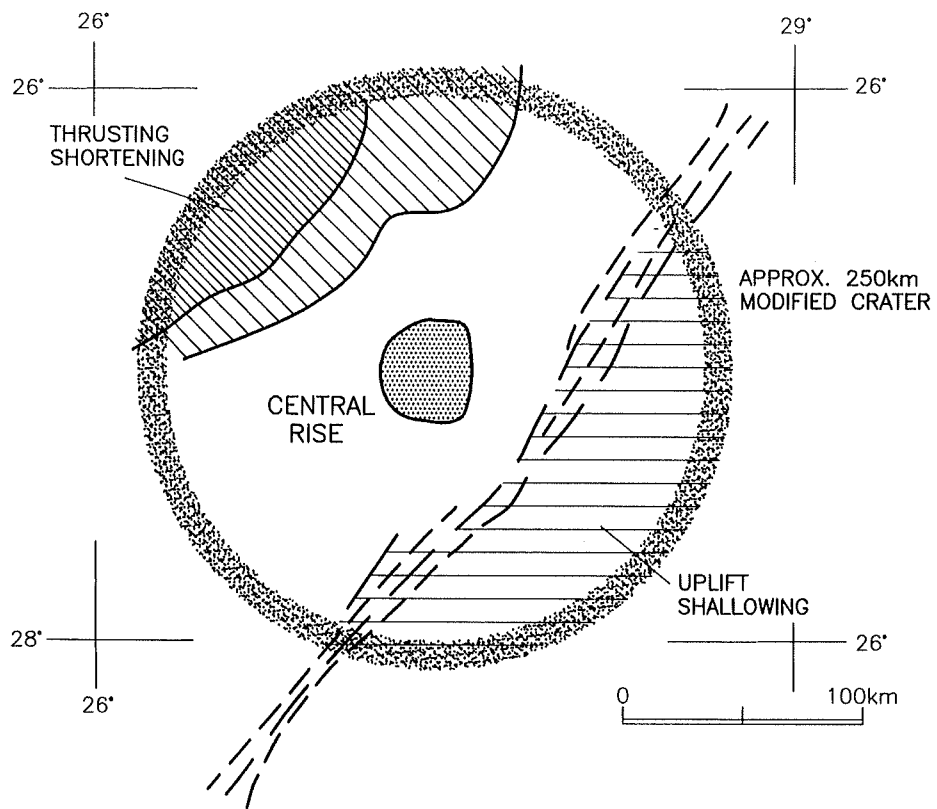


*Figure 26: Reconstruction of the extension of the Vredefort crater. The NW edge of the present Vredefort Structure is displaced inwards by about 65km, and the whole SW segment is uplifted several km along a fairly straight SSW-NNE running flexure/lineament. The dotted line shows the approximate outline of a restored circular crater basin with a diameter of about 250km.*

An alternative way to restore the original shape of the southeastern part of the impact basin would be to counteract the effects of northwesterly directed thrusting along surfaces striking in a southsouthwest-northnortheasterly direction. The displacement due to thrusting would, then, be of the order of more than 50 km in northwesterly direction. Post-impact, northwesterly directed, thrusting related to ca. 1 to 1.2 Ga Namaqua-Natal activity along the

southern margin of the Kaapvaal Craton has been evidenced by several workers and most recently emphasized by Friese et al. (1995). The region of the Witwatersrand Basin and its environs has also provided ample evidence for magmatic activity, which has been linked to Kibaran (Grenvillian, ca. 1 Ga) tectonism (e.g., Reimold et al., 1995c; Friese et al., 1995).

The post-impact deformation by thrusting may locally have preserved sediments and ejecta of the impact-induced ring basin underneath overthrust units. A large volume of such ejecta would consist of unshocked sedimentary cover rocks derived from the transition zone between zero and low shock pressures just beneath the pre-impact free surface.

In very large impact basins, post-impact adjustments of the crust may result in the development of radial and/or tangential graben structures. These patterns may overprint the modified crater (MC), but may be recognizable by their crater-related symmetry and/or extension. The formation of such secondary basins depends on the prevailing geothermal gradient and the resulting rheological layering of the lithosphere. Soft, crustal layers will adjust by flow and, in response, shallow brittle layers will be disrupted. These effects may extend outwards from the centre of the impact structure up to several crater radii. Melosh (1989) refers to this phenomenon as '*viscous decay*'.

#### *The pre-impact cover thickness*

The sedimentary-volcanic sequence of the ring basin must correspond to the whole (or at least a major part) of the pre-impact cover sequence in the region. Its average thickness is estimated on the basis of stratigraphic thicknesses suggested by Fletcher and Reimold (1989) to about 15 km. This value is in good agreement with barometric estimates by Gibson and Wallmach (1995), based on pre-impact metamorphic assemblages in the Lower Witwatersrand Supergroup. The MC crater diameter and the cover thickness define, in essence, two other important dimensions: the TC diameter and the EC depth. According to scaling rules given by Melosh (1989), the transient crater (TC), corresponding to a final crater diameter of 250 km, would have had a diameter of about 125 to 162 km. Its depth at present can not be estimated: the relation of growth of the central rise with respect to crater diameter for large complex craters is still unknown; thus, the depth scaling found for smaller craters would lead to a severe over-estimation of the TC depth.

As the crystalline basement at the outer edge of the crater is currently exposed, the whole cover sequence as well as the sediments potentially accumulated in post-impact times within the basin must have been eroded to a considerable depth. Consequently, all of the cover of the central rise, including impact melt and ejecta, would now be removed as well. Erosion has cut deeply into the Vredefort Dome. Together with the pre-impact sedimentary-volcanic rocks, some alloigenic breccia, such as *suevite*, may, however, still be preserved in the ring basin.

#### *Estimation of the extension of shock effects*

The next step in the reconstruction of the Vredefort crater relies on the interpretation of the reflection seismic profile by Durrheim et al. (1991). In this publication, a marked lateral zoning of the seismic reflectivity of the crust (Figure 27) was noted, but remained

unexplained. In this study, the published reflection seismic section across the NW basin is used to identify the extension of shock-induced deformation of the crust around the point of impact. This provides a key to the energy imparted by the impact event. It will be shown in a sequence of figures how other important parameters related to the cratering process can, then, be deduced and how they are combined with the above-derived dimensions and the results of the gravity modelling. The results of this reconstruction are summarized in Table 7.

#### *Extent of the plastic deformation regime*

Figure 27 shows the interpretation of the Trans-Witwatersrand reflection seismic section by Durrheim et al. (1991), with the linear vertical scale being equivalent to the horizontal scale. The original TWT scale was, thus, stretched using the velocity-depth relations of the refraction seismic study by Durrheim and Green (1992). It was, then, assumed that the horizontal reflective pattern seen in the crystalline basement to the northwest is typical of the undisturbed crust. Inclined reflectors at the base of the crust (B) and in the upper crust (A) have, thus, been restored to a horizontal position and, in the case of the uppermost crustal reflector, joined (see also the alternative interpretation of this feature given below). The crustal velocity (and, thus, density or composition), equivalent to the gravity crustal background model, is marked with horizontal lines and represents the undisturbed crust.

In Figure 28, the observed terminations of reflective patterns are interpreted as the limit between shock-induced plastic and brittle deformation. Taking the lower crustal terminations as the characteristic measure, a depth extension of about 70 km is obtained for material, in which the HEL is exceeded. The outwards directed lobe in the upper crust is interpreted as the extension of that limit, for two reasons: 1) The presence of high temperatures where the felsic crystalline rocks have significantly lower viscosity (as compared to the mafic lower crust). This assumption is valid already on the basis of the increased radioactive decay, which, at 2 Ga ago, was twice as high as present conditions, in addition to the existence of a sedimentary cover with significantly lower thermal conductivity (conductivity values for some typical lithologies are given in Jones, 1988), which caused pronounced heating of the underlying crystalline basement. In addition, recent metamorphic studies (Gibson and Wallmach, 1995; Stevens et al., 1996) strongly suggest an elevated geothermal gradient within the Witwatersrand Basin and its environs at the time of impact. The felsic upper crystalline crust could, thus, be plasticized with relatively little additional energy, widening the extension of the HEL. 2) The compositional structure with sediments and felsic rocks (having a lower transition pressure to HEL) in the upper crust and mafic rocks in the lower crust (having a higher transition pressure, see Table 3.1 in Melosh, 1989) is significant. Both these effects will cause an outward shift of the HEL. Towards the surface, the location of the HEL can not be determined, but it must asymptotically approach the free surface at the site of the impact.

Inward terminating seismic reflectors have also been reported from the Siljan crater (Juhlin, 1991). In this structure, termination occurs well within the crystalline core, indicating less extension of the HEL and, as a consequence, a crater collapse within a mixed, outer brittle and inner plastic, regime. In the Siljan study these seismic reflectors were found,

**Table 7. Vredefort Crater Dimensions Resulting from this Modelling**

Parameter	Derived by	Calculated Value, km	Observed Value Comments
Final crater diameter	interpretation of extension of circular sedimentary basin	DF = 250 km	
Central rise width	0.19 ... 0.25 x DF	48...62	55
Potential central ring diameter	0.5 x DF	125	in NW basin remaining 12 km
Stratigraphic uplift	0.08 x DF	20	
Transient crater diameter	0.5 ... 0.65 x DF	DT = 125 ... 162	
TC depth	0.25 ... 0.33 x DT	39 ... 51	not applicable for complex craters
Crater rim height	0.036 x DT	HR = 4.5 ... 5.8	
Rim ejecta thickness	0.5 x HR	2.8	
Rim injecta thickness	0.5 x HR	2.8	
Width of rim rise	0.3 x DT / 2	39 ... 49 rise	
Continuous ejecta blanket	2.3 x DT	356	
Largest ejecta block size	0.3 x sqrt (DT)	4	
Largest terrace width	0.1 x DT	15	
Excavated crater depth	0.125 x DT	16 ... 20	
Pre-impact sedimentary Cover thickness		15	assumed on basis of geology
Melting depth	shock wave scaling central uplift density Granophyre density termination of lower crustal reflectors	12.5 ... 19 <15 <35	
Extension of HEL		70	
Volume of ejecta	see appendix for calculation	7 x 10 <sup>4</sup> km <sup>3</sup>	
Volume of injecta	" " " "	6 x 10 <sup>4</sup> km <sup>3</sup>	
Depth of erosion	whole sed. cover is eroded	>15	
Deepest part of excavated crater	0.22 DT	27 ... 36	
Formation time of TC	sqrt (TC/gravity)		1.9 min 3.8 min
Formation time of modified crater			
Upper limit of viscosity for central rise formation	See appendix for derivation	1 x 10 <sup>12</sup> Pa s	
Impact energy	see appendix for calculation	3 . 10 <sup>19</sup> J	
Seismic magnitude	see appendix for calculation	14	

**Table 8. Shock Pressures Needed to Exceed the Hugoniot Elastic Limit for Different Rocks  
(after Melosh, 1989)**

	GPa
Sediments	< 1
Granite	3
Granodiorite	4.5
Gabbro	ca. 6
Mantle rocks	9

**Table 9. Shock Pressures Needed to Melt  
Minerals and Rocks (after Melosh, 1989)**

	GPa
Quartz	50
Plagioclase	50
Pyroxene	40 to 65
Olivine	70
Typical crustal rocks	appr. 50
Typical mantle materials	appr. 70

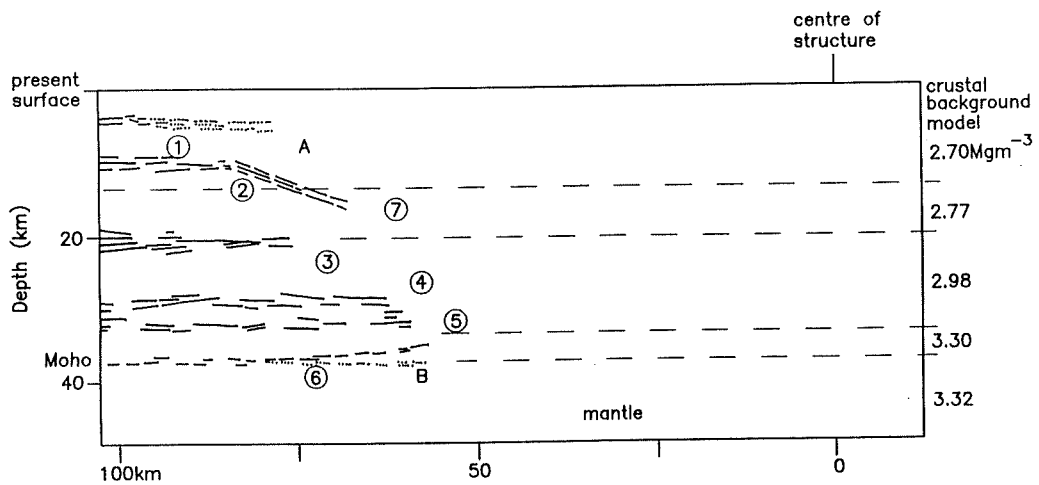


*Figure 27: Results derived from the NW-SE trending reflection seismic profile through the NW sector of the Witwatersrand Basin and extending into the central part of the core of the Vredefort Dome (after Durrheim et al., 1991). The original section has been converted to equal vertical and horizontal scales. All seismic reflectors are seen to terminate towards the centre of the structure (1-5). The lowest reflector (interpreted to be just on top of the Moho) has been brought back into a horizontal position (B) and the inclined reflector in the upper crust has been moved into an assumed original position (A) (see text for alternative interpretations).*

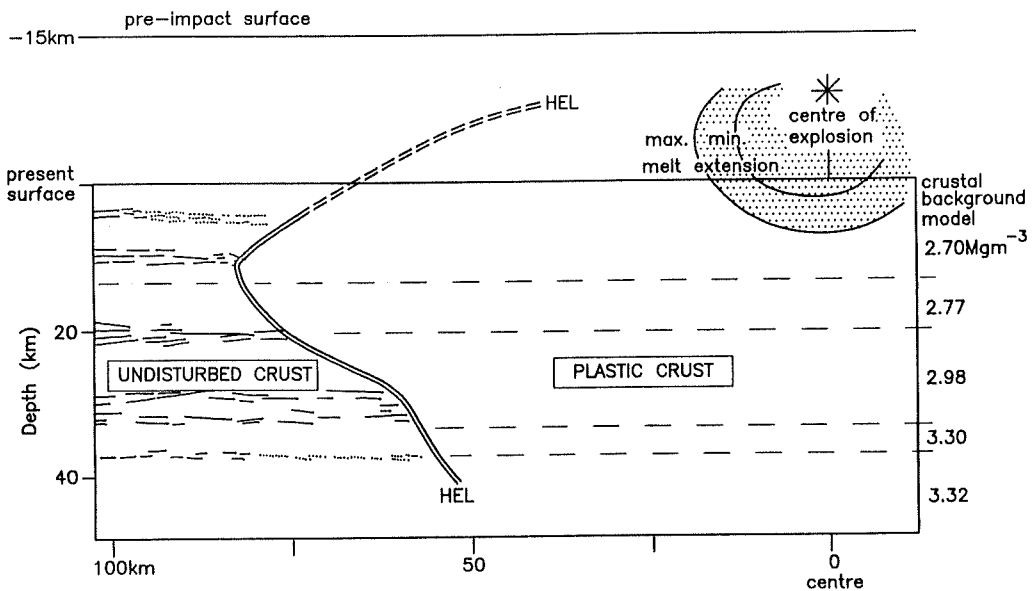


*Figure 28: The termination of seismic reflectors is interpreted as the boundary, inside of which rocks were brought above the Hugoniot Elastic Limit (HEL) by the shock wave. The outward bulge in the upper crust is caused by the enhanced thermal regime residing under an estimated cover of 15 km. Around the centre of explosion, shock melting occurs at a depth, which depends on the projectile density and velocity. These limits were calculated from the location of the normal HEL in the lower crust using the diagram relating projectile size and velocity to pressure given by Melosh (1989). The centre of explosion is located 5 km below the surface.*

by drilling, to be caused by mafic sills. [The termination of reflectors was, however, erroneously interpreted by Juhlin and Pedesen (1993) as an indicator of the position of the transient crater TC.]

#### *Estimate of the extent of melt formation*

The 70 km radial extension of the HEL provides a basis to estimate the potential extension of melt formation, the next higher degree of impact deformation (Figure 25B). Melosh (1989) related shock effects to projectile dimensions and velocities (his figure 5.3), thus providing a means to estimate a provisional range of projectile diameters or velocities. These, in turn, provide a range for the potential depth of melting. These estimates were presented for iron projectiles (the nature of the Vredefort projectile is of course uncertain) and an anorthosite-gabbro target composition (the density of which is comparable to that of lower crustal rocks). These conditions are appropriate for a HEL position in the lower crust. The generally felsic composition of the upper crust would require slightly less energy to melt. The derived melt limit is, therefore, a conservative value. This exercise results in an interval where the limit of melting is very likely to have occurred, and which is given by the curves marked 'max' and 'min' melt extension, respectively, in Figure 28).

The extension of melting can roughly be tested by a consideration of composition of actually identified impact melt dykes and the composition of their host rocks. The density of Granophyre of  $2.8 \text{ Mgm}^{-3}$  indicates a parent rock composition of intermediate  $\text{SiO}_2$  content, found at depths of about 20 km below the cover rocks (according to the velocity-density structure of the crust). The impact melt is, however, found within felsic rocks with densities typical for the uppermost crystalline crust. This observation can only be explained if the melt represents sources that once were located within the cover rocks or in the upper part of the crystalline basement, as melting down to 20 km below the cover would produce gigantic volumes of intermediate (e.g., dioritic) melt. This deduction is supported by the clast population in the Granophyre, which includes a large proportion of supracrustal material. It is, therefore, possible that melting only reached the uppermost part of the crystalline basement, which is in agreement with the minimum melt extension curve in Figure 28.

#### *Effects of the excavation flow*

It is now possible, by combining the parameters derived from modelling of the final crater dimension and the shock-induced zonation, to consider the subsequent evolution of the crater. Figure 29 shows the crater formation by the mass displacements described previously. The volume of spall of material from the upper, unshocked, cover rocks is considerable and is deposited as the basal ejecta sequence outside the crater, thus introducing a crater-related lithology which is atypical for the ordinary sedimentary cover sequences, but made up of similar material. The subsequently ejected material is mainly composed of shocked cover rocks, with extensive mixing of source lithologies, but generally building up a deposit in stratigraphically reversed order, in comparison with the original stratigraphic sequence of the cover strata. Melt bodies, mainly derived from crystalline strata within the cover sequence, may also be ejected. Melt from the crystalline basement (if any) will not be ejected, but stays in the crater as displaced masses lining the TC and injected deeper into the basement, outwards into the crater wall, and up into the sedimentary cover outside of the transient

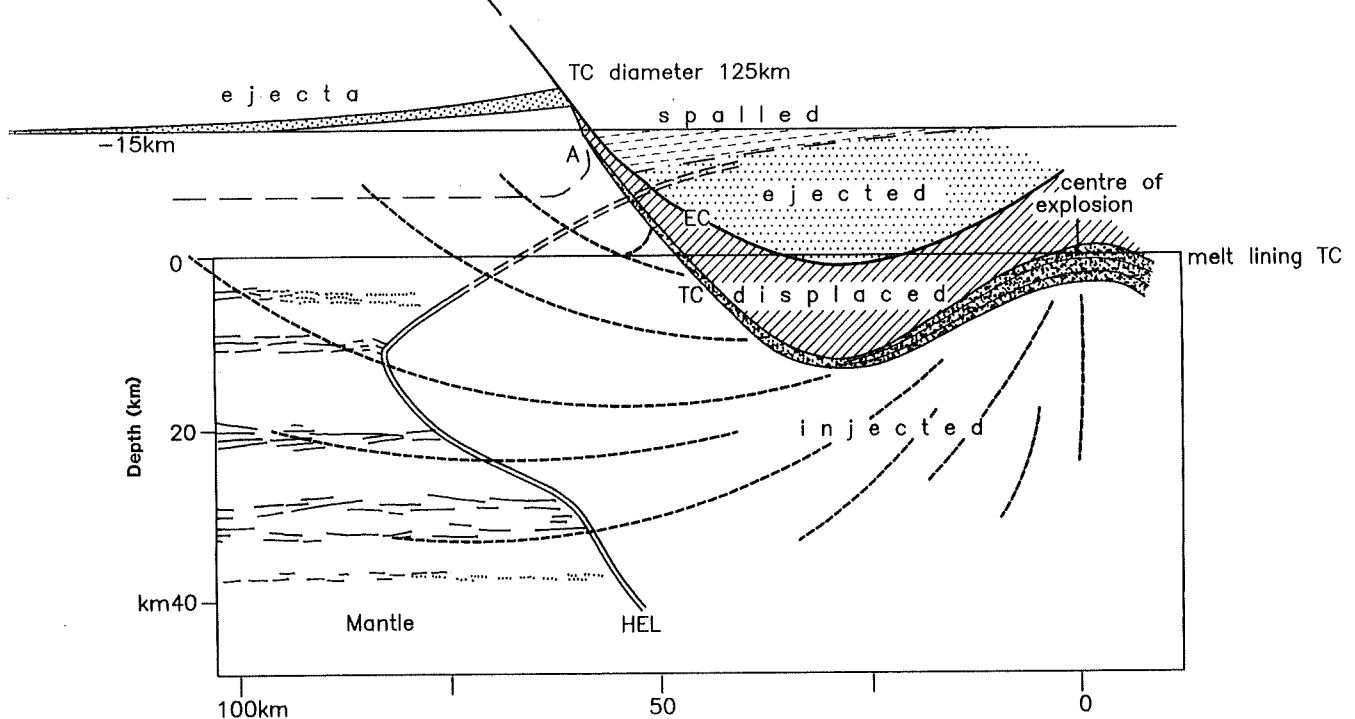


*Figure 29: The excavation and injection flow as derived from the estimated crater diameter and cover thickness. The spall regime is the source for unshocked ejecta. Flow lines, along which (in a very generalized way) material is moving away from explosion centre, were calculated using the flow model described by Melosh (1989). The position of the resultant free surface (the transient crater, TC) can only be approximated. Its most important aspect is the well developed central rise, which is already on its way up while the crater still expands laterally. Vertically under the explosion centre, material is just pushed into the basement and not ejected. Notice the upturning of cover and basement structures along the TC wall.*

crater. This injection follows the directions of flow lines, as indicated in Figure 29, which correspond to the flow model (Z-model with  $Z=3$ ) described by Melosh (1989). In this reconstruction, the most uncertain parameter is the shape of the TC and the position of the central rise at the moment when the excavation flow has ceased. Experiments cited by Melosh (1989) indicate that the central rise is well on its way before the crater is fully evolved laterally. The position of the deepest excavation reaches to at least 15 km depth - barely into the upper crust. This depth can be scaled against the radius of the transient crater with a factor 0.22 (for derivation of this quantity refer to Appendix II.).

#### *The collapse flow*

The position of the TC is critical for the next phase of crater evolution, the collapse of the transient crater. The collapse is initiated along the deepest flow surface cut by the TC floor, which will act as a detachment region for the mass influx. Still, a large portion of the crater surroundings behaves plastically with an outer load of ejecta covering a segment of brittlely deformed uppermost crust. For the formation of craters with a central rise, crustal viscosity must be less than a limiting value proportional to the crater size. For Vredefort, this limiting viscosity is estimated to about  $1 \cdot 10^{12}$  Pa s.

Figure 30 shows the reconstructed collapsed crater. Its accessible parts and the gravity modelling should confirm this reconstruction. The deepest flow surface cut by the TC defines the edge of the modified crater, when approaching the surface. The flow line model referred to produces a modified crater (MC) diameter that is twice the diameter of the TC. The collapsed masses fall into four different categories (labelled 1 - 4 in Figure 30): the essentially downward displaced cover rocks, the inward displaced cover rocks, the basement wedge above the detachment region, and the upwards displaced basement of the central rise, respectively. The oblique reflectors emphasized in the interpretation of the reflection seismic profile (Figure 27) align to the basal flow surface and can, therefore, be interpreted alternatively as either rock material (e.g., melt) injected during the excavation and injection flow, or as intense shearing in the basal detachment region, in addition to the inwards displacement and tilting of the uppermost reflector in the crystalline basement.

#### *Position of melt bodies after collapse*

The colliding flows from the rim collapse and the central rise collapse form the complexities of the collar of the central rise. The TC occurs now in at least two locations separated by the collar sequence. The lower TC position contains most of the impact melt lining and would constitute a conical, outwards dipping, structure ("dyke system"), which would be relatively enriched in clasts (or grading into fragmental breccia) at its base. Repetition of fragments of the melt lining may be produced by stacking of lithologies. Potentially, a melt sheet may have collected within the depression of the central rise (now eroded), from which melt dykes may intrude down into the basement. As all the mass flows occur within minutes, any larger melt body would only freeze at its margins and only fully crystallize in its final position after completion of the collapse. This scenario could also explain the contrasting observations that some Granophyre dykes contain clast-rich zones, an obvious formation process for which would be gravitational settling in a horizontal setting, on their eastern, others on their western, margin (Reimold and Colliston, 1994). Alternatively, some of these melt dykes could have formed by injection from a, now eroded, melt body on top of the central rise. The relatively undeformed state of these dykes suggests that this second hypothesis, which has also been favoured by Therriault (1992) and Therriault et al. (1996), is the most likely one. In this scenario, the crystalline core represents the solid rock volume below the melt zone, indicating that melting could have reached only into (but not below) the uppermost basement lithologies. This would confine melting to depths around 20 km. The more mafic composition of the Granophyre would, then, be inherited from lithologies in the uppermost basement or cover rocks (shales, greenstone remnants, intermediate-mafic intrusives) located within the zone of melting (Figure 28).

#### **Comparison with modelling results**

All impact-induced material flow is strictly ordered, with the only exceptions occurring at free surfaces, resulting in large volumes of neatly ordered lithologies. They have, however, been subject to plastic deformation and injection, changing their pre-impact nature significantly, especially towards the centre of the crater where the injection flow has been denser. It can also be noted that it is not required that the mantle was involved in the mass flow at all; its location is essentially unchanged. Only a slight rise of, at maximum, 4 km can be envisaged. The reasons for this are the rheologic layering (the upper mantle

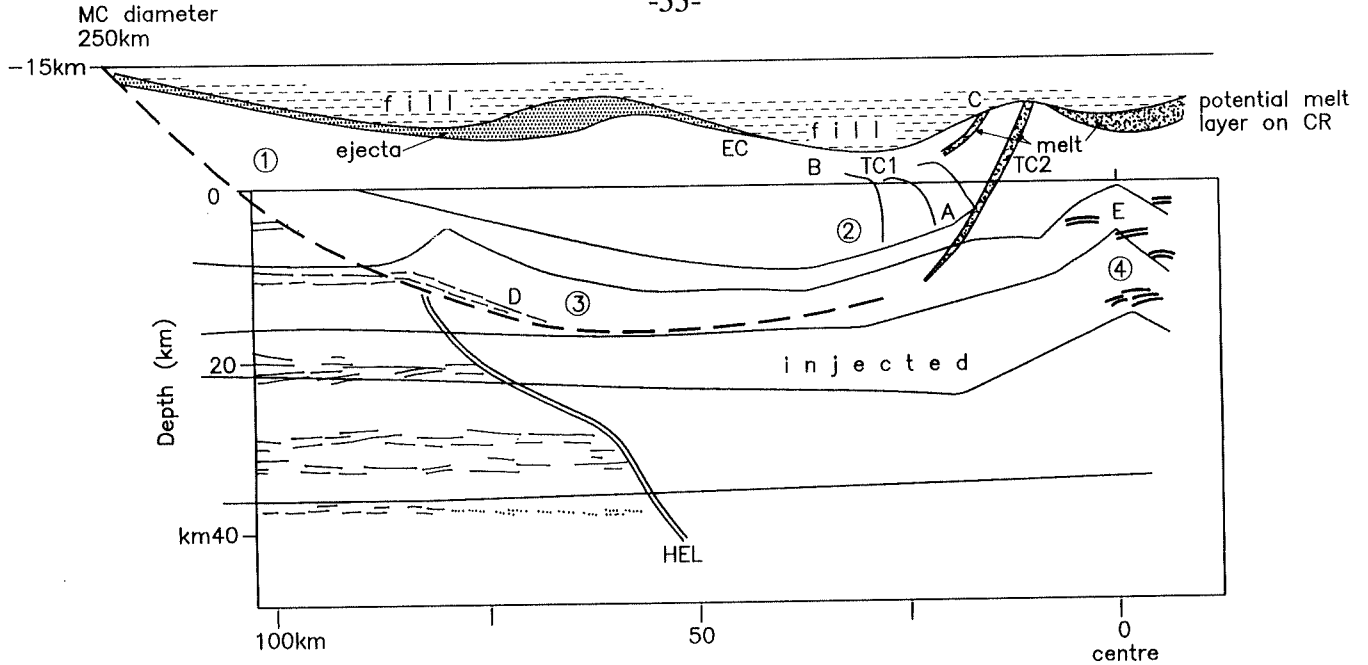


**Figure 30:** This diagram shows the collapsed crater which has widened to its final diameter. The collapse flow occurs mainly above a detachment zone related to the position of the TC, when the excavation flow is halted, and to the flow surface connecting this point with the perimeter of the modified crater. The collapse of the central rise is the last event in the modification flow. The central rise disperses discordantly against the incoming crater wall and may develop into a ring rise. The result is a complex repetition of the TC surface around the central rise perimeter. Potential melt volumes will occur along the TC and especially on top of the central rise. Displaced masses belong to 4 different categories: 1 - downfaulted brittle cover rocks, 2 - radially inward-displaced, mainly plastically deformed, cover rocks, 3 - inward-displaced, plastically deformed, basement rocks from the uppermost crust, and 4 - upward-displaced, plastically deformed, basement rocks from deeper positions of the upper crust and from the lower crust. The weak seismic reflectors interpreted by Durrheim et al. (1991) in the centre of the structure are marked. The main structural boundaries of the nearby (but not long this exact trend) located gravity model are shown for comparison.

having high viscosity) and the shock-induced rheologic changes, which concentrate the mass flow in the more plastic crust with drastically decreased viscosity.

The gravity modelling, in essence, confirms the reconstruction made by the combined approaches starting with the MC diameter of 250 km and with the HEL at about 70 km distance from the impact. All the basins surrounding the CR show a similar structure with a basement wedge approximately at 125 km radial distance, a basin depth of about 10 km, and overturned cover rocks, abutting against the crystalline basement, around the central rise, and the outer melt dyke in the basement being positioned in the extension of the lowest level of the TC. Figure 31 shows how the collapse flow and MC crater shape are related in section and in plan view, and Figure 32 summarizes how these results were constrained by observations. The complexity of the collapse flow makes all estimates of the crater extension based on shock criteria within the MC highly uncertain.

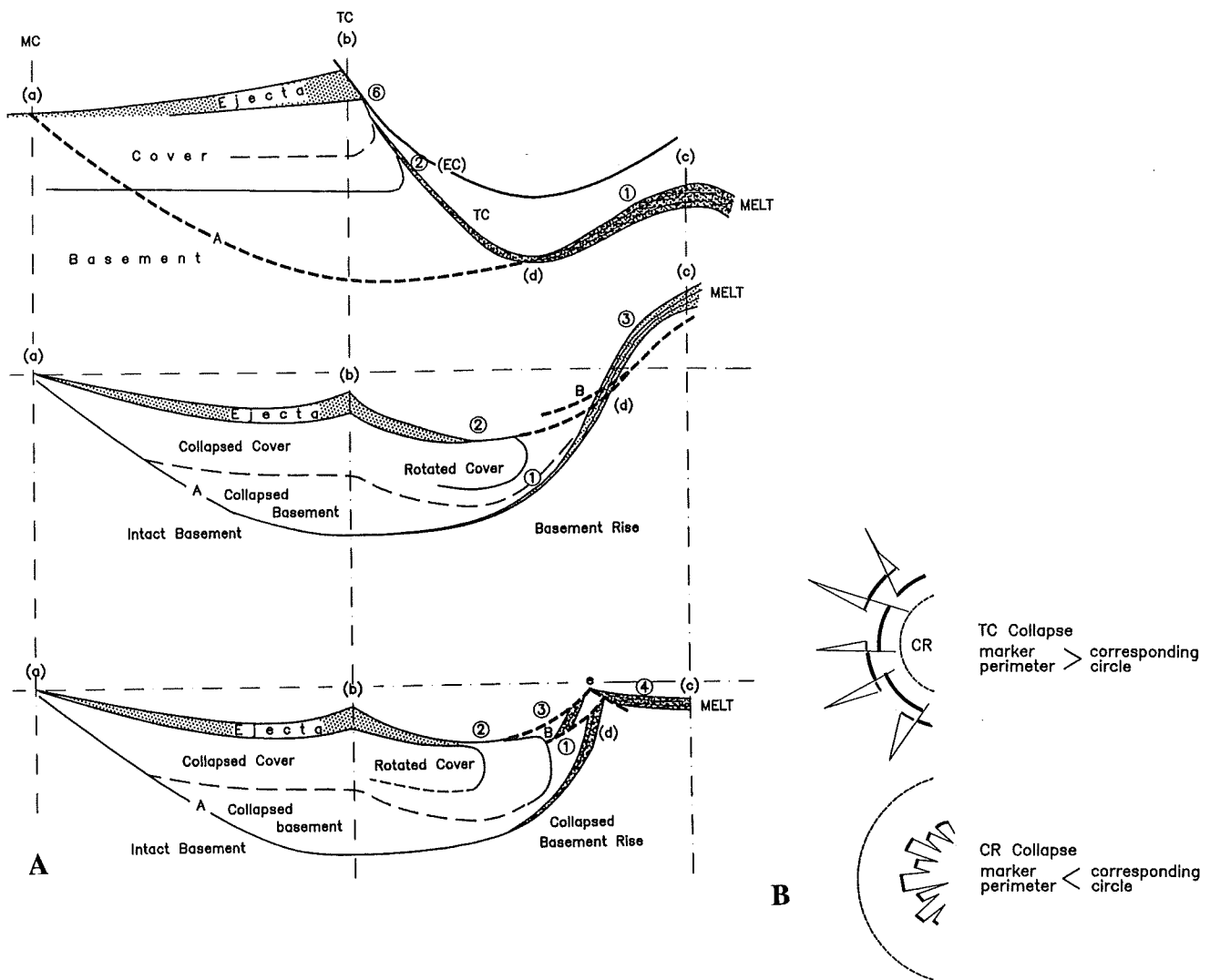


*Figure 31: Schematic description of the collapse flow and resulting structures.*

*A: Section showing the critical points (a,b,c,d), ie. the modified crater edge, the TC crater edge, the centre of the structure, and the point where the flow line joining (a) is intersected by the TC. Along the TC, melt will be concentrated around the central rise (region 1) and dispersed along the crater wall (region 2). Two detachment surfaces develop (A) along the flow line between a and d and (B) from the position of d, when the central rise starts to collapse. The resultant inward flow of the crater wall and the outward flow of the central rise eventually create a complex pattern of repeated strata. The melt from region 1, which originally was above point d (3), is now separated into an outward directed flow and a part collected on top of the central rise (4).*

*B: Plan view showing the effects of structural shortening of the inward-moving wall flow (resulting in marker perimeters larger than the corresponding circle and layer repetition) and the dispersion of the outward-moving central rise (resulting in marker perimeters smaller than the corresponding circle).*

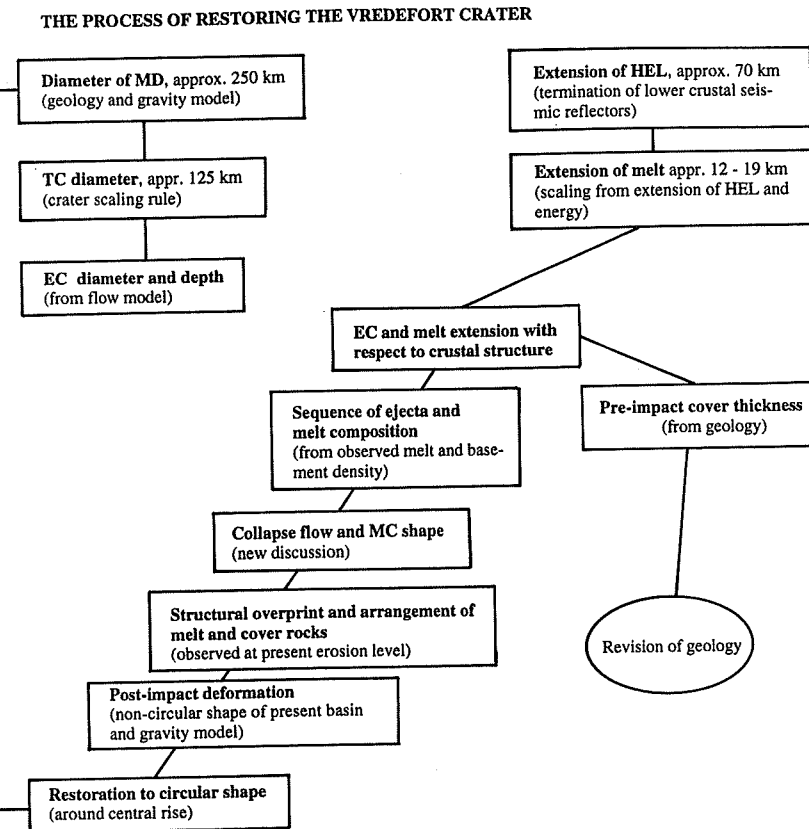


*Figure 32: Flow chart for the reconstruction of the Vredefort crater.*

Significantly, earlier attempts at estimating the original diameter of this impact structure, through scaling of the radial distances (from the center of the central rise), at which certain deformation features such as shatter cones, pseudotachylitic breccias, or shock-characteristic microdeformations in rock-forming minerals can still be observed, in comparison with empirical relationships derived from the study of other confirmed impact structures, have led to very similar values for the original diameter of the Vredefort impact structure: Therriault et al. (1993) suggested an original diameter between 180 and 300 km, but Therriault et al. (1995) revised this figure to 335 km. We wish to stress that our figure of about 250 km must be regarded as a conservative estimate, as, for example, the original (pre-impact) thickness of cover strata is not well constrained. An average thickness of the Witwatersrand-Transvaal Supergroups succession of about 15 km, as assumed in this study, was, for example, suggested by Fletcher and Reimold (1989). Note, however, that there are good reasons to consider the thickness of the cover strata with caution - as discussed below.

### **Characteristic geological features created by the crater-forming sequence of events**

#### *Shock effects and mass flow*

Figure 33 shows the shock-induced structure superimposed on a crust with lithologies similar to those in the central Kaapvaal Craton at about 2 Ga ago. Also shown are the different regions of typical mass flow during the subsequent excavation. The impact melt is seen to form mainly in the sedimentary cover and reaching the crystalline basement at A.

This level is dependent on the cover thickness and the impact energy. Intrusive bodies within the cover rocks and parts of the basement will contribute to the melt, while the sediments themselves are unlikely to form much melt. Along the surface, an outward increasing volume of unshocked cover rocks is spalled, forming the basal layers of a growing ejecta deposit outside the expanding crater. The ejected, shocked material is mainly derived from cover strata. A large portion of impact melt is not ejected out of the crater, but rather displaced along the evolving crater floor. A significant volume is injected into the basement. In the vertical direction, below the point of impact, the pre-impact layering of the crust will be preserved during the displacement. The outwards directed flow will, on the other hand, mix the different lithologies.

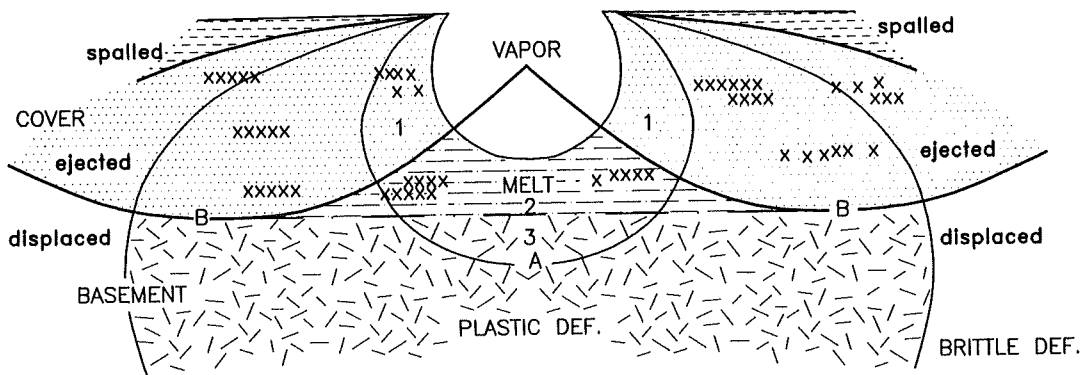


*Figure 33: Schematic detail of the region around the explosion centre showing spalled, ejected, and displaced volumes, separated by bold lines, together with a cover-base ment interface and the extension of shock zoning containing vapour (V), melt (M), plastic (P), and brittle (B) deformation of rocks, separated by thin lines. The position of the cover-base ment interface at (B) is critical for the formation of basement ejecta and the position of the melt-plastic deformation interface at (A) for the amount of basement-derived melt. The ejected melt (1) will be composed of cover rocks, whereas the displaced melt may be composed of cover-(2) and basement-(3) derived material.*

#### *Transient crater wall and rim*

Figure 34 illustrates what is thought to have happened along the evolving TC wall and rim. The ejecta will accumulate at the crater rim and early formed ejecta will be incorporated into later formed ones, as the crater grows. The ejecta arrive at the ground in roughly reversed stratigraphic order. They will contain a mixture of rocks deformed to different degrees of shock metamorphism, a mixture of shocked lithologies and melt volumes. The most typical rock type that is produced is suevite, a rudite containing mineral and lithic clasts, as well as fragments of melt (Hörz, 1965). The crater rim is gradually pushed outwards and near the ground it may move along thrust surfaces, as observed in the Popigai (Masaitis et al., 1975) and Ries (Stöffler and Ostertag, 1983; cf. also Chao et al., 1978) craters. These thrusts overrun and repeat ejecta layers and upper cover rocks. Along the TC, melt and breccia is dispersed and mixed, pushed down (with less mixing), and injected following a typical flow line pattern. This injection causes the rim to rise significantly. The

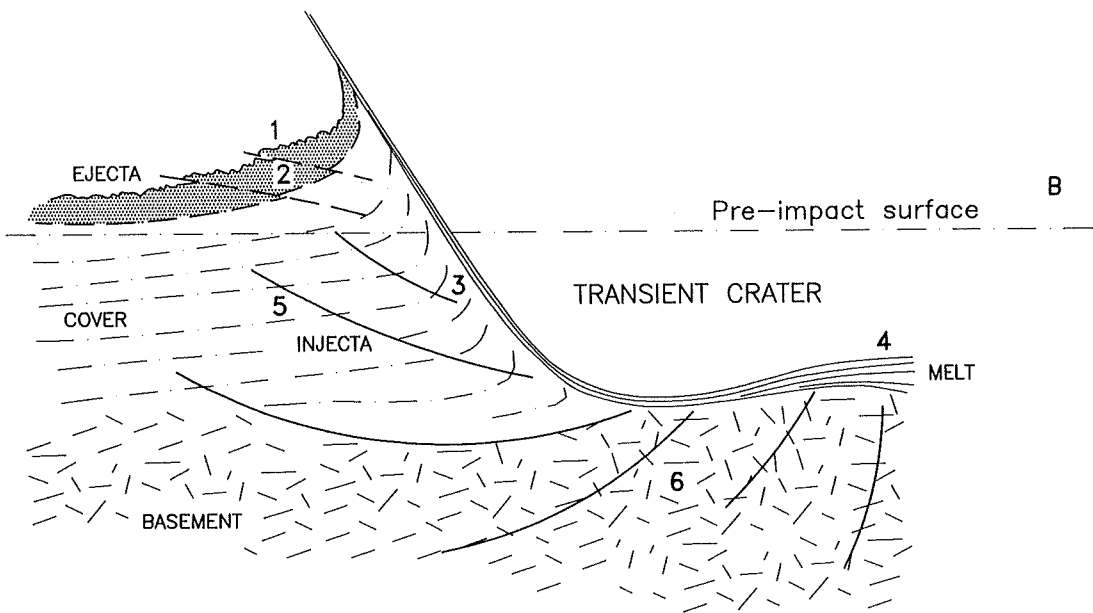


*Figure 34: Schematic detail of the evolving free surface (TC) and structures in the crater wall and on the crater rim. The spall flow deposits large plates of unshocked, but rotated, surface rocks as the first ejecta layer. These are followed by products from the excavation flow deposited essentially in reverse order of their original stratigraphic order. Outward thrusting of near-surface rocks and of ejecta may result in complex rim formations with basement overlying ejecta (2). The top layer (1) consists of material from the deepest level of excavation. The structures along the crater wall are bent upwards (3), where injecta cut the existing structures. These injecta cause the rim to rise. Melt occurs as coherent volume in the centre (4) and strongly dispersed along the crater wall. Below the evolving free surface, material is injected into the basement along the directions of flow lines. These are directed downwards at the crater floor (6) and upwards in the crater wall (5).*

excavation flow also bends structures upwards in a zone near the TC, including the cover-basement interface. The structures, either original or impact-generated, are cut by the injecta with angles that depend on their radial and vertical positions. The upward-directed injection flow, thus, may create ring structures dipping inward, while the downward directed injection flow may create structures dipping away from the crater centre. If the excavation reaches into the basement, an ejecta layer dominated by clasts of crystalline rocks will be deposited on top of the previously ejected cover sequence.

#### *Rim collapse*

Figure 35 represents the collapse features forming from the TC. The crust above the flow level tangential to the lowest position of the TC will flow into the crater. This flow level cuts the surface at about twice the TC radius and marks the lateral extension of the MC. Cover rocks with overlying ejecta and parts of the basement are rotated in blocks with inwards decreasing dimensions, building up a megabreccia (MB) formation with very complex structure (compare Figure 4 showing parts of the Siljan MB). Below the detachment

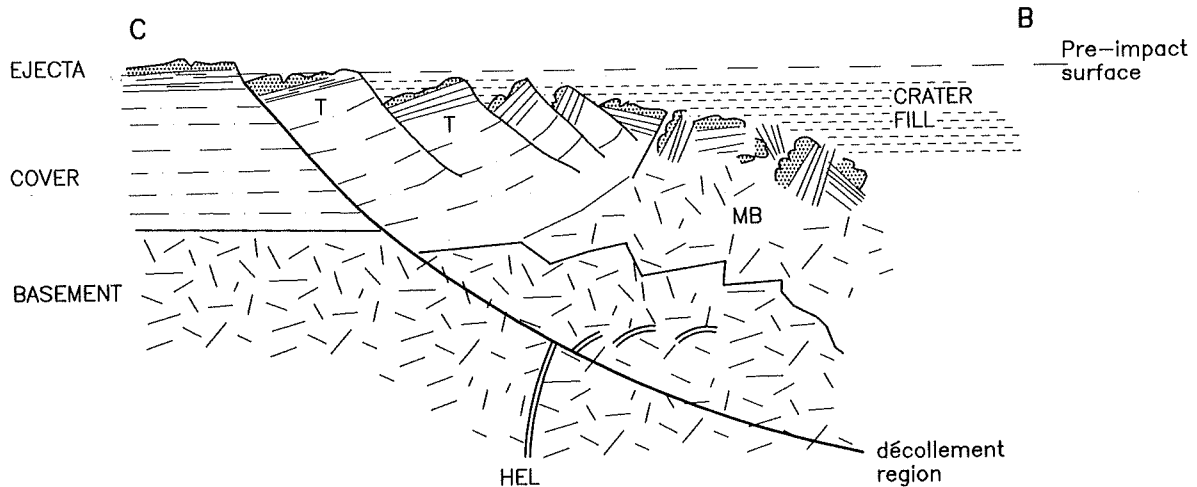


*Figure 35: Schematic detail of the collapse of the crater wall. Ejecta-covered surface rocks are downfaulted and form terraces (T), and are tilted with increasing angles towards the crater centre, where they form a megabreccia (M). Along the periphery, larger terraces form. Below the detachment region, the shock-induced deformation limit, the HEL, is preserved in its approximately original position. A ring morphology may appear in the position of the former TC rim (B). The final crater edge at (C) is covered with a thin ejecta layer. Sediments derived from erosion products of ejecta and basement may finally fill the impact basin.*

flow surface, the shock-induced features may be preserved in their approximately original position in the crater periphery. The injecta limit and the transition from plastic to brittle shock deformation may, thus, be seen in very deeply eroded craters. The inward flow of material would result in thickening, folding, or other tectonic repetitions of markers, thereby increasing their length over that of a corresponding circle. This detail was pointed out by Manton (1965) for the Vredefort Structure and by Wilshire and Howard (1968) for the Sierra Madera complex impact structure.

### *Central rise collapse*

Finally, Figure 36 is an attempt to envisage how the collapse of the TC evolves in the centre of the crater. A central rise (CR) evolves in the TC already during excavation/injection times, and it is usually assumed that its rise commences before the onset of the collapse phase. The timing of this phase with respect to the crater wall collapse is still unclear. It seems, however, that the central rise is the last feature to settle in the modified crater (MC). The return flow of the CR will, thus, meet the inflow of the crater wall, resulting in complex structures involving repetitions of both units. The outflow of CR material disperses marker horizons, which results in a shorter perimeter than the corresponding length of a circle. A ring-shaped CR may form by the stacking of lithologies. If a larger impact melt body existed at the bottom of the TC, it would now be found at the top of the CR. In the ring position, material from the CR return flow mixes and overruns material from the TC wall return flow, and repetition due to thrusting can be expected to occur (a three times repeated marker has been found in that position in the Siljan crater (Juhlin, 1991, and references therein).

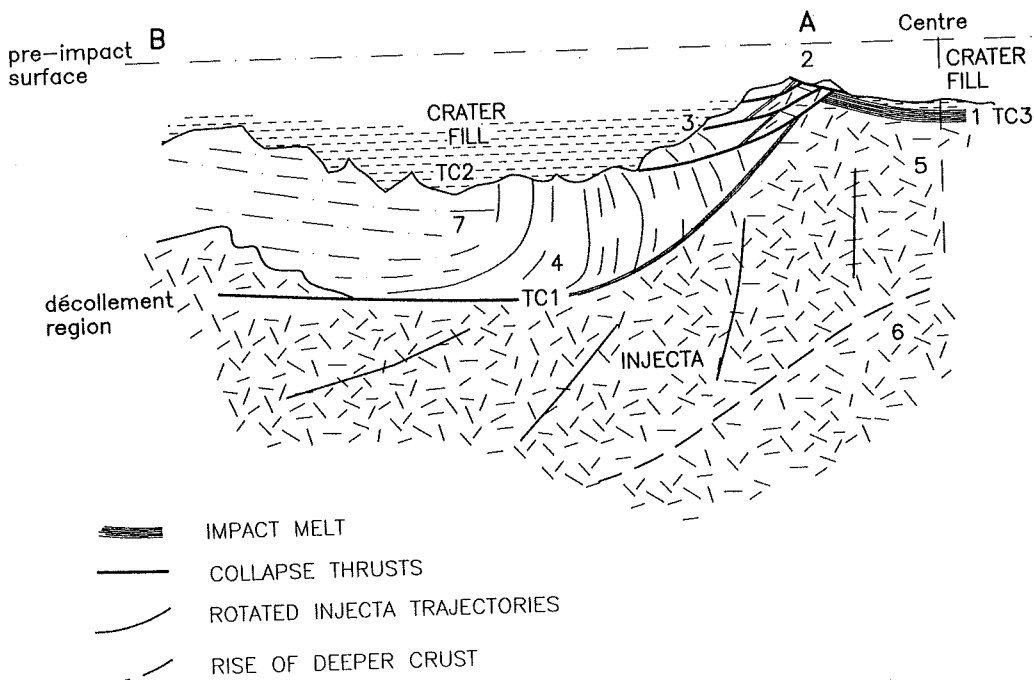


*Figure 36: Schematic detail of the collapse of the central rise. Melt covered basement rocks from an overheightened central rise collapse back into the crater and abut against the flow from the crater wall, which mainly involves cover sequences. The central part of the central rise collects a coherent melt body (1), which may intrude downwards to form dykes (5). A ring may appear at (A), on top of a complex thrust fan with repeated melt and basement sequences (3). Some of the collapsed rock mass slides towards the centre (2). The structures of the incoming crater wall are rotated into steep and overturned positions (4). The former crater wall is now essentially horizontal, and, at its top position, ejecta may adhere to blocks of cover rocks (7). The former TC rim may form a ring feature (B). In deeper parts of the central rise, deeper crust is brought into a higher crustal position (6). The complexity of the collapse flows results in repetitions of the former TC free surface (TC 1-3).*

The incoming crater wall is rotated by more than 90 degrees, which produces an overturned collar structure around the CR. The former TC floor is now represented several times: in the section containing the melt lining around the central rise (now under the wall sequence), the section containing dispersed melt and breccia lining the outer TC floor (now dispersed on top of the wall sequence), and as melt bodies from the collapsed CR, which has overrun that flow, making up the top unit. The structures in the former crater wall that were upturned by the excavation flow may now be seen as upward closing folds. Also the injection flow directions have been rotated, being differently oriented in different parts of the MC. Ejecta would remain on top of rotated blocks outside the collar sequence. Along a given erosion surface, the central rise will, from the TC location to the centre, exhibit a cross-section of the crust originally located below the interface between vapor and melt. This effect is caused by the downward directed mass flow during the excavation stage, which preserves the occurring lithologies from ejection. This cross-section is, however, severely distorted by large-scale injection and deformation to so far unknown depths.

### Remaining effects of the impact event on the crust

That a large impact event can create serious local changes of the Earth's crust is obvious. What is less clear, however, is how much of these changes could still be observed after 2 billion years of erosion. Stratigraphic effects typically observed in large impact structures include:

- preservation of large amounts of pre-impact cover rocks and underlying basement;
- significant ring basin subsidence, which may extend to great depths;
- the central rise brings deep crustal lithologies to a higher level;
- the central rise forms a deep-reaching structure.

It is, therefore, likely that a very large impact structure, formed in continental crust, is never fully erased from the Earth's crust - unless it would be completely destroyed by large-scale plate tectonic processes or a later, even larger, impact event. Large impact structures formed in oceanic crust may become subducted into the Earth's mantle within periods of a few 100 Ma.

Another specific aspect of large impact structures, which concerns the rearrangement of the post-impact crust, is that ejecta on crater rims are deposited in reverse stratigraphic order, compared to the stratigraphy of the pre-impact target geology. These inverted stratigraphic sequences constitute a significant thickness of the order of several kilometers and will, subsequently, become part of the ring basin, where they are progressively rotated to steeper orientations. While the transient crater (TC) expands, the rim region is displaced outwards by radial thrusting (as, for example, reported from the Ries and Popigai impact structures - Masaitis et al., 1975; Stöffler and Ostertag, 1983, respectively). This thrusting can, locally, repeat stratigraphic units. As ejecta are deposited simultaneously, a new layer of impact breccia may discordantly cover obliquely oriented layers, which are uncovered - or stacked - by thrusting. The rim region is, therefore, a place of very complex impact-related rearrangement of lithologies - creating a specific, new, stratigraphic sequence. This rim region will finally be part of the ring basin (RB). The first crater fill is related to the crater environs. In craters formed in continental settings, the crater fill will contain erosion-reworked ejecta transported down from all sorts of slopes. In craters formed in marine environments, an initial resurge deposit is followed by a crater-specific sequence of marine sediments, often of anoxic nature (Lindström et al., 1994). If, for example, the original cover rock was sandstone, neither ejecta nor redeposited ejecta would differ significantly from that sandstone; however, the total stratigraphic thickness may have increased considerably (see Figure 37).

Also within the ring basin, specific impact-related tectonic phenomena take place. An example for these processes from the Siljan Structure is shown in Figures 3 and 4. Large rotated blocks of brecciated cover rocks are re-assembled into a new formation, together with some impact melt and ejecta. Higher up in the stratigraphy, these breccias are followed by post-impact crater-fill sediments. Thinned and repeated (at Siljan, up to three times, Juhlin 1991) cover sequences line the lower part of the central rise. Within the rise region, the basement is strongly brecciated and a new lineation is typically observed in previously undeformed granites. When the oversteepened central rise collapses, the top units will slide radially outwards, overrun lower parts of the same units and, thereby, generate repetitions

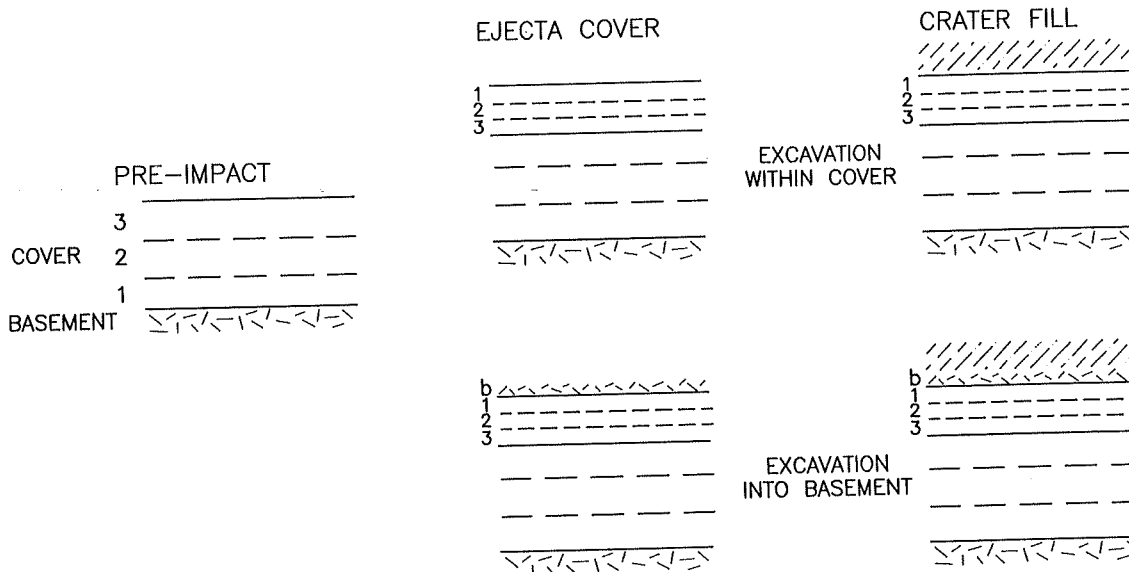


*Figure 37: An outline of the stratigraphic complexities, which can be expected to be created during modification outside of the crater rim. The original cover stratigraphy is, in essence, found to be reversed in the ejecta layer. A top layer of basement-derived breccia may occur, if the excavation flow cuts into the basement. The increased relief caused by the impact promotes the formation of an early crater fill mainly composed of reworked ejecta. It may, thus, appear as if there existed a much thicker than realistic cover sequence before impact (if the crater basin is interpreted as an ordinary sedimentary sequence). (Not to mention the potential of misinterpretation of the structural complexities induced by the impact).*

(also observed at Siljan). Pre-impact marker horizons may be rotated in a systematic way, together with impact injecta (so-called dyke breccias - e.g., Stöffler et al., 1979; Lambert, 1981), occurrences of which may extend outwards from the transient crater zone.

The estimated amount of ejecta from a 250-km-diameter Vredefort impact structure is about  $7 \cdot 10^4$  km<sup>3</sup>, which was deposited as a 1-2 km thick layer within the region of 1 transient crater radius outside of the TC. The amount of injecta is similarly impressive at about  $6 \cdot 10^4$  km<sup>3</sup>, which are expected to occur within the rim region up to ca. 1.6 TC radii from the centre, around and below the TC (for derivation of these values, cf. Melosh, 1989).

Durrheim et al. (1991) mentioned a series of relatively short, often convex, reflectors within the central rise (Figure 27). Such features are also known from the Siljan Structure (Juhlin, 1991), where they have been interpreted as flow features produced when the central rise formed, and, later, collapsed. Alternatively, these reflectors could represent pre-impact lithological contrasts, which could have been deformed during collapse of the central rise.

The authors propose that Durrheim et al. (1991) could have overestimated the thickness of the sedimentary-volcanic sequence under the overturned 'collar' around the central rise. The depth of the mega-breccia region around the central rise can certainly not be estimated on the basis of pre-impact stratigraphic thicknesses, as outlined above.

In Figure 29, a large region below the TC is labelled 'injected'. Injecta may also

occur outside of the TC wall, and injecta will also have occurred in the 10 km section of pre-impact cover rocks, outside of the transient crater region. Upon formation of the modified crater (MC), these injecta will become part of the mega-breccia formations. In addition, impact melt bodies can be expected to exist in the zone between the TC outline and the present central rise. The detachment of the RB from its basement was also noticed by Durrheim et al. (1991), who mentioned that faults observed in the sedimentary sequence did not distort seismic reflectors in the crystalline basement.

#### *Post-impact thermal effects*

Two specific post-impact thermal effects can be observed in very large impact structures. One is related to the central rise region, where deep crustal rocks are brought to higher positions in the crust (e.g., McCarville and Crossey, 1996). These rocks may have been at an elevated temperature, dependent on the pre-impact geothermal gradient in the impact region. Upon central rise formation, the elevated thermal energy will diffuse into the surrounding rocks, resulting in a radial thermal gradient. The regions from where the CR material originates are, on the other hand, cooled.

The other thermal effect is related to the thermal energy stored in an impact melt body and in the strongly shock-metamorphosed rocks below such a body. At its upper surface, this melt volume is in equilibrium with vapor and, thus, has a very high temperature, which exceeds temperatures of endogenically generated melts by far. At its bottom, the melt body is in equilibrium with shocked, plastically deformed, rocks of elevated temperatures. Dispersion of impact melt can be two-fold: first, a melt pool may accumulate above the central rise region and, second, impact melt may become intermixed with downfaulted cover rocks and ejecta/injecta in the zone surrounding the central rise. Heat will diffuse from a superheated melt body into the surrounding rocks, resulting in variably directed, local, thermal gradients, which eventually will grade into the general temperature, at least in the central parts of the MB, rise around the central rise region. Temperature may well rise above that in the sub-MB basement, and temperature distribution will take the form of an inverted thermal gradient. An impact melt layer on top of the central rise will induce a reversed thermal gradient down into the crystalline basement, further increasing its temperature above the already elevated level related to the uplift.

As a result of the new heat fluxes, extensive hydrothermal activity will arise in the megabreccia zone around the central rise, especially where, as in the case of the Vredefort Structure, fluid-bearing rocks are an important constituent of the regional stratigraphy. At this point, it is not clear which path fluids originating within the central rise region will take, as any assumptions concerning heat flow directions for this region are seriously hindered by the lack of information concerning the volume and locus of the main impact melt volume. It can, however, be stated that much of the hydrothermal veining in the core region has been attributed to Archean processes, but that weakly deformed vein quartz occurrences of up to several meters extent are known from various areas in the granitoid basement exposed in the core. It may be worth while to examine the fluid inclusion characteristics of such occurrences. It is likely, however, that fluids would have moved away from the heat source and, thus, flowed outwards from the central rise region into the surrounding ring basin.

In the central rise region, high temperature metamorphic changes may result in partial melting and extensive annealing. Both these features are well-known from large areas of the core of the Vredefort Dome. In addition, newly formed ferrimagnetic minerals may acquire a remanent magnetization upon cooling through their Curie temperature interval (Hart et al., 1995).

In recent years, significant evidence for hydrothermal activity, throughout the mineralized 'Witwatersrand Basin', at about 2 Ga ago has been collected (e.g., Boer et al., 1993, 1994; Frimmel, 1994; Trieloff et al., 1994; Reimold, 1994; various papers in Reimold, 1995b). Particularly the chronological data provided by Trieloff et al. (1994) strongly suggest that the Vredefort event was responsible for, at least, some, if not most of this activity, which apparently affected much of the mining areas in an arc surrounding the Vredefort Dome. While a serious effort to understand the nature and formation conditions of these fluids has already begun, it may be important to trace fluid characteristics from the mining areas towards the Vredefort Dome, the central rise region.

#### *Possible occurrences of impact breccias*

The Vredefort Dome is the type locality for so-called *pseudotachylite* breccia (Shand, 1916). Similar breccias have been observed, more or less abundant, in the basements to a number of other impact structures - and are a frequently observed feature of tectonically initiated fault or shear zones. Regarding the Vredefort impact structure, specific concentrations of such breccias are observed within the central rise, particularly in the granitoids of the core, and along major bedding-parallel faults in the ring basin (e.g., Reimold and Colliston, 1994). Many impact workers are convinced that the existence of massive breccia of 'pseudotachylite'-like appearance can be used as a diagnostic criterion for the recognition of impact structures. Unfortunately, at least one apparently tectonically generated occurrence of massive 'pseudotachylite' has been described by Camacho et al. (1995) from central Australia (and the occurrence of tectonically formed pseudotachylite in the Ivrea Zone contains, at least locally, massive developments of such fault breccia - S.Siegesmund, pers, commun, 1995). What is worse, a wide variety of breccia types, including cataclasite, mylonitic rocks, bona fide friction melt, as well as impact melt have been indiscriminately classified as 'pseudotachylite'. This is a flaw that has also become entrenched into the Vredefort literature. Reimold (1995a) reviewed this dilemma and resorted to calling the abundant breccias from the Vredefort Structure 'pseudotachylitic breccias', until a proper nomenclature would have been developed.

In addition to the well described 'pseudotachylitic breccias' from the Vredefort Dome and environs, several other breccia types are known from the Witwatersrand Basin. At several intervals within the stratigraphy of the Witwatersrand Supergroup, *diamictites* have been described (e.g., SACS, 1980). And that the Granophyre breccia locally occurring within the core of the Vredefort Dome represents impact melt, has already been discussed. In contrast, the literature does not contain any reports of other impact melt or alloigenic (e.g., suevitic) breccia occurrences from the region of the Vredefort impact structure yet.

## What is missing in the Vredefort Structure?

### *Ejecta*

In the modified impact crater (MC), a significant proportion of the rocks must consist of ejecta. Excavation flow will extend downwards to about 0.125 of the transient crater diameter (i.e., when assuming a 15 km thick pile of cover rocks, it would barely extend into the crystalline basement by a few kilometres). The largest part of the ejecta is, thus, made up of both shocked and unshocked cover sediments and volcanics, besides impact melt, which was mainly derived from these rocks (if any significant amount of impact melt was generated at all, cf. below). It may be difficult, if not impossible, to distinguish ejected unshocked cover rocks from their in situ equivalents, unless their textural properties (e.g., inverted stratigraphic settings which can not be related to tectonic folding) would indicate that they are 'out-of-place'. There should be, however, some discordant rock bodies, which, if they were recognized in the past, were probably related to faulting. So far, no ejecta have been identified in the MB basin, although they almost certainly exist.

### *Impact melt*

The other, largely missing lithology expected to be found in a large impact structure is impact melt. However, porous cover rocks are not likely to produce much impact melt, and carbonate-rich strata, such as the carbonates of the Transvaal Supergroup, must be expected to rather dissociate than to form melt (see Melosh, 1989). Support for this conclusion comes, for example, from the Ries Crater, where a relatively small melt volume (e.g., papers in Schmidt-Kahler, 1977) can be explained with the thick sedimentary cover in this region. Lack of a large impact melt volume is also a feature of the Lake St. Martin impact crater (Canada), where carbonates constitute an important component of the pre-impact stratigraphy (e.g., Reimold et al., 1990b). Significant impact melt volumes are generally associated with impact structures formed in predominantly crystalline target regions, or where consolidated metasediments and crystalline basement prevail.

The depth of impact melting in the Vredefort impact structure was estimated at up to 19 km below the explosion centre. Much of the melt formed from cover strata was probably ejected (compare Figure 29). In contrast, only a minor volume of the basement-derived melt would have been ejected. Some part of this melt would have been dispersed along the TC wall and, upon collapse of the central rise, the main part ended up on top of the CR, in the form of a melt complex possibly similar to that of the Sudbury impact structure (the Sudbury Complex - e.g., Stöffler et al., 1994; Deutsch et al., 1995). In the case of less deep melting (i.e., down to the lower limit of about 12 km from the explosion centre), no crystalline basement would have been melted and no melt complex could be expected. Regarding the composition of impact melt formed in the Vredefort event, the evidence at hand in the form of analytical data for Granophyre (e.g., Reimold et al., 1990a; Therriault, 1992) dykes in the core of the Vredefort Dome favours that much of the impact melt generated was extremely homogeneous. Significantly, impact melt bodies occurring in impact structures of widely variable sizes (<20 - >80 km diameters) have been reported to be characterized by very homogeneous compositions (e.g., Reimold, 1982 and papers ref. therein). However, comparing with the massive, heterogeneous impact melt volume of the Sudbury impact

structure, the original size of which at about 250 km (Deutsch et al., 1995) is of the same magnitude as the original diameter of the Vredefort Structure, may suggest a different scenario: chemically heterogeneous melt may be produced in the central parts of large craters, where the excavation flow is downward directed, whereas melt along the outer parts of the TC are homogenized. In order to better understand impact melt formation in the Vredefort impact event, it would be interesting to search for dispersed melt bodies in the ring basin. In this context it must be mentioned that the stratigraphy of the 'Witwatersrand basin' is characterized by an abundance of felsic to mafic intrusions. Most of the studied intrusions have been classified as pre-Vredefort or post-Vredefort magmatic formations, but several authors, in the past, invoked Bushveld-Vredefort related mafic intrusions. These would be the obvious candidates to pursue as possible impact melt formations.

### *Injecta*

Other types of impact breccias, such as suevitic or fragmental impact breccias (e.g., Stöffler et al., 1979) have, not been identified to date in the Vredefort Structure. This does, however, not mean that such breccias are completely absent. In the view of this new impact model for the region of the Witwatersrand basin, it is necessary to carefully reconsider the nature of any breccia occurring in and around the Vredefort Dome.

### *The Projectile*

Estimation of the size of the (asteroid or comet) projectile, which formed the Vredefort impact structure, results in figures around 5 to 10 kilometers diameter, with major uncertainties not only caused by the lack of knowledge of the type of material and, thus, its density, but also by the uncertain velocity of the bolide. Projectiles causing such large impact structures are generally believed to be nearly entirely vaporized. Therefore, any chance of recognizing traces of the bolide is reduced to searches for projectile-derived chemical contamination of impact breccia, especially impact melt breccia, and in distal ejecta. Such searches are further limited to attempts to identify slight enrichments of elements, which are generally enriched in extraterrestrial materials in comparison to their concentrations in crustal rocks. The elements most widely used are siderophile elements, such as Ni, Co, or Ir, as well as Cr (it is referred here to the extensive literature regarding the K/T Boundary impact). It is, however, in every case necessary to prove beyond doubt that no terrestrial source (for example mantle-derived rocks) could be responsible for enrichments of these elements, before a relationship to the projectile can be invoked.

Several chemical studies of the Granophyre (impact melt) did not reveal any significant enrichments of these elements (e.g., Reimold et al., 1990a and papers cited therein). However, a recent Re-Os isotope study of Granophyre by Koeberl et al. (1996) indicates an about 0.02% contamination from an extraterrestrial source.

It may be possible that some parts of this very large projectile were not vaporized and, instead, remained unshocked as spalled fragments. These parts theoretically could be dispersed among the ejecta and injecta, and could be, by good fortune, detected.

## "Impact tectonics" and metamorphism

### *The crater region*

In the case of relatively old impact structures, the regional tectonic history may be very complex. However, the strongest distortions observed in such areas would be associated with the impact event. Regarding Vredefort, the tectonic history must be unravelled with increasing time, through comparison of structural deformation in exposed parts of the impact structure with deformation styles in the wider environs that were not impact-affected. As the impact event will have rheological effects different from normal crustal tectonic processes, deformation of the crater interior will appear different from that outside of the impact structure.

For a long time after the impact event, the crust around the impact structure will adjust to the impact-generated stresses. In the region characterized by plastic and brittle shock-induced deformation, the crust behaves in a less cohesive manner. In consequence, deformation will tend to dissipate within this weaker part of the crust and spread over larger volumes (as compared to surrounding undisturbed regions) - thus minimizing the strain on single deformation structures, but multiplying their number. In this way, the crater will deflect the deformation patterns seen in the surrounding terrane. An instructive example is the Sudbury Structure, where exterior thrusts spread into a shear fan on reaching the crater formations (Pye et al., 1984 and references therin). A similar effect is actually seen in the northwestern sector of the Vredefort ring basin, where the crater edge has been pushed into the ring basin producing a large shear bulge (Figure 26). Within the crater, the traditional ways of interpreting metamorphic (pressure-temperature) effects must take into consideration the large-scale thermal anomaly created by the impact event. The central rise, for example, does not represent the extremely deep crustal section one would expect from the study of pressure-temperature indicators, when normal crustal layering is assumed. Instead, they represent relatively high crustal levels overprinted by an inverted thermal gradient (cf. also Stevens et al., 1996).

### *The ring basin*

Before any pre-impact tectonic patterns can be interpreted, the post- and syn-impact deformation patterns need to be understood. In the interior of the crater structure, all pre-impact deformation patterns have to be expected to be thoroughly overprinted and disrupted. Estimates of thicknesses of the original cover rocks based on traditional endogenic geological interpretation must be reduced with regard to the possibility of impact cratering-induced stratigraphic repetition - in the crater rim during formation of the transient crater and in the central rise during its collapse (cf. above). The processes leading to ring basin formation are also capable of repeating and/or rotating strata. In addition, all estimates of post-impact erosion, based on pressure-temperature estimates of exposed crust, must take into account the elevated temperature caused by the impact event in the original cover rocks. As both phenomena tend to result in overestimation of sequence thicknesses, a reduction of the presently assumed basin depths is inevitable. The gravity modelled basin depths are generally up to 30% less than previously anticipated (see paragraph on gravity model results).

In the 'Witwatersrand Basin', all tectonic features have been interpreted so far as endogenically produced phenomena. However, when examining the metasedimentary exposures even at the outer edge of the basin, surprisingly intense faulting, brecciation, fracturing, and - often observed - striation is noticed (for example, throughout the Johannesburg-Roodepoort-Krugersdorp area in the northeast). It has been known for a long time that the present basin is complexly deformed and that much of this deformation is related to post-Transvaal processes (e.g., McCarthy et al., 1986, 1990; Roering et al., 1990). However, despite intense study, no comprehensive tectonic model for either the basin-wide deformation or the existence of the central rise has been put forward. It is noteworthy that some published local cross-sections from areas of the Basin are comparable to typical megabreccia patterns with discontinuities and block rotations (compare, for example, Figures 38, after Roering et al., 1990), closely resembling the chaotic arrangement of blocks in the ring basin of the Siljan impact structure.

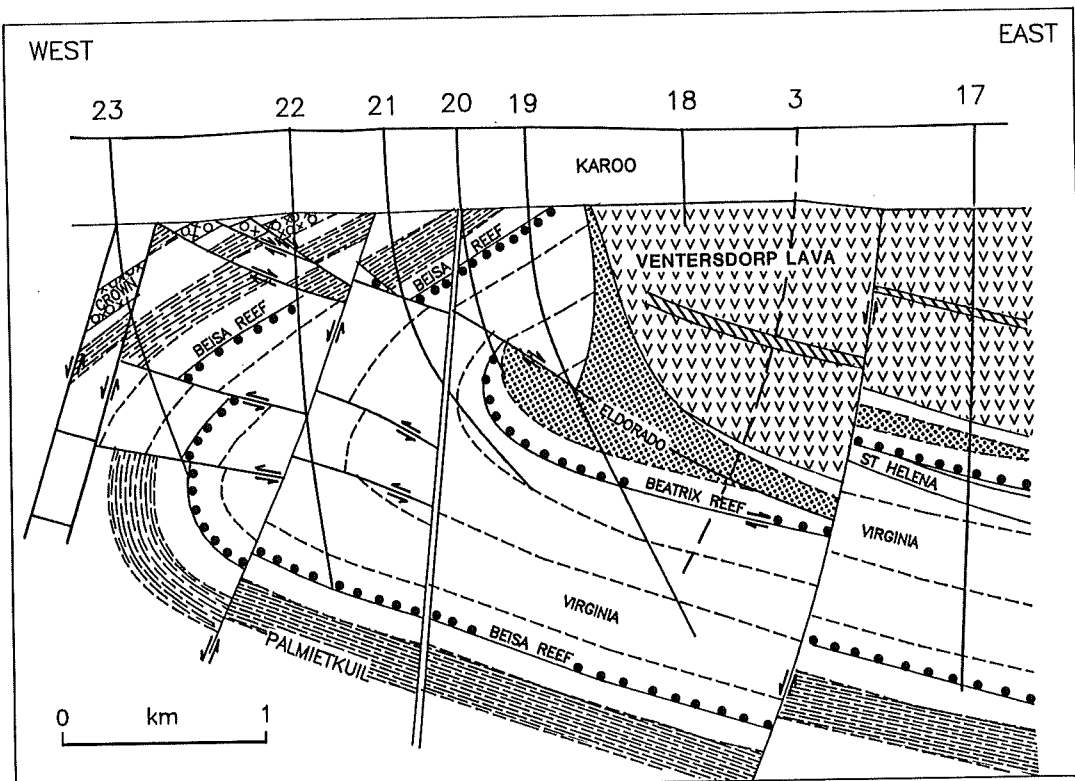


*Figure 38: A section through a mine in the southwestern part of the Witwatersrand Basin. Beisa Gold and Uranium Mine: The structural pattern shown resembles the complex megabreccia structure of an impact ring basin. Folding is essentially inferred and not seen where drilling cuts the actual geological structure, so that instead, faulting is exclusively observed. After Roering et al. (1990) and Tweedie (1986).*

#### *The central rise*

The few available structural geological treatments of the central rise or parts of the central rise of the Vredefort Structure (Stepto, 1979, 1990; Brink, 1986; Colliston, 1990; Colliston and Reimold, 1990; Minnitt et al., 1994) have emphasized the brittle-ductile

deformation patterns seen in the high grade crystalline rocks. These have conventionally been attributed to pre-impact Archaean tectonics. In order to confirm that this is correct, the tectonic effects of the modification stage of the impact event need to be assessed. As the basement rocks were at significantly elevated temperature, any deformation will largely have been of ductile nature. Additional characteristic features of the CR are 1) the injection of a large volume of material along steeply inclined flow lines (vertical in the centre), pushing aside pre-existing rocks, and 2) the collapse of the CR piling up a ring rise feature of stacked and dispersed lithologies. The injected material may contain cover units, as well as melt and breccia volumes. Dispersed melt bodies of variable small sizes that formed below the crater floor by the passage of the shock wave may become deformed along the CR flow pattern.

There is, so far, no case known where a sufficiently large central rise region could be studied in tectonic detail, although some useful data exist (e.g., from the drilling of the Siljan Structure - Juhlin, 1991 - and the Puchezh Katunki Structure - Masaitis et al., 1994). At Sudbury, the high grade metamorphic envelope below and outside of the impact melt complex has been attributed to the effects of the impact event; this includes formation of secondary melts in the granulite facies basement rocks (Pye et al. 1984). Similar melting, on a local scale, has also been observed in the core of the Vredefort Dome and has been attributed to local compression or decompression melting induced by the impact event (Dence, 1985; Hart et al., 1991; Stevens et al., 1995, 1996).

Impact-induced flow patterns are potentially revealed by foliation and lineation trends in central rise rocks, by folding, and flow- or shear-induced layering. So far, such features have not been interpreted in terms of impact-related tectonics. The entire Siljan central rise, comprised predominantly of granitic rocks, is striated in a characteristic way with a radially symmetric orientation (Figure 39). Pre-impact ductile tectonic patterns will, with certainty, be reactivated by impact deformation, resulting in new lineations and rotation, and, in places, completely new structural patterns.

## SUMMARY AND CONCLUSIONS

In summary, the following strategy was used for the modelling of the Vredefort Structure:

- Available refraction seismic data provided constraints for the background crustal density structure;
- reflection seismic data were used to identify the onset of impact-induced deformation;
- surface geology and measured rock physical properties provided further constraints for the modelling calculations.

This was followed by an attempt to reconstruct the Vredefort impact structure following the procedures detailed in the flow chart for this process (Figure 32). As there are large uncertainty limits for any parameter estimated, those estimates that, wherever possible, best reproduced the observed situation were chosen. In this regard, the position of the shock-induced HEL is critical. The present interpretation that rocks, which were driven beyond their HEL, will lose their structure (as seen in the seismic reflectivity patterns) should be tested in other impact structures, as, so far, it is only supported by the findings from the approximately 60 km diameter Siljan crater (Juhlin, 1991) and appears to be consistent with



*Figure 39: Granitic rock from the central rise of the Siljan crater showing typical penetrative striations formed either by the shock wave (plastic deformation region) or during the central rise and collapse flows. Photograph by H. Henkel.*

our results for the Vredefort Structure. For very large craters, this limit may provide the only potentially undisplaced indicator, at depth, of the original shock-induced structure.

The results<sup>1</sup> of our attempt to reconstruct the original Vredefort impact structure are summarized in Table 7. The pre-impact cover thickness is probably the most uncertain estimate, which has direct consequences for how deeply the excavated crater and the zone of impact melt generation extended into the crust. A lesser cover thickness would result in more crystalline ejecta and a larger melt volume derived from crystalline rocks. The crater collapse flow was modelled by us in a new way (Figure 31), based on the following critical geometric relations: (1) That the wall influx occurs essentially above a detachment region

following the deepest flow surface (of the excavation/injection flow) that is cut by the transient crater, and (2) that the central rise collapse evolves into thrust stacking along its inflection perimeter upon meeting the wall collapse flow. As a consequence, the TC free surface, at the onset of the wall collapse, has an already well developed central rise.

The following impact-generated structural features appear to characterize the Vredefort impact structure:

- A very complex structure is likely for the ring basin (as already seen along its periphery);
- hydrothermal alteration may be extensive throughout the whole basin;
- the central rise structure is also very complex and represents a real challenge to distinguish impact-related from older deformation features;
- the crust-on-edge model does not satisfy the modelling results, as only the succession of collar strata is found to be on-edge;
- there is no apparent support for the assertion that mantle material could have been significantly uplifted - not even a significant perturbation of the Moho is indicated (in contrast to what has been frequently quoted for very large terrestrial craters).

This modelling study showed that

- the entire preserved part of an originally sedimentary Witwatersrand Basin represents the eroded remnant of an impact structure;
- the Vredefort impact structure has been significantly distorted by post-impact tectonics, with the exception of its central part, where structures are in their impact-determined positions; this conservation effect is related to the long-lasting rheologic weakening of the crust affected by the impact event;
- the impact structure was probably formed in a thick cover sequence, a fact that minimized the shock deformation of the crystalline basement and resulted in a limited production of melt;
- the impact crater formed almost entirely within crust that was above its HEL, which resulted in a crater structure that was extensively modified due to viscous decay;
- the remaining structural uplift is about 12 km, a value which was calculated from the position of intracrustal interfaces around the central rise in the gravity model;
- a profound thermal aureole is seen in and around the central rise, which was the cause of resetting of the remanent magnetization of all involved rocks;
- erosion has been moderate, in essence removing the cover rocks surrounding the crater and the potential crater fill, but leaving the amazing thickness of up to about 13 km of pre-impact cover rocks in the ring basin;
- the southeastern part of the structure was up-tilted, resulting in the different appearance of the central rise collar in the southeastern and northwestern sectors, and in the lesser thickness of remagnetized rocks in the southeastern part of the core of the central uplift;
- in consequence, the present shape of the central rise is not the result of compressional tectonics, as proposed by Colliston (1990);
- the mantle was not involved in the formation of the impact structure (ultra-mafic rocks in the central rise region must, therefore, be related to crustal evolution);

- the interface between felsic upper crust and mafic lower crust is not exposed in the central rise - which is contrary to the crust-on-edge model;
- high-grade metamorphic zoning is most likely the result of a combination of pre-impact thermal conditions and thermal overprinting due to the impact event.

A new model was tested for the collapse flow of large craters (a necessary step in the reconstruction of any crater event starting with a transient crater), which demands early onset of the development of a central rise already during the excavation stage. In consequence, the TC depth calculation on the basis of a parabolic geometry (which is also the reason for the belief that the mantle must have been involved in the formation of the Vredefort impact structure) can not be applied for very large craters.

The determination of the position of the HEL is a new aspect in the reconstruction of large craters. It is very likely that the onset of plastic behaviour at the HEL is responsible for the termination of undisturbed crustal reflective patterns (as seen in reflection seismic data from the Siljan and Vredefort structures). This limit is also the only geometrically preserved shock structure, as material closer to the impact centre has been strongly radially and vertically displaced by the collapse flow. The arrangement of shock indicators along any erosion surface can, therefore, not be used to assess the extension of the shock structure (unless properly reconstructed).

Further study of the Vredefort structure has great potential for enhancing our knowledge of the physical processes governing the formation of large terrestrial impact structures. This structure provides a unique window into the deeper level of the central uplift region of a large, complex impact structure. In addition, the new and completely different view of the Witwatersrand Basin as the remnant of an impact basin demands thorough reassessment of the tectonics of this region (for example with regard to separation of pre- and post-impact structures), study of the hydrothermal system generated by the impact event, and reevaluation of known metamorphic data, and further detailed metamorphic studies - not only of the Vredefort Dome, but along radial traverses into the surrounding basin. Comparison with the structural and metamorphic situations in and around other large terrestrial impact structures, such as the Sudbury Structure in Canada and the Uppland Structure in Sweden, will provide invaluable information concerning formation and evolution of large, complex, impact structures and their "environmental" effects. Continued detailed mapping, reexamination of drillcore, and metamorphic and fluid studies will contribute much valuable data for a better understanding of the Witwatersrand Basin and of impact cratering in general.

#### ACKNOWLEDGEMENTS

The authors would like to thank the following persons who have directly contributed to this study: Dr Luc Antoine of the Department of Geophysics at the University of the Witwatersrand for the preparation of gravity and magnetic profile data and for invaluable discussion; Dr J. Stokes for the computation and graphics of the flow model; Dr. Richard Viljoen (Consulting Geologist, Gold Fields of S. Africa Pty. Ltd.) for his interest and support, especially for making available important drilling information and geophysical data; Mr. P. Fletcher, for sharing some of his stratigraphic knowledge with us; Mr. Andy Friese for discussion of the vibroseis data for the southeastern sector of the Vredefort Dome; and

Ms. Sharon Saedt (Gold Fields of S. Africa Pty. Ltd.) for providing the gravity image shown as Figure 10. Lyn Whitfield and Di Du Toit supported us with the drafting of numerous figures, and Henja Czekanowska assisted with photography. Drs. Luc Antoine and Roger Gibson critically read an earlier version of this manuscript and their comments are much appreciated.

## REFERENCES

- Andreoli, M.A.G., Ashwal, L.D., Hart, R.J., Smith, C.B., Webb, S.J., Tredoux, M., Gabrielli, F., Cox, R.M., and Hambleton-Jones, B.B., The impact origin of the Morokweng Ring Structure, southern Kalahari, South Africa (abstract), *Cent. Geocongress, Geol. Soc. S. Afr.*, Johannesburg, Ext. Abstr., 541-543, 1995.
- Antoine, L.A.G., Nicolaysen, L.O., and Niccol, S.L., Processed and enhanced gravity and magnetic images over the Vredefort structure and their interpretation, *Tectonophys.*, 171, 63-74, 1990.
- Bisschoff, A.A., The petrology of the igneous and metamorphic rocks in the Vredefort Dome and the adjoining parts of the Potchefstroom Syncline, *Ph.D. diss.*, Univ. of Pretoria, Pretoria, 230pp. (unpubl.), 1969.
- Bisschoff, A.A., The dioritic rocks of the Vredefort Dome, *Trans. Geol. Soc. S. Afr.*, 75, 31-45, 1972a.
- Bisschoff, A.A., Tholeiitic intrusions in the Vredefort Dome, *Trans. Geol. Soc. S. Afr.*, 75, 1972b.
- Bisschoff, A.A., The petrology of some mafic and peralkaline intrusions in the Vredefort dome, South Africa, *Trans. Geol. Soc. S. Afr.*, 76, 27-52, 1973.
- Boer, R.H., Reimold, W.U., and Graney, J.R., Physico-chemical conditions of gold remobilization in the Ventersdorp Contact Reef, Witwatersrand Basin, in: *The VCR Revisited*, Carletonville, West. Transv. Branch, Geol. Soc. S. Afr., 92-94, 1993.
- Boer, R.H., Reimold, W.U. and Kesler, S.E., Conditions of gold mineralization in the Ventersdorp Contact Reef, Witwatersrand Basin, *Cent. Geocongress, Geol. Soc. S. Afr.*, Johannesburg, Ext. Abstr., p.696, 1995.
- Brink, M.C., Tektoniese en stratigrafiese ontwikkeling van die Witwatersrand-Supergroep en verwante gesteentes in die gebied noord en oos van Klerksdorp, *Ph.D. diss.*, Randse Afrikaanse Universiteit, Johannesburg, 317pp. (unpubl.), 1986.
- Carmichael, R.S. (Ed.), Practical Handbook of Physical Properties of Rocks and Minerals, CRC Press, Boca Raton, Florida, 741 pp., 1989.
- Chao, E.C.T., Hüttner, R., and Schmidt-Kaler, H., Principal exposures of the Ries meteorite crater in southern Germany, Geol. Surv. Bavaria, 84pp., 1978.

Coetzee, H. and Kruger, F.J., Geochronology and Sr-isotope geochemistry of the Losberg Complex and the limits of Bushveld Complex magmatism, *S. Afr. J. Geol.*, 92, 37-41, 1989.

Colliston, W.P., A model of compressional tectonics for the origin of the Vredefort structure, *Tectonophys.*, 171, 115-118, 1990.

Colliston, W.P. and Reimold, W.U., Structural studies in the Vredefort Dome: Preliminary interpretations of results on the southern portion of the structure, Univ. of the Witwatersrand, Johannesburg, *Econ. Geol. Res. Unit Inf. Circ.*, 229, 31p., 1990.

Corner, B., Crustal framework of the Kaapvaal Province from geophysical data (abstract), *Abstr. Proterozoic Crustal and Metallogenic Evolution Conf.*, Windhoek, p.9, 1994.

Corner, B. and Wilsher, W.A., Structure of the Witwatersrand basin derived from interpretation of aeromagnetic and gravity data, in: *Exploration '87, Geol. Surv. Can. Spec. Vol.*, 3, 532-546, 1989.

Corner, B., Durrheim, R.J. and Nicolaysen, L.O., Relationships between the Vredefort structure and the Witwatersrand basin within the tectonic framework of the Kaapvaal craton as interpreted from regional gravity and aeromagnetic data, *Tectonophys.*, 171, 49-61, 1990.

Corner, B., Reimold, W.U., Brandt, D. and Koeberl, C., Evidence for a major impact structure in the Northwest Province of South Africa - The Morokweng impact structure (abstract), *Lunar Planet. Sci.*, XXVII, 257 - 258, 1996.

Dence, M.R., Axial melts in central peaks of complex impact structures, *Meteoritics*, 20, 635-636, 1985.

Deutsch, A., Grieve, R.A.F., Avermann, M., Bischoff, L., Brockmeyer, P., Buhl, D., Lakomy, R., Müller-Mohr, V., Ostermann, M., Stöffler, D., The Sudbury Structure (Ontario, Canada): a tectonically deformed multi-ring impact basin, *Geol. Rdsch.*, 84, 697-709, 1995.

Duane, M.J. and Kruger, F.J., Geochronological evidence for tectonically driven brine migration during the Early Proterozoic Kheis Orogeny of Southern Africa. *Geophys. Res. Lett.*, 18, 975-978, 1991.

Durrheim R.J., Nicolaysen, L.O., and Corner, B., A deep seismic reflection profile across the Archean-Proterozoic Witwatersrand basin, South Africa. Continental Lithosphere: Deep seismic reflections. *AGU Geodynamics Series*, 22, 213-224, 1991.

Durrheim R.J., and Green, R.W.E., A seismic refraction investigation of the Archaean Kaapvaal craton, South Africa, using mine tremors as the energy source. *Geophys. J. Int.*, 108, 812-832, 1992.

Fletcher, P. and Reimold, W.U., Some notes and speculations on the pseudotachylites in the Witwatersrand Basin and the Vredefort Dome, *S. Afr. J. Geol.*, 92, 223-234, 1989.

French, B.M., Orth, C.J. and Quintana, L.R., Iridium in the Vredefort Bronzite Granophyre: impact melting and limits on a possible extraterrestrial component, *Proc. 19th Lunar Planet. Sci. Conf.*, 733-744.

Friese, A.E.W., Charlesworth, E.G. and McCarthy, T.S., Tectonic processes within the Kaapvaal Craton during the Kibaran Grenville orogeny: Structural, geophysical and isotopic constraints from the Witwatersrand Basin and environs, Univ. of the Witwatersrand, Johannesburg, *Econ. Geol. Res. Unit Inf. Circ.*, 292, 67p., 1995.

Frimmel, H., Metamorphism of Witwatersrand Gold, *Explor. Mining Geol.*, 3, 357-370, 1994.

Geovista, GMM Gravity and magnetic modelling, Users Manual, Geovista AB, Luleå, Sweden, 41pp., 1994.

Gibson, R.L. and Wallmach, T., Low pressure-high temperature metamorphism in the Vredefort Dome, South Africa: anticlockwise pressure-temperature path followed by rapid decompression, *Geol. J.*, 30, 319-331, 1995.

Gibson, R.L., Reimold, W.U., and Wallmach, T., Metamorphosed pseudotachylite from the Lower Witwatersrand Supergroup, Vredefort Dome, South Africa, *Tectonophys.*, in revision, 1996.

Green, R.W. and Chetty, P., Seismic refraction studies in the basement of the Vredefort structure, *Tectonophys.*, 171, 105-113, 1990.

Grieve, R.A.F. and Masaitis, V.L., The economic potential of terrestrial impact craters, *Int. Geol. Rev.*, 36, 105-151, 1994.

Grieve, R.A.F., Langenhorst, F. and Stöffler, D., Shock metamorphism of quartz in nature and experiment: II. Significance in geoscience, *Meteoritics and Planet. Sci.*, 31, 6-35, 1996.

Hart, R.J., Nicolaysen, L.O. and Gale, N.H., Radioelement concentrations in the deep profile through Precambrian basement of the Vredefort structure, *J. Geophys. Res.*, 86, 10639-10652, 1981.

Hart, R.J., Andreoli, M.A.G., Smith, C.B., Otter, M.L. and Durrheim, R., 1990a, Ultramafic rocks in the centre of the Vredefort structure: possible exposure of the upper mantle, *Chem. Geol.*, 83, 233-248, 1990a.

Hart, R.J., Andreoli, M.A.G., Tredoux, M. and de Wit, M.J., Geochemistry across an exposed section of Archaean crust at Vredefort: with implications for mid-crustal discontinuities, *Chem. Geol.*, 82, 21-50, 1990b.

Hart, R.J., Andreoli, M.A.G., Reimold, W.U. and Tredoux, M., Aspects of the dynamic and thermal metamorphic history of the Vredefort cryptoexplosion structure: implications for its origin, *Tectonophys.*, 192, 313-331, 1991.

Hart, R.J., Hargraves, R.B., Andreoli, M.A.G., Tredoux, M., and Doucouré, C.M., Magnetic anomaly near the centre of the Vredefort structure: Implications for impact related magnetic signatures, *Geology*, 23, 277-280, 1995.

Henkel, H., Petrophysical properties (density and magnetization) of rocks from the northern part of the Baltic shield, *Tectonophys.*, 192, 1-19, 1991.

Henkel, H., Geophysical aspects of meteorite impact craters in eroded shield environment, with special emphasis on electric resistivity, *Tectonophys.*, 216, 63-89, 1992.

Henkel, H., Standard diagrams of magnetic properties and density - a tool for understanding magnetic petrology, *J. Appl. Geophys.*, 32, 43-53, 1994.

Henkel H., and Lilljequist, R., Large impact in the Baltic shield with special attention to the Uppland structure. *Lunar Planet. Inst. Contr. No. 790*, 38-40, Houston, Texas, 1992.

Henkel, H., Lee, M.K., and Lund, C-E., An integrated geophysical interpretation of the 2000 km Fennolora section of the Baltic shield. In: R. Freeman, P. Giese, and St. Mueller (Eds), *The European Geotraverse: Integrated Studies*, 67-76. European Science Foundation, Strasbourg, France, 1994.

Hildebrand, A.R., Penfield, G.T., Kring, D.A., Pilkington, M., Carmargo, Z.A., Jacobsen, S.B., and Boynton, W.V., Chicxulub crater: A possible Cretaceous-Tertiary boundary impact crater on the Yucatán Peninsula, Mexico, *Geology*, 19, 867-871, 1991.

Hische, R., Geologische Kartierung und petrographische Untersuchungen am westlichen Kraterrand der Siljan-Impaktstruktur in Mittelschweden (Kopparbergslän), *Msc. thesis*. Westfälische Wilhelms Universität, Münster, Germany, 145p. (unpubl.), 1991.

Hörz, F., Untersuchungen an Riesgläsern, *Beitr. Miner. Petrol.*, 11, 621-661, 1965.

Jackson, G.M., Palaeomagnetic study and magnetic modelling of the Vredefort dome. *B.Sc thesis*, Univ. of the Witwatersrand, Johannesburg, 46p. (unpubl.), 1982.

Jackson, M.C., Geochemistry and metamorphic petrology of Dominion Group metavolcanics in the Vredefort area, South Africa, *S. Afr. J. Geol.*, 97, 62-77, 1994.

Jones, M.Q.W., Heat flow in the Witwatersrand basin and environs and its significance for the South African shield geotherm and lithosphere thickness. *J. Geophys. Res.*, 93, B4, 3243-3260, 1988.

Juhlin, C., Scientific summary report of the Deep Gas Drilling Project in the Siljan ring impact structure, Vattenfall Utvecklings AB., Report U(G) 1991/14. Älvkarleby, Sweden, 278p., 1991.

Juhlin, C., and Pedersen, L.B., Reflection seismic investigations of the Siljan impact structure, Sweden, *J. Geophys. Res.*, 92, B13, 14113-14122, 1987.

Juhlin, C., and Pedersen, L.B., Further constraints on the formation of the Siljan impact crater from seismic reflection studies, *Geol. För. Stockholm Förh.*, 115-2, 151-158, 1993.

Kamo, S.L., Reimold, W.U., Krogh, T.E., and Colliston, W.P., Shocked zircon in Vredefort pseudotachylite and the U-Pb zircon age of the Vredefort impact event, *Cent. Geocongress Geol. Soc. S. Afr.*, Johannesburg, Ext. Abstr., 566-569, 1995.

Koeberl, C., Reimold, W.U. and Shirey, S.B., A Re-Os isotope study of the Vredefort Granophyre: Clues to the origin of the Vredefort Structure, South Africa, *Geology*, in revision, 1996.

Lambert, P., Breccia dikes: Geological constraints on the formation of complex craters, in: Schultz, P.H. and Merrill, R.B. (Eds.), *Multi-Ring Basins, Proc. Lunar Planet. Sci.*, 12A, 59-78, 1981.

Leroux, H., Reimold, W.U. and Doukhan, J.-C., A T.E.M. investigation of shock metamorphism in quartz from the Vredefort dome, South Africa, *Tectonophys.*, 230, 223-239, 1994.

Lindström, M., Floden, T., Grahn, Y., and Kathol, B., Post-impact deposits in Tvären, a Middle Ordovician crater south of Stockholm, Sweden, *Geol. Mag.*, 131, 91-103, 1994.

Manton, W.I., The orientation and origin of shatter cones in the Vredefort Ring, In: Geological Problems in Lunar Research. *New York Acad. Sci. Ann.*, 123, 1017-1049, 1965.

Masaitis, V.L., Mikhaylov, M.V., and Sleninovskaya, T.V., The Popigai meteorite crater, Nauka Press, Moscow, 124p., 1975.

Masaitis, V.L., Maschchak, M.S., Naumov, M.V., and Raikhlin, A.I., Large Astroblemes of Russia, VSEGEI, St. Petersburg, Russia, 32p., 1994.

Maxwell, D.E., Simple Z-model of cratering, ejection and the overturned flap, in: *Impact and Explosion Cratering* (edited by D.J. Roddy, R.O. Pepin, and R.B. Merrill, Pergamon press, New York, pp.1003-1008, 1977.

McCarthy, T.S., Charlesworth, E.G. and Stanistreet, I.G., Post-Transvaal structural features of the northern portion of the Witwatersrand Basin, *Trans. Geol. Soc. S. Afr.*, 89, 311-324, 1986.

McCarthy, T.S., Stanistreet, I.G. and Robb, L.J., Geological studies related to the origin of the Witwatersrand Basin and its mineralization - an introduction and a strategy for research and exploration, *S. Afr. J. Geol.*, 93, 1-4, 1990.

McCarville, P. and Crossey, L.J., Post-impact hydrothermal alteration of the Manson Impact Structure, in: *The Manson Impact Structure, Iowa: Anatomy of an Impact Crater* (edited by C. Koeberl and R.R. Anderson), *Geol. Soc. Amer. Spec. Pap.*, 302, 275-316, 1996.

Melosh, H.J., Impact Cratering - a geologic process. *Oxford Monogr. on Geol. and Geophys.*, 11, 245p., 1989.

Militzer, H. and Weber, F. (eds.), Angewandte Geophysik, Band 1, Gravimetrie und Magnetik, Akademie-Verlag, Berlin, 353pp., 1984.

Minnitt, R.C.A., Reimold, W.U. and Colliston, W.P., The geology of the Greenlands Greenstone Complex and selected granitoid terranes in the southeastern quadrant of the Vredefort Dome, Univ. of the Witwatersrand, *Econ. Geol. Res. Unit Inf. Circ.*, 281, 46p., 1994.

Moonsamy, B.C., The petrography and geochemistry of a layered ultramafic intrusion at Majuba Colliery, south of Amersfoort, South Eastern Transvaal. Is it a Bushveld satellite?, *B.Sc. Hons. Diss.*, Univ. of the Witwatersrand, Johannesburg, 44p. (unpubl.), 1995.

Nel, L.T., The Geology of the Country Around Vredefort, *Geol. Surv. S. Afr. Spec. Publ.*, 6, 134p., 1927.

Nicolaysen, L.O. and Reimold, W.U., Editors, Proc. Int. Worksh. Cryptoexpl. and Catastr. in the Geol. rec., with a Special Focus on the Vredefort Structure, *Tectonophys.*, 171, 422p., 1990.

Olesen, O., Kaada, K., and Tveten, E., Petrophysical properties of a prograde amphibolite-granulite facies transition at Sigerfjord, Västerålen, northern Norway. *Tectonophys.*, 192, 33-39, 1991.

Pybus, G.Q.J., Geological and Mineralogical Analysis of Some Mafic Intrusions in the Vredefort Dome, Central Witwatersrand Basin, *M.Sc. diss.*, Univ. of the Witwatersrand, Johannesburg, 376pp. (unpubl.), 1996.

Pybus, G.Q.J., Reimold, W.U., Colliston, W.P. and Smith, C.B., Mineralogical and chemical classification of mafic intrusives in the central region of the Witwatersrand Basin, *Cent. Geocongress, Geol. Soc. S. Afr.*, Johannesburg, Ext. Abstr., 581-584, 1995.

Pye, E.G., Naldrett, A.J., and Giblin, P.E., Editors, The Geology and Ore Deposits of the Sudbury Structure, *Ontario Geol. Surv. Spec. Vol.*, 1, 603p., 1984.

Reimold, W.U., The impact melt rocks of the Lappajärvi meteorite crater, Finland: Petrography, Rb-Sr, major and trace element geochemistry, *Geochim. Cosmochim. Acta*, 46, 1203-1225, 1982.

Reimold, W.U., A review of the geology and deformation related to the Vredefort structure, South Africa, *J. Geol. Educ.*, 41, 106-117, 1993.

Reimold, W.U., Hydrothermal Witwatersrand gold mineralization caused by the Vredefort mega-impact event?, *Abstr. Int. Conf. on New Developments Regarding the K/T Event and other Catastrophes in Earth History, Lunar Planet. Inst. Contr. No. 825*, 91-92, Houston, Texas, 1994.

Reimold, W.U., Pseudotachylite in impact structures - generation by friction melting and shock brecciation?: A review and discussion, *Earth-Science rev.*, 39, 247-264, 1995a.

Reimold, W.U., Comp., Proc. Symp. Economic Significance of Metamorphism and Fluid Movement within the Witwatersrand Basin, Univ. of the Witwatersrand, *Econ. Geol. Res. Unit., Inf. Circ.*, 296, 56p., 1995b.

Reimold, W.U., Impact cratering - A review, with special reference to the economic importance of impact structures and the southern African impact crater record, *Earth, Moon and Planets*, 70, 1995c.

Reimold, W.U. and Wallmach, T., The Vredefort structure under review, *S. Afr. J. Sci.*, 87, 412-417, 1991.

Reimold, W.U. and Colliston, W.P., Pseudotachylites of the Vredefort Dome and the surrounding Witwatersrand basin, South Africa, In: *Large Meteorite Impacts and Planetary Evolution*, B.O. Dressler, R.A.F. Grieve, and V.L. Sharpton, V.L. (Eds), *Geol. Soc. Amer. Bull.*, 293, 177-196, 1994.

Reimold, W.U., Colliston, W.P. and Robertson, A.S., Chronological and structural work in the Vredefort Dome, *Geocongress '88, Geol. Soc. S. Afr.*, Durban, Ext. Abstr., 501-504, 1988.

Reimold, W.U., Horsch, M. and Durrheim, R.J., The 'Bronzite'-Granophyre from the Vredefort Structure - a detailed analytical study and reflections on the origin of one of Vredefort's enigmas, *Proc. 20th Lunar Planet. Sci. Conf.*, 433-450, Lunar Planet. Inst., Houston, 1990a.

Reimold, W.U., Barr, J.M., Grieve, R.A.F. and Durrheim, R.J., Geochemistry of the melt and country rocks of the Lake St. Martin impact structure, Manitoba, Canada, *Geochim. Cosmochim. Acta*, 54, 2093-2111, 1990b.

Reimold, W.U., Gibson, R.L., Colliston, W.P., Layer, P.W., Pybus, G.Q.J., Armstrong, R.A., and Smith, C.B.,  $^{40}\text{Ar}$ - $^{39}\text{Ar}$  dating and Sm-Nd isotopic analysis of mafic intrusions in the central portion of the Witwatersrand Basin, *Cent. Geocongress, Geol. Soc. S. Afr.*, Johannesburg, Ext. Abstr., 585-588, 1995a.

Reimold, W.U., Gibson, R.L., Friese, A., and Layer, P.W., A chronological framework for the Witwatersrand basin - with emphasis on metamorphic/hydrothermal events, in: *Proc. Symp. Econ. Significance of Metamorphism and Fluid Movement within the Witwatersrand Basin* (comp. by Reimold, W.U.), Univ. of the Witwatersrand, *Econ. Geol. Res. Unit, Inf. Circ.*, 296, 30-37, 1995b.

Reimold, W.U., Meshik, A.P., Smit, G., Pravditsseva, O.V., and Shukolyukov, Yu.A., U-Xe dating of Witwatersrand uraninite: Implications for post-2 Ga overprinting, *Geochim. Cosmochim. Acta*, 59, 5177-5190, 1995c.

Robb, L.J. and Meyer, F.M., The Witwatersrand Basin, South Africa: Geological framework and mineralization processes, Univ. of the Witwatersrand, *Econ. Geol. Res. Unit., Inf. Circ.*, 293, 37p., 1995.

Roering, C., Barton, J.M., and Winter, H. de la R., The Vredefort structure: A perspective with regard to new tectonic data from adjoining terranes, *Tectonophys.*, 171, 1-22, 1990.

SACS (South African Committee for Stratigraphy), *Stratigraphy of South Africa*, Part 1: Lithostratigraphy of the Republic of South Africa, South West Africa/Namibia and the Republics of Bophutatswana, Transkei and Venda (Kent, L.E., comp.), Dept. of Mineral and Energy Affairs, Governm. Printer, Pretoria, 690p., 1980.

Schmidt-Kahler, H. (Publ.), Ergebnisse der Ries-Forschungsbohrung 1973: Struktur des Kraters und Entwicklung des Kratersees, *Geol. Bavaria*, 75, 470p., 1977.

Shand, S.J., The pseudotachylite of Parijs (O.F.S.) and its relation to 'trap-shotten gneiss' and 'flinty crush-rock', *Quart. J. Geol. Soc. London*, 72, 198-221, 1916.

Sharpton, V.L., Burke, K., Camargo-Zanoguera, A., Hall, S.A., Lee, S., Marín, L.E., Suàrez-Reynoso, G., Quezada-Muñeton, J.M., Spudis, P.D., and Urrutia-Fucugauchi, J., Chicxulub multiring impact basin: Size and other characteristics derived from gravity analysis, *Science*, 261, 1564-1567, 1993.

Slawson, W.F., Vredefort core: a cross-section of the upper crust?, *Geochim. Cosmochim. Acta*, 40, 117-121, 1976.

Smit, P.J., and Maree, B.D., Densities of South African rocks for the interpretation of gravity anomalies. *Geol. Surv. S. Afr. Bull.*, 48, 37p., 1966.

Spray, J.G., A physical basis for the frictional melting of some rock-forming minerals, *Tectonophys.*, 204, 205-221, 1992.

Spudis, P.D., *The Geology of Multi-Ring Impact Basins*, Cambridge Univ. Press, 263p., 1993.

Stepto, D., A geological and geophysical study of the central portion of the Vredefort dome structure. *Ph.D. diss.*, Univ. of the Witwatersrand, Johannesburg, 378p. (unpubl.), 1979.

Stepto, D., The geology and gravity field in the central core of the Vredefort structure, *Tectonophys.*, 171, 75-103, 1990.

Stevens, G., Gibson, R.L. and Droop, G.T.R., Low=pressure granulite facies metamorphism in the core of the Vredefort Dome: Getting to the root of the problem, in: *Proc. Symp. The Economic Significance of Metamorphism and Fluid Movement Within the Witwatersrand Basin* (Comp. Reimold, W.U.), Univ. of the Witwatersrand, *Econ. Geol. Res. Unit., Inf. Circ.*, 296, 44-48, 1995.

Stevens, G., Gibson, R.L. and Droop, G.T.R., Polyphase granulite metamorphism in the Vredefort Dome: A window into the deep Kaapvaal Craton at 2.06 Ga, Univ. of the Witwatersrand, *Econ. Geol. Res. Unit, Inf. Circ.*, 297, 27pp., 1996.

Stöffler, D., Knöll, H.-D., and Maerz, U., Terrestrial and lunar impact breccias and the classification of lunar highland rocks, *Proc. Lunar Planet. Sci. Conf. 10th*, 639-675, 1979.

Stöffler, D., and Ostertag, R., The Ries impact crater, *Fortschr. Miner.*, 61, 71-116, 1983.

Stöffler, D., Deutsch, A., Avermann, M., Bischoff, L., Brockmeyer, P., Buhl, D., Lakomy, R. and Müller-Mohr, V., The formation of the Sudbury Structure, Canada: Toward a unified impact model, in: *Large Meteorite Impacts and Planetary Evolution* (edited by Dressler, B.O., Grieve, R.A.F., and Sharpton, V.L.), *Geol. Soc. Amer. Spec. pap.*, 293, 303-318, 1994.

Theriault, A.M., Field study, petrology, and chemistry of the Vredefort Granophyre, South Africa, *M.Sc. diss.*, Univ. of Houston, Houston (Texas), 347p. (unpubl.), 1992.

Theriault, A.M., Reid, A.M. and Reimold, W.U., Original size of the Vredefort Structure, South Africa (abstract), *Lunar Planet. Sci.*, XXIV, 1419-1420, 1993.

Theriault, A.M., Grieve, R.A.F., and Reimold, W.U., How big is Vredefort? (abstract), *Meteoritics*, 30, 586-587, 1995.

Theriault, A.M., Reimold, W.U. and Reid, A.M., The Vredefort granophyre: Field studies, *S. Afr. J. Geol.*, 99, 1-21, 1996.

Trieloff, M., Reimold, W.U., Kunz, J., Boer, R.H. and Jessberger, E.K.,  $^{40}\text{Ar}$ - $^{39}\text{Ar}$  thermochronology of pseudotachylites at the Ventersdorp Contact Reef, Witwatersrand Basin, *S. Afr. J. Geol.*, 97, 365-384, 1994.

Tweedie, K.A.M., The discovery and exploration of beisa Gold and Uranium mines in the southern extension of the Welkom Gold Field, in: *Mineral Deposits of Southern Africa* (edited by Anhaeusser, C.R. and Maske, S.), Geol. Soc. S. Afr., Johannesburg, 541-550, 1986.

Walraven, F. and Elsenbroek, J.H., Geochronology of the Schurwedraai Alkali Granite and associated nepheline syenite and implications for the origin of the Vredefort Structure, *S. Afr. J. Geol.*, 94, 228-235, 1991.

Walraven, F., Armstrong, R.A. and Kruger, F.J., A chronostratigraphic framework for the north-central Kaapvaal Craton, the Bushveld Complex and the Vredefort structure, *Tectonophys.*, 171, 23-48, 1990.

Wilshire, H.G., and Howard, K.A., Structural patterns in central uplifts and cryptoexplosion structures as typified by Sierra Madera, *Science*, 162, 258-261, 1968.

## APPENDIX

### I. Comparison of measured magnetic properties of central core rocks

It was found in the course of magnetic modelling that the high q-values cited by Hart et al. (1995) were far too high to reproduce the measured magnetic anomalies. Some of the data cited by Hart et al. (1995) were measurements first reported by Jackson (1982), who already noted this discrepancy. Jackson could not model the observed anomalies with the high remanences determined and, instead, used values reduced by a factor of 10. The original SI scaled magnetic susceptibility data of Jackson (1982) were converted by Hart et al. (1995) to cgs units. Hart et al. also reported estimates of the magnetite content of Vredefort rocks, which they derived from CIPW norm calculations. In comparison with their susceptibility data, these values are also too high by a factor of approximately 10. Because of these problematics, it was decided to determine a large number of new susceptibility data for rocks of the Vredefort core in order to obtain more reliable data for this crucial modelling parameter. In Figure 40 these data are compared. It is clear that similar susceptibilities have been measured in all three cases and the type values are in reasonable agreement. However, magnetite contents, as reflected in the susceptibility data, are in the 0.1 vol% range, one order of magnitude lower than the values reported by Hart et al. (1995) based on CIPW norm estimates.

The q-values obtained by Jackson (1982) and applied by Hart et al. (1995) are given in Figure 41. They cover a similar range with an average around 40. In the modelling, the use of type susceptibilities and q-values around 2 to 3 results in rather good reproduction of the measured anomalies.

It is, therefore, concluded that there still exists a basic problem regarding the q-values reported for Vredefort rocks in the past. These values are not readily reconciled with the known properties of magnetic minerals (compare Figure 11B). Neither the quoted magnetite contents in Hart et al. (1995) nor the high q-values in Jackson (1982) and Hart et al. (1995) can be brought in agreement with observed magnetic anomalies. Even if part of the magnetite is so fine-grained that it would only carry remanent magnetization, the related q-values could only be higher than the values applied in this modelling by a factor of 2. We conclude that it is not likely that the actual q-values of important Vredefort rocks are much higher than the values used in this study. And to assume that excessively high q-values could be the result of impact magnetizations is not supported by any data reported to date.

### II. Calculation of flow lines

In accordance with Melosh (1989), the flow model by Maxwell (1977) appears to provide results, which are in good agreement with the results of experimental cratering and observed

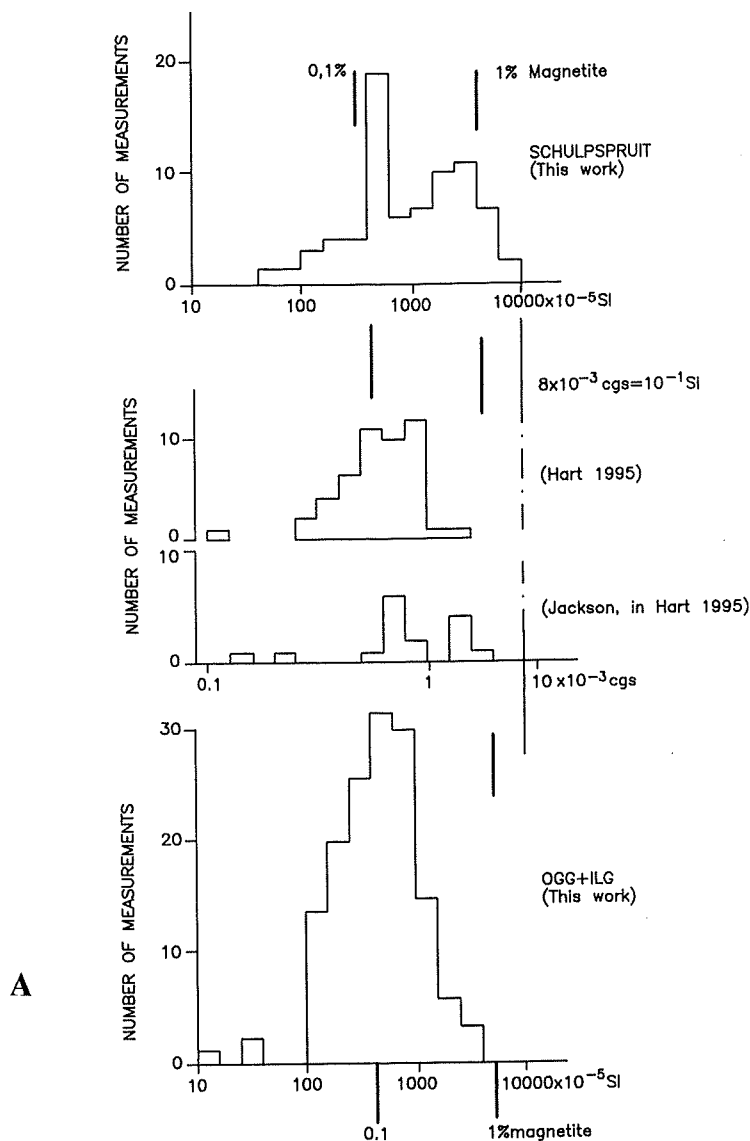


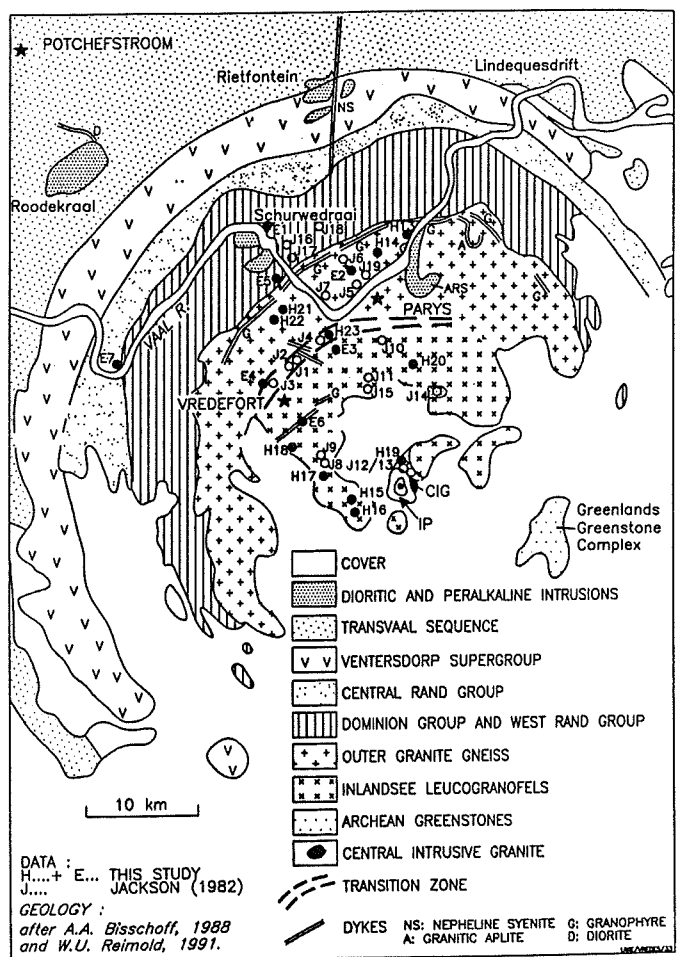
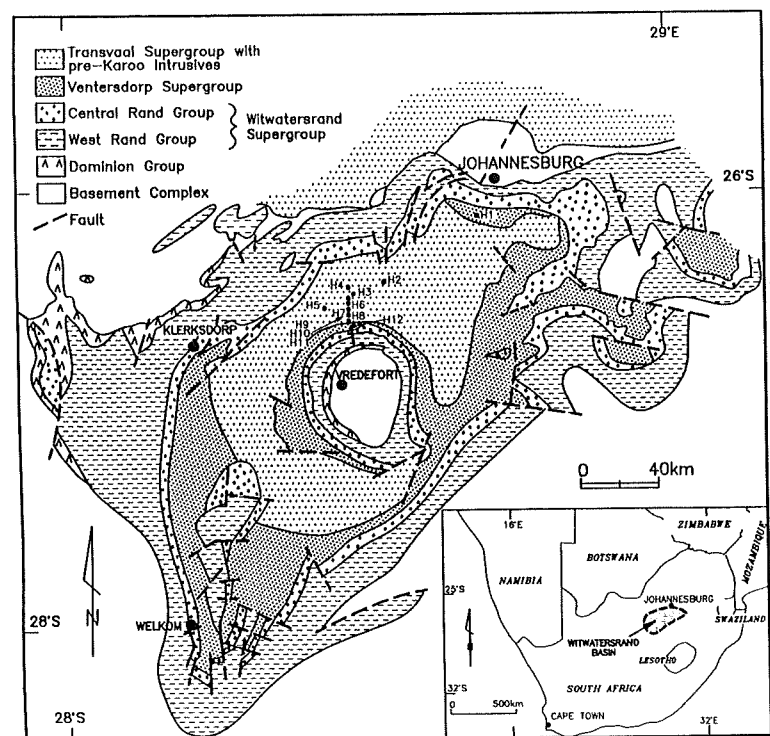
*Figure 40: A: Comparative histograms of magnetic susceptibilities for rocks in the core of the Vredefort Dome; B: Measurement stations for susceptibility data of various lithologies (compare Tables 3 and 4) in the central Witwatersrand Basin and south of Johannesburg; C: Measurement stations for susceptibility data obtained within the Vredefort Dome (compare Tables 3 and 4).*

crater shapes. The z-parameter in this context was found to be close to 3. In polar coordinates ( $r$  - radius and  $v$  - angle and  $R$  as the location where the flow line cuts the surface) such a flow line is described as:

$$r = R (1 - \cos v)^{1/(z-2)} \quad \text{or, when } z=3 \text{ and } r = R (1-\cos v); \text{ or in cartesian coordinates:}$$

$$x = r \cos v \quad \text{and} \quad y = r \sin v$$

To find the location of  $x$  and  $y$ , where the flow line reaches its minimum:



$$r = R (1 - x/r) = R - Rx/r$$

$$r^2 = Rr - Rx$$

$$r^2 - Rr + Rx = 0$$

$$r = R/2 + \sqrt{(R^2/4 - Rx)} \quad \text{or} \quad r = R/2 (1 + \sqrt{1 - 4x/R}).$$

$x$  will achieve its maximum, when  $1 - 4x/R = 0$  and  $x = R/4$  and  $r = R/2$ ; when  $\cos v = x/r = 1/2$ , i.e.  $v = 60$  degrees,  $x = r/2$ , then

$$\sin v = y/r = \sqrt{3}/2, \quad y = r\sqrt{3}/2 = 0.22r.$$

As  $v$  is independent of  $R$ , all minima for different  $R$  will be located on the line inclined by 60 degrees. A family of flow lines for  $z=3$  is reproduced in Figure 42; as they are self similar, they can be applied to any crater dimension at different scales.

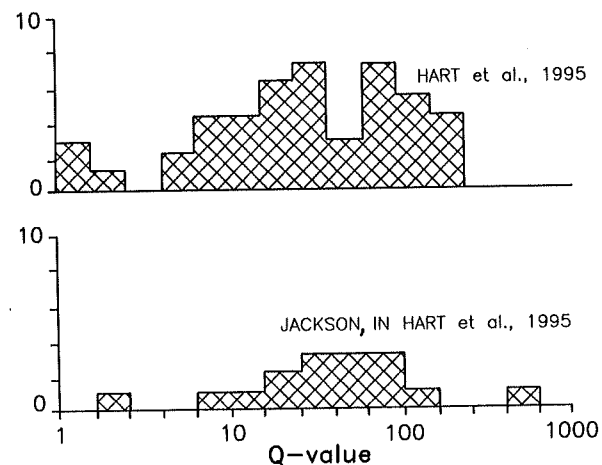


Figure 41: Comparative histograms of  $q$ -values determined for core lithologies.

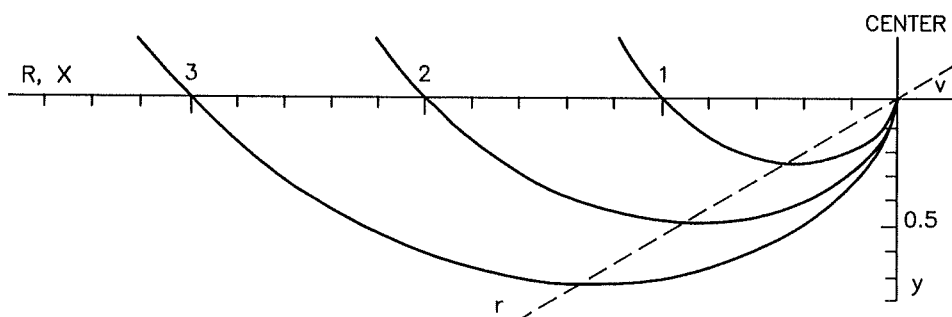


Figure 42: Flow lines calculated for the flow model presented in Melosh (1989) and using  $z=3$ . The lines can be rescaled to analyze the flow conditions for any crater size.

### **III. Calculation of how to delimit the viscosity factor for modelling of the central rise formation**

The viscosity ( $\nu$ ) necessary for the immediate formation of a central rise is related to gravity ( $g$ ), the TC diameter ( $d$ ), and the density ( $m$ ) of crustal material:

$$\nu = m \pi^{3/2} g^{1/2} d^{3/2} = \sqrt{m \pi^3 g d^3}; \text{ when } m = 2.9 \text{ Mgm}^{-3}, g = 10, \text{ and } d = 1.25 \times 10^5 \text{ m,}$$

$$\nu = \sqrt{(2.9 \cdot 10^6 \cdot 10 \cdot \pi^3 \cdot 1.25^3 \cdot 10^{15})} = 1 \cdot 10^{12} \text{ Pa s}$$

### **IV. Calculation of impact energy**

The energy  $E$  depends on the projectile mass ( $M$ ) and velocity ( $V$ ):

$$E = 1/2 M V^2.$$

For projectile radii 3.9 ... 2.5 km and velocities 15 ... 45 km s<sup>-1</sup>, the energy will be

$$E = 1/2 \cdot 4/3 \cdot \pi \cdot 3.9^3 \cdot 10^9 \cdot 15^2 \cdot 10^6 = 3 \cdot 10^{19} \text{ J}$$

### **V. Calculation of seismic magnitude**

The seismic magnitude  $S$  is:

$$S = 0.67 \cdot 10 \log E - 4.87;$$

inserting  $E = 3 \cdot 10^{19}$ , gives  $S = 14$ .

### **VI. Calculation of melt extension from the extension of HEL**

The diagram from Melosh (1989) relating shock effects to projectile properties is reproduced in Figure 43. This diagram illustrates the arising amounts of vapor and melt, and the position of the HEL for an anorthosite gabbro target and an iron projectile. In the Vredefort case, the composition of the projectile is unknown. The anorthosite gabbro target composition is a reasonable approximation for the composition of the lower crust, where the extension of the HEL is indicated by the termination of seismic reflectors. The two entries HEL and melt are shown with their intersections with the curves for a projectile having an impact velocity of 45 and 15 km s<sup>-1</sup>, respectively. The obtained parameter  $D/r$  (depth extension and projectile radius) has the values 5, 9.5, 18, and 28. For a measured HEL extension (i.e.  $D$ ) of 70 km, the projectile radii of 3.9 and 2.5 km are obtained, corresponding to the impact velocities of 15 and 45 km s<sup>-1</sup>, respectively. The melt extension is then found by using these radii, resulting in values of 19 and 12.5 km for velocities of 15 and 45 km s<sup>-1</sup>, respectively.

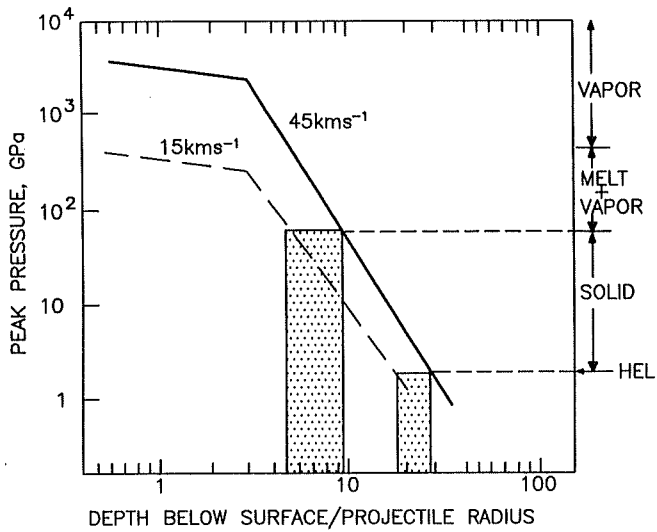


*Figure 43: Diagram relating impact pressure to irreversible phase changes in target material (after Melosh, 1989), for a target composition of anorthosite gabbro and an iron projectile, and for two different impact velocities. The HEL and the melt-solid interface result in an interval of extensions and projectile sizes.*

## VII. Calculation of displaced masses

The rim elevation is calculated as 0.036 times the TC diameter, which gives 4.5 and 5.8 km for TC diameters of 125 and 162 km, respectively. The rim rise is approximated with a triangle of this height and a base of 0.6 times half the TC diameter, i.e. 38 and 49 km + the extension into the crater from the rim position, which is the same as the rim height, if the ejecta angle is 45 degrees (a value obtained in the flow model, when  $z = 3$ ). The volume  $V$  of this rotational symmetric triangle is its area  $A$  times the radius  $r$  to its mass centre.

$$V = 2 \pi A r$$

The mass centre in the radial extension is found from the average of the radial distances of the triangle corners:

$$r(\min) = 125 - 4.8 + (0 + 38 + 4.5) / 3 = 135 \text{ km}$$

$$r(\max) = 162 - 5.8 + (0 + 49 + 5.8) / 3 = 174 \text{ km}$$

$$V(\max) = ((38 + 4.5) \cdot 4.5) / 2 \cdot 2 \pi \cdot 135 = 4 \cdot 10^4 \text{ km}^3$$

$$V(\max) = ((49 + 5.8) \cdot 5.8) / 2 \cdot 2 \pi \cdot 174 = 2 \cdot 10^5 \text{ km}^3.$$

The ejecta volume can be calculated using a triangular approximation of the excavated crater, where the excavation depth and its radial position are derived from the flow model (with  $z = 3$ ). The depth is 0.125 times the TC diameter, i.e. 15.6 and 20.25 km for TC diameters of 125 and 162 km, respectively. The radial position is at 0.22 times the TC diameter, i.e. at 27.5 and 35.6 km, respectively. The volume  $V$  of a conical section is a

function of its height  $h$ , the larger radius  $R$  and the smaller radius  $r$ :

$$V = (1/3) \pi h (R^2 + Rr + r^2);$$

and when the central, not excavated volume  $1/3 \pi h r^2$  is subtracted, this gives

$$V = (1/3) \pi h (R^2 + Rr); \text{ it follows that}$$

$$V(\min) = (1/3) \cdot \pi \cdot 15.6 \cdot (62.5^2 + 62.5 \cdot 27.5) = 6 \cdot 10^4 \text{ km}^3$$

$$V(\max) = (1/3) \cdot \pi \cdot 35.6 \cdot (81^2 + 81 \cdot 35.6) = 1 \cdot 10^5 \text{ km}^3.$$

\_\_\_\_oOo\_\_\_\_